A parton shower algorithm based on Catani-Seymour dipole factorisation

S. Schumann

Institut für Theoretische Physik, TU Dresden,
D–01062 Dresden, Germany, and
School of Physics, The University of Edinburgh,
EH9 3JZ, Edinburgh U.K.
E-mail: steffen@theory.phy.tu-dresden.de

F. Krauss

Institute for Particle Physics Phenomenology, Durham University,
Durham DH1 3LE, U.K.
E-mail: frank.krauss@durham.ac.uk

ABSTRACT: In this publication the implementation of a new parton shower model based on the Catani-Seymour dipole factorisation, as first suggested by [1, 2], is discussed. First results obtained with the new algorithm are compared with experimental data.

KEYWORDS: Jets, QCD, Parton Model, Hadronic Colliders.

Contents

1. Introduction

In the past decades, parton shower Monte Carlo programs, such as PYTHIA [3, 4] or HER-WIG [5, 6] have been indispensable tools for planning and analysing particle physics experiments at different colliders. It can be anticipated that they will play a similarly prominent rôle in the LHC era.

There are a number of reasons for the success of these workhorses. One of the most important ones rests in their ability to bridge the gap between few-parton final states, as described by fixed-order perturbative calculations, and the real world, where a multitude of hadrons etc. fills the detectors of the experiments. The transformation of the partons of perturbation theory into the visible hadrons, hadronisation, is a direct consequence of the confinement property of QCD. Currently, this phenomenon can be described in terms of phenomenological models only, which depend on various phenomenological parameters tuned to data. These parameters and hence the validity of the models in turn depends on the properties (such as the flow of energy and other QCD quantum numbers) of the parton ensemble; therefore it is important that these properties are kept under control. It is the merit of parton showers that they provide a well-understood, theoretically sound and universal framework of translating the few-parton states of fixed-order perturbation theory, calculated at some high scale, with multi-parton states at much lower scales, of the order of a few Λ_{QCD}, where hadronisation sets in. In so doing the parton showers help guarantee the validity of the tuned parameters of the hadronisation models.

To achieve this translation of few-parton to multi-parton states, the parton shower programs rely on correctly describing QCD particle production in the dominant soft and collinear regions of phase space, giving rise to the bulk of radiation. It is in this region, where the complicated radiation pattern of multiple particle emission factorises into nearly independent - up to ordering in terms of a suitably chosen parameter - individual emissions of single partons. This approximation, namely expanding around the soft or collinear limit, ultimately leads to the resummation of the corresponding leading logarithms, which are then typically encapsulated in exponential form in the Sudakov form factors. Their probabilistic interpretation in fact is the central feature allowing for a straightforward implementation in an event generator, producing unweighted events. Due to the resummation of leading logarithms it should thus not be too surprising that the parton shower programs more than often produce answers for QCD-related questions, which approximate exact results very well.

However, the quality of the answers provided by the parton shower approximation alone relies on whether the question is related to the soft and/or collinear region in the phase space of particle production. If this is not the case, for example because of the relevance of hard emissions or of non-trivial correlations of particles, the quality of parton shower

results tends to deteriorate. In such cases, evidently a full quantum mechanical treatment as provided by fixed-order calculations becomes mandatory. Therefore, the problem of systematically including higher-order effects into parton shower programs has been in the center of research in the past few years. In principle, there have been two major avenues of investigation. One dealt with the question of how to include the correct QCD next-to leading order correction to total cross sections [7]–[9], and has led to an implementation ready for use by the experiments in form of the MC@NLO code [10]. The other considered the inclusion of tree-level multi-leg matrix elements into the simulation [11]–[15], and has lead to two types of algorithms being implemented. One, based on [11, 12], is the cornerstone of the event generator SHERPA [16]–[18] and an alternative formulation of the same algorithm, proposed in [13], has been implemented in ARIADNE [19, 20]. The other merging algorithm, based on [14, 15], has been incorporated in ALPGEN [21], MADGRAPH/MADEVENT [22]–[24], and HELAC [25, 26]. Although it is not entirely clear how these two approaches relate in detail, some first comparisons [27] show an interesting and assuring degree of agreement.

As one of the most recent outcomes of this line of research, it became apparent that in order to systematically improve the event generators by including higher-order corrections, also the parton shower algorithms themselves must be ameliorated. Some developments in this direction include an improved treatment of angular ordering and massive partons in HERWIG++ [28] or the introduction of a new $k_\perp$-ordered shower in PYTHIA [29]. More recently, and motivated by the wish to include loop-level calculations in a more straight-forward and systematic manner, the application of subtraction terms, prevalent in QCD next-to leading order calculations, has been proposed. This paper reports on the construction of a parton shower based on such subtraction terms. It uses the Catani-Seymour dipole formalism [30, 31] and the corresponding subtractions as a starting point.[1] This formulation of a parton shower has been proposed for the first time in [1, 2]. A similar ansatz relies on antenna subtraction terms [33, 34] and has been presented recently in [35].

The paper is organised as follows: After briefly introducing the idea of parton shower algorithms based on subtraction terms in section 1.1 and a short review of the subtraction formalism of Catani-Seymour in section 1.2, section 2 states the basic construction principles of the proposed shower description. In section 3 the actual parton shower built on Catani-Seymour subtraction terms is constructed. The most general massive and the massless case for all the possible QCD splitting types are discussed in detail, and the modifications needed to include splittings of supersymmetric particles are discussed. The analytic expressions for the first shower emission from various core processes are compared with the corresponding exact tree-level matrix element calculations in section 4. In section 5 predictions obtained with the developed shower formalism are confronted with experimental data and other calculations. The focus hereby is on hadron production in e^+e^- collisions, and Drell-Yan and QCD jet production at the Fermilab Tevatron. Section 6 is devoted to the summary, conclusions, and an outlook on further developments.

---

[1]This approach has also been employed in a parallel project, [32].

1.1 Parton showers based on subtraction methods

Since its formulation almost a decade ago, the Catani-Seymour dipole formalism [30, 31] has been widely used in the calculation of next-to leading order (NLO) corrections in QCD, see for instance [36]–[43].

Such calculations typically face the problem of infrared divergences in both the real and the virtual parts of the NLO correction. In principle, such divergences are not really a problem, since for physically meaningful observables, the Kinoshita-Lee-Nauenberg theorem [44, 45] guarantees their mutual cancellation. To technically perform this cancellation, however, the divergences need to be regularised, which is usually performed by dimensional regularisation, i.e. continuing the calculation to d dimensions. There, the infrared divergences manifest themselves as poles in $1/(4-d)$ or $1/(4-d)^2$. To deal with the poles and achieve the cancellation, subtraction methods may be used. In general, they rely on the fact that the infrared divergences in the real correction part follow an universal pattern. This allows to construct simplified terms in a process-independent way that encapsulate all infrared divergences occurring in the full matrix element. Then, subtracting these terms from the real-correction matrix elements will yield an infrared-finite result, such that this subtracted matrix element can be safely integrated numerically in four dimensions. In addition, the subtraction terms are chosen such that they can be analytically integrated in d dimensions over the phase space of the additional soft or collinear particle causing the divergences. This yields the poles in $1/(4-d)$ or $1/(4-d)^2$, which are then added to the virtual part of the correction, and thus cancel the poles there.

The catch with the subtraction methods is that the subtraction terms can be constructed locally from the (colour-ordered) Born matrix element. In the Catani-Seymour method, for instance, pairs of particles are interpreted as emitting particle and spectator and are subjected to a splitting kernel creating a third particle. In this splitting process, one of the particles actually splits, while the recoil is compensated for by the spectator, which may be interpreted as its colour partner. At the same time, the phase space factorises exactly into a phase space over the original particles, already present at the Born level, and into a phase space of the additional particle emerging in the splitting. This exact factorisation corresponds to an exact mapping of the two original momenta (emitter and spectator) onto three four-momenta. At each point of the procedure all particles remain on their respective mass shell.

This is why constructing parton showers based on such methods currently is being pursued by different groups. It is clear that these showers, in full conformance with original formulations employing the splitting of individual, single partons, are based on the universal soft and collinear dominance of QCD radiation. Similar to the original shower algorithms, the emerging large logarithms occurring with each individual parton emission can be resummed in a straightforward way through a Markovian process. This, in principle, renders both formulations formally equivalent. On the other hand, however, showers based on subtraction terms have the practical advantage that the conservation of four-momentum is built in with particles that remain on their mass shell at any given point.[2] It can be

---

[2] It is interesting to note that the latest refinements of the parton showers in HERWIG and PYTHIA also

anticipated that these features ultimately will allow for a more transparent merging with multi-leg matrix elements and a drastically alleviated matching with full NLO calculations.

1.2 Short review of the Catani-Seymour subtraction method

The Catani-Seymour subtraction method has been introduced in [30] for massless partons and it has been extended to massive partons in [31]. To fix the notation for the rest of the paper, it will be briefly reviewed here.

The essence of this method is embedded in the dipole factorisation formula

$$|\mathcal{M}_{m+1}|^2 = \sum_{i,j} \sum_{k \neq i,j} \mathcal{D}_{ij,k} + \sum_{i,j} \sum_a \mathcal{D}_{ij}^a + \sum_{a,i} \sum_{k \neq i} \mathcal{D}_k^{ai} + \sum_{a,i} \sum_{b \neq a} \mathcal{D}^{ai,b} + \dots . \quad (1.1)$$

The individual dipole contributions $\mathcal{D}$ provide the correct approximation of the $(m+1)$-parton matrix element squared in the different singular regions of phase space.[3] In each term i, j and k denote final-state partons and a and b stand for initial-state partons. The first sum always runs over the two particles to be combined, whereas the second sum takes care of the spectators. Accordingly, the four terms correspond to the splitting of a final-state parton accompanied by a final-state or initial-state spectator and emissions off incoming particles in the presence of a final-state or an initial-state spectator, respectively. Finally, the dots in the equation above denote some potential finite terms which do not exhibit any divergence.

For the case of final-state emitters with a final-state spectator, for instance, the individual dipole contributions read [30]

$$\mathcal{D}_{ij,k} = -\frac{1}{2p_i p_j} \langle m 1, \dots, \widetilde{ij} \dots, \tilde{k}, \dots, m+1 | \frac{\mathbf{T}_k \cdot \mathbf{T}_{ij}}{\mathbf{T}_{ij}^2} \mathbf{V}_{ij,k} | 1, \dots, \widetilde{ij} \dots, \tilde{k}, \dots, m+1 \rangle_m, (1.2)$$

when all the involved partons are assumed to be massless. The occurring m-parton states are constructed from the original $(m+1)$-particle matrix element by replacing the partons i and j with the new parton $\widetilde{ij}$, the emitter, and the original parton k with $\tilde{k}$, the spectator. In the massless case, their momenta are given by

$$\tilde{p}_{ij}^\mu = p_i^\mu + p_j^\mu - \frac{y_{ij,k}}{1 - y_{ij,k}} p_k^\mu \quad \text{and} \quad \tilde{p}_k^\mu = \frac{1}{1 - y_{ij,k}} p_k^\mu, \quad (1.3)$$

where the dimensionless, Lorentz-invariant quantity $y_{ij,k}$ is given by

$$y_{ij,k} = \frac{p_i p_j}{p_i p_j + p_i p_k + p_j p_k}. \quad (1.4)$$

It is simple to show exact four-momentum conservation, i.e. $\tilde{p}_{ij}^\mu + \tilde{p}_k^\mu = p_i^\mu + p_j^\mu + p_k^\mu$, with all particles on their mass shell. In the matrix element on the right hand side of eq. (1.2), the $\mathbf{T}_{ij}$, $\mathbf{T}_k$ are the colour charges of the emitter and spectator, respectively, and the $\mathbf{V}_{ij,k}$

---

put more emphasis on the notion of a colour-connected partner compensating recoils etc. [28, 29].

[3]Note that squared matrix elements shall always be understood as properly normalised with respect to the colour degrees of freedom of incoming particles.

are matrices in the emitter's spin and colour space, responsible for its branching. The operators $\mathbf{V}_{ij,k}$ also depend on the dimensionless, Lorentz-invariant quantities

$$\tilde{z}_i = \frac{p_i p_k}{p_i p_k + p_j p_k} = \frac{p_i \tilde{p}_k}{\tilde{p}_{ij} \tilde{p}_k} \quad \text{and} \quad \tilde{z}_j = \frac{p_j p_k}{p_i p_k + p_j p_k} = \frac{p_j \tilde{p}_k}{\tilde{p}_{ij} \tilde{p}_k} = 1 - \tilde{z}_i \,. \tag{1.5}$$

For instance, for the case of a quark splitting in the final state with a final-state spectator, i.e. $q_{ij} \rightarrow q_i + g_j$, where s and s' denote the spins of $\widetilde{ij}$ and i, respectively, and where the subscripts label the momenta,

$$\langle s | \mathbf{V}_{q_i g_j, k}(\tilde{z}_i, y_{ij,k}) | s' \rangle = 8\pi\mu^{2\epsilon} \alpha_{\mathrm{s}} C_{\mathrm{F}} \left[\frac{2}{1 - \tilde{z}_i (1 - y_{ij,k})} - (1 + \tilde{z}_i) - \epsilon(1 - \tilde{z}_i) \right] \delta_{ss'} \,. \tag{1.6}$$

Here, $\epsilon = (4 - d)/2$, with d the number of dimensions. Similar expressions emerge for the other QCD splittings or when masses are included. However, as a general property, the matrices $\mathbf{V}_{ij,k}$ do not become singular, if any of the scalar products $p_i p_j$, $p_i p_k$ or $p_j p_k$ vanishes, and therefore the only soft or collinear divergences in the dipole terms $\mathcal{D}_{ij,k}$ are related to $p_i p_j \rightarrow 0$.

The collinear limit of the two final-state partons i and j originating from a splitting $\widetilde{ij} \rightarrow i + j$ is defined through their relative transverse momentum $k_\perp \rightarrow 0$. This limit can be investigated by decomposing the momenta as

$$p_i^\mu = z p^\mu + \frac{-k_\perp^2}{z} \frac{n^\mu}{2pn} + k_\perp^\mu \,, \tag{1.7}$$

$$p_j^\mu = (1 - z) p^\mu + \frac{-k_\perp^2}{1 - z} \frac{n^\mu}{2pn} - k_\perp^\mu \,, \tag{1.8}$$

where the lightlike p^μ defines the collinear direction and n^μ is an auxiliary lightlike vector that specifies the spacelike transverse momentum $k_\perp^\mu$, with $k_\perp^2 = -\mathbf{k}_\perp^2$, through $pk_\perp = nk_\perp = 0$. Then, in the collinear limit, the scalar product $p_i p_j$ reads

$$p_i p_j = -\frac{k_\perp^2}{2z(1 - z)} \,, \quad k_\perp^2 \rightarrow 0 \,, \tag{1.9}$$

and the dipole variables are given by

$$y_{ij,k} \rightarrow -\frac{k_\perp^2}{2z(1 - z)pp_k} \,, \qquad \tilde{z}_i = 1 - \tilde{z}_j \rightarrow z \,,$$
$$\tilde{p}_k^\mu \rightarrow p_k^\mu \quad \text{and} \quad \tilde{p}_{ij}^\mu \rightarrow p^\mu \,. \tag{1.10}$$

It can then be shown that in this limit the matrices $\mathbf{V}_{ij,k}$ become proportional to the Altarelli-Parisi splitting kernels,

$$\mathbf{V}_{ij,k} \rightarrow 8\pi\mu^{2\epsilon} \alpha_{\mathrm{s}} \hat{P}_{(ij),i}(z, k_\perp; \epsilon) \,. \tag{1.11}$$

In this limit the only remaining dependence of the dipole contributions $\mathcal{D}_{ij,k}$ on the spectator k resides in its colour factor $\mathbf{T}_k$ and it can be shown that eq. (1.2) reproduces the well-known universal collinear behaviour of the $(m + 1)$-parton matrix element,

$$_{m+1}\langle 1, \, \ldots, \, i, \, \ldots, \, j, \, \ldots, \, m + 1 || 1, \, \ldots, \, i, \, \ldots, \, j, \, \ldots, \, m + 1 \rangle_{m+1}$$
$$\xrightarrow{k_\perp \rightarrow 0} \frac{4\pi\mu^{2\epsilon}\alpha_{\mathrm{s}}}{p_i p_j} {}_m\langle 1, \, \ldots, \, ij, \, \ldots, \, m+1 | \hat{P}_{(ij),i}(z, k_\perp; \epsilon) | 1, \, \ldots, \, ij, \, \ldots, \, m+1 \rangle_m \,, \tag{1.12}$$

where again, the kernel $\hat{P}$ is a d-dimensional Altarelli-Parisi splitting function.

In contrast, the limit where p_j becomes soft is given by $p_j^\mu = \lambda q^\mu$ with $\lambda \to 0$ and q^μ some, in principle arbitrary, four-vector. In this limit, the dipole variables become

$$y_{ij,k} \to 0\,, \qquad\qquad \tilde{z}_i = 1 - \tilde{z}_j \to 1\,,$$
$$\tilde{p}_k^\mu \to p_k^\mu \qquad\qquad \text{and} \qquad\qquad \tilde{p}_{ij}^\mu \to p_i^\mu\,, \tag{1.13}$$

and $\mathbf{V}_{ij,k}$ tends to

$$\frac{1}{1 - \tilde{z}_i(1 - y_{ij,k})} \xrightarrow{\lambda \to 0} \frac{1}{\lambda} \cdot \frac{p_i p_k}{(p_i + p_k)q}\,. \tag{1.14}$$

Therefore,

$$\lambda \mathbf{V}_{ij,k} \xrightarrow{\lambda \to 0} 16\pi\mu^{2\epsilon}\alpha_s \mathbf{T}_{ij}^2 \frac{p_i p_k}{(p_i + p_k)q}\,. \tag{1.15}$$

It can thus be shown that the well-known soft limit of the $(m+1)$-parton matrix element is recovered, namely

$$_{m+1}\langle 1,\,\ldots,\,i,\,\ldots,\,j,\,\ldots,\,m+1 || 1,\,\ldots,\,i,\,\ldots,\,j,\,\ldots,\,m+1 \rangle_{m+1}$$
$$\xrightarrow{\lambda \to 0} -\sum_{i,k \neq i} \frac{8\pi\mu^{2\epsilon}\alpha_s}{\lambda^2(p_i q)}\,_m\langle 1,\,\ldots,\,ij,\,\ldots,\,m+1 | \frac{\mathbf{T}_k \cdot \mathbf{T}_i(p_i p_k)}{(p_i + p_k)q} | 1,\,\ldots,\,ij,\,\ldots,\,m+1 \rangle_m. \tag{1.16}$$

Taken together, these considerations and similar reasoning for the other dipole contributions translate into the dipole formula, eq. (1.1), to provide a point-wise approximation to the full $(m+1)$-parton matrix element, which exactly recovers all the soft and collinear divergences.

Before starting the discussion on the construction of a parton shower algorithm from the Catani-Seymour dipole formula in section 2 the generalisation of eq. (1.9) to the massive case and the analogous result for the splitting of an initial-state parton shall be briefly repeated.

First, re-consider the splitting $\widetilde{ij} \to i + j$ from above. This time, however, both the emitter and the splitting products are allowed to be massive, the corresponding mass shell conditions read $p^2 = m_{ij}^2$, $p_i^2 = m_i^2$ and $p_j^2 = m_j^2$. However, in order to avoid on-shell decays it is required that $m_{ij} \leq m_i + m_j$. The momenta p_i and p_j can then again be written in a Sudakov parametrisation according to

$$p_i^\mu = zp^\mu + \frac{-k_\perp^2 - z^2 m_{ij}^2 + m_i^2}{z} \frac{n^\mu}{2pn} + k_\perp^\mu\,, \tag{1.17}$$

$$p_j^\mu = (1-z)p^\mu + \frac{-k_\perp^2 - (1-z)^2 m_{ij}^2 + m_j^2}{1-z} \frac{n^\mu}{2pn} - k_\perp^\mu\,, \tag{1.18}$$

with $n^2 = 0$ and $k_\perp$ perpendicular to both p and n. Identifying $k_\perp^2 = -\mathbf{k}_\perp^2$ the invariant mass of partons i and j is now given by

$$(p_i + p_j)^2 = \frac{\mathbf{k}_\perp^2}{z(1-z)} + \frac{m_i^2}{z} + \frac{m_j^2}{1-z}\,, \quad \mathbf{k}_\perp^2 \to 0\,. \tag{1.19}$$

Accordingly, the collinear singularity is shielded when at least one of the two partons has a finite mass.

Finally, consider the case when final-state parton i becomes collinear to an initial-state parton a. This corresponds to the splitting $a \to \widetilde{ai} + i$, with $\widetilde{ai}$ the initial-state parton that enters the m-parton process. Considering only massless initial states, all the partons involved in the splitting are consistently taken to be massless. Decomposing the final-state momentum p_i according to

$$p_i^\mu = (1-x)p_a^\mu + \frac{-k_\perp^2}{1-x}\frac{n^\mu}{2p_a n} + k_\perp \,, \tag{1.20}$$

the collinear limit is reached for

$$p_a p_i = \frac{\mathbf{k}_\perp^2}{2(1-x)}\,, \quad \mathbf{k}_\perp^2 \to 0\,, \tag{1.21}$$

with $\mathbf{k}_\perp^2$ the magnitude of the spacelike transverse momentum vector $k_\perp$, namely $k_\perp^2 = -\mathbf{k}_\perp^2$. The definitions eq. (1.19) and eq. (1.21) constitute the basic relations for identifying the transverse momentum vector for the different splitting types in terms of the respective splitting variables used to describe the branchings, see section 3.

2. Construction of the algorithm

To formulate a parton shower algorithm based on the Catani-Seymour dipole formulae, the corresponding splitting operators $\mathcal{D}$ that describe the emission of an additional parton from an arbitrary m-parton state have to be analyzed and rewritten in a suitable form, before they can be used for a showering algorithm. To this end, a number of issues has to be resolved:

- First of all, only the four-dimensional expressions of the splitting kernels $\mathcal{D}$ will enter the parton shower. In addition, spin correlations are neglected by employing the spin-averaged form of the splitting kernels only. This manipulation is straightforward and a detailed discussion is therefore not necessary. The resulting splitting kernels depend on the actual configuration of emitters and spectators in the initial- and final state and they will be listed in the corresponding parts of section 3.

- In order to keep the probabilistic notion enabling simulation, to use a Markovian formulation for the showering process and to facilitate the hadronisation at the end of the shower, issues concerning colour correlations have to be solved. While the original Catani-Seymour dipole formulae consider all colour correlations, the shower will account only for the leading terms in $1/N_c$. This will be further discussed in section 2.1.

- Also, the phase space factorisation and the corresponding combination procedure is effectively inverted to construct the kinematics of the individual splittings. This yields splitting kernels for $1 \to 2$ QCD branchings that allow for the inclusion of finite

parton masses in quite a general way. Each splitting parton thereby is accompanied by a single colour-connected spectator parton compensating the recoil of the splitting. The only exception here are initial-state splittings in the presence of an initial-state spectator, where the recoil is taken by all final-state partons of the event. The introduction of the spectator allows to assemble the shower kinematics such that four-momentum conservation can be ensured after each individual branching with all external partons on their mass-shell. Accordingly, this parton shower algorithm can be stopped at any intermediate stage as well as started again for a partially evolved parton ensemble. However, the exact procedure for reconstructing the kinematics of each splitting again depends on whether the emitter and spectator are in the initial- or final state, respectively. The corresponding formulae are listed in section 3.

- The actual shower evolution variable specifying and ordering subsequent emissions is chosen to be the transverse momentum between the splitting products for branching final-state partons and the transverse momentum with respect to the beam for emissions from the initial state, collectively denoted by $\mathbf{k}_\perp$. The physics underlying this choice will be further detailed in section 2.2.

- Furthermore, choices have to be made concerning the scales entering the QCD running coupling constant, α_s, and the parton distribution functions when initial-state partons are present. This will be discussed in section 2.3.

- Based on these considerations, appropriate Sudakov form factors are constructed that determine the probability for a certain branching process not to occur for a given range of the evolution variable, $\mathbf{k}_\perp$. These Sudakov form factors constitute the basis of the actual Monte Carlo showering algorithm. Again, their specific form depends on the details of emitter and spectator parton and they will thus be given in corresponding parts of section 3, too.

- This section closes with some general considerations concerning the treatment of parton masses, cf. section 2.4.

2.1 Colour factors and spectators

The starting point for every parton shower evolution is a given set of partons and their momenta from a fixed-order matrix element calculation. In the large-N_c approximation a colour flow can be assigned to each parton configuration. Since in most cases the initial matrix element calculation is already summed and averaged over the colours of final and initial partons, the assignment typically is performed a posteriori in different ways in different codes. However, as a result the partons entering the parton shower after this assignment have a well-defined colour, and, due to the large-N_c limit, one or two uniquely assigned colour partners.[4] Motivated by considerations on the colour dynamics for soft emissions in

---

[4]Representing the colour flow pictorially by coloured strings of partons, two configurations emerge, namely open or closed strings. An open string consists of a colour-triplet state followed by colour octets and ends with a colour anti-triplet. Mapping the colour flows, initial-state quarks (colour triplets) correspond to

the Catani-Seymour formalism, in a corresponding shower formulation the spectator parton accompanying a given splitting is colour-connected to the emitter parton. For the case of a splitting gluon/gluino then there are always two possible colour partners, whereas splitting (anti-)quarks/squarks will have only one spectator parton candidate. Following this reasoning, the initial partons will enter the parton shower stage in well-defined pairs of potential emitters and spectators. The subsequent parton shower will not change this feature.

To formalise the treatment of colour inside the parton shower presented here, consider the colour-operators present in the Catani-Seymour dipole contributions. In the large-N_c limit, they are easily calculated for any m-parton state at the price of losing colour correlations beyond $1/N_c$. However, in this limit only two cases need to be considered. Independent of the actual spectator flavour, the colour algebra for a splitting (anti-)quark/squark yields,

$$-\frac{\mathbf{T}_k \cdot \mathbf{T}_{ij}}{\mathbf{T}_{ij}^2} \to 1 + \mathcal{O}\left(\frac{1}{N_c^2}\right) , \tag{2.1}$$

whereas a splitting gluon/gluino results in

$$-\frac{\mathbf{T}_k \cdot \mathbf{T}_{ij}}{\mathbf{T}_{ij}^2} \to \frac{1}{2} + \mathcal{O}\left(\frac{1}{N_c^2}\right) . \tag{2.2}$$

For convenience, these two results can be combined by introducing $\mathcal{N}_{ij}^{\mathrm{spec}}$, the number of possible spectators the emitting parton possesses, then

$$-\frac{\mathbf{T}_k \cdot \mathbf{T}_{ij}}{\mathbf{T}_{ij}^2} \to \frac{1}{\mathcal{N}_{ij}^{\mathrm{spec}}} + \mathcal{O}\left(\frac{1}{N_c^2}\right) . \tag{2.3}$$

2.2 Ordering parameter

Having the individual splitting process under control, i.e. having at hand the corresponding splitting kernel with all relevant colour factors and the way the kinematics of the emission is constructed, the full showering algorithm with its sequence of splittings can be addressed. While the individual splitting kernel properly takes into account the soft and collinear divergent regions, in the parton shower itself these regions are cut away and, formally speaking, combined with the virtual bits to yield a probabilistic description of the splitting process. The cut on the soft and collinear region implies the emergence of corresponding logarithms of the cut parameter, which the parton shower aims to resum. Technically, this resummation is achieved by arranging the individual emissions in a Markov chain, treating each emission on the same footing, and by ordering the emissions with some ordering parameter. This has been detailed in textbooks such as [46]. In different parton shower implementations, there are different ordering parameters realised, such as the invariant mass of the splitting particle [47]–[49], the opening angle of the pair [28, 50], or their

---

final-state anti-quarks (colour anti-triplets), whereas initial-state anti-triplets can be treated as final-state triplets. A closed colour string corresponds to a configuration of colour-octet partons only. Accordingly, the end of a closed string is colour-connected to its beginning and therefore the whole colour string is invariant under cyclic permutations of its individual constituents.

relative transverse momentum [19, 29]. At the level of doubly leading logarithms, these choices are all equivalent, but there are substantial differences on the level of next-to leading logarithms, i.e. on the level of single soft logarithms. This is closely tied with the treatment of quantum coherence effects [51]–[54], which are properly taken into account by ordering subsequent emissions through their respective opening angles [50]. In [55] it has been shown that another way of properly accounting for coherence effects is evolving in a dipole-like picture with subsequent emissions ordered by transverse momenta.

In the implementation presented here, the parton shower will be ordered by transverse momenta, i.e. by the $\mathbf{k}_\perp$ in eqs. (1.19) and (1.21). Apart from the proper treatment of quantum coherence effects, this choice has additional benefits: First of all, as will be discussed in the next section, cf. section 2.3, by ordering with $\mathbf{k}_\perp$ the ordering parameter also enters as the relevant scale in the coupling constant and the parton distribution functions. Second, the definition used here allows for a shower formulation on the basis of Lorentz-invariant quantities, see for instance e.g. eqs. (1.4) and (1.5). Also, ordering by $\mathbf{k}_\perp$ immediately implies that the parton shower cut-off is related to some minimal transverse momentum necessary to resolve partons, which seems quite appealing in terms of the physical interpretation of such a resolution criterion. Last but not least an ordering by transverse momenta appears to allow for quite a straightforward merging of the parton shower with multi-leg tree-level matrix elements in the spirit of [11, 12]. The merging method presented there is based on Sudakov suppression weights for matrix elements, which are constructed from the transverse momenta of their nodes, and on a vetoed parton shower respecting the minimal scale of a $k_\perp$-jet definition.

In the parton shower evolution each colour-singlet is separately evolved. To this end, all emitter-spectator dipoles are iterated over and for each of those configurations a $\mathbf{k}_\perp$ is chosen according to the corresponding Sudakov form factor. The dipole with the largest $\mathbf{k}_\perp$ is selected to split according to the kinematics detailed below. As long as this largest $\mathbf{k}_\perp$-value is larger than the infrared cut-off $\mathbf{k}_{\perp,0}$, the shower evolution will continue, and this largest $\mathbf{k}_\perp$ of the current evolution step serves as the maximal scale for all dipoles in the colour-singlet in the next splitting step.

2.3 Scales to be chosen

When discussing the details of a parton shower implementation, some care has to be taken in the choice of various, in principle undetermined, occurring scales. There are a number of choices to be made, namely:

- The evolution variable and the related evolution cut-off:
  As already discussed in the previous section, in this implementation the relative transverse momentum of the produced parton w.r.t. its emitter has been chosen as the relevant evolution variable. It is given by eqs. (1.19) and (1.21). Correspondingly, a cut-off has to be set as a tuning parameter, to stay away from phase-space regions where the perturbative expansion for the running coupling is divergent. The choice of this cut-off is dictated by two aspects. First of all, it seems to be more attractive to try to assign as much phase space for particle creation to the, in princi-

ple, well-understood perturbative parton shower rather than to a phenomenological hadronisation approach such as the Lund string fragmentation [56, 57] or a cluster model [58]–[60]. This implies that the cut-off should be as small as possible. On the other hand, it is clear that perturbative QCD breaks down and loses its predictive power at small scales. This is best exemplified by the infrared behaviour of the running coupling which exhibits a Landau pole at Λ_{QCD}. As will be discussed in the next item, since the running coupling in the shower is evaluated at a scale related to $\mathbf{k}_\perp$, this feature of QCD prohibits cut-offs in the region of Λ_{QCD}. Therefore, a suitable choice seems to be a cut-off $\mathbf{k}_{\perp,0}$ of the order of $1\,\mathrm{GeV}$, sufficiently separated from the Landau pole.

- The argument of the running coupling constant, μ_R:
  In the previous item it has been already hinted at the choice typically made in parton showers, to take the running coupling at scales of the order of $\mathbf{k}_\perp$. The reason for this choice is that it incorporates and resums some of the higher-order corrections to the splitting. Specifically, in this implementation the choice is to take $\mu_R^{\mathrm{F.S.}} = \mu_R = \mathbf{k}_\perp$ if the emitter is a final-state particle and $\mu_R^{\mathrm{I.S.}} = \mu_R = \mathbf{k}_\perp/2$ if the emitter is a parton in the initial state.[5]

- The argument of the parton density functions, μ_F:
  Similar to the case of the running coupling constant, a choice has also been made at which scale to take the parton distribution functions, if necessary. In parton showers, there are typically two answers, namely to either again take the transverse momentum or to use the virtual mass of the initial emitter. Here the choice again is to use $\mu_F = \mathbf{k}_\perp$.

2.4 General considerations on massive particles

Taking into account finite quark mass effects in the Standard Model (SM) clearly is of importance when producing heavy quarks, bottom or top quarks, in a hard scattering process. In addition, many extensions of the SM introduce new strongly-interacting heavy particles, whose QCD radiation needs to be modeled to understand the patterns of particle and energy flows in their production and eventual decays. Prime examples are scalar quarks and gluinos in supersymmetric theories [61] or heavy excitations of the SM quark and gluon fields in models with additional space-time dimensions [62]. While at lepton colliders heavy objects only appear in the process' final state, at hadron colliders charm and bottom quarks can also constitute the partonic initial state. An example where these are of phenomenological relevance is the associated production of heavy quarks and scalar Higgs particles in supersymmetric models, which is a promising channel to gain deeper insight into the mechanism of electroweak symmetry breaking, see for instance [63] and references therein.

In the following section, QCD splitting operators will be derived, that fully take into account finite masses of partons in the final state. This includes both emission from heavy

---

[5]The latter choice of an additional factor of $1/2$ is motivated by the improved performance in the description of the transverse momentum of the lepton pair in Drell-Yan processes.

particles but also the splitting of gluons into heavy quarks such as charm or bottom. Splittings of gluons into heavier objects or branchings of heavy states into other heavy objects are beyond the scope of this work as they are not well modeled by the soft or quasi-collinear approximation and should rather be described with full matrix elements. For all the formulae presented in section 3, the massless limit is smoothly obtained when setting the parton masses to zero. This will be explicitly examined for some of the important results there.

Throughout this work, incoming QCD partons will always be treated as massless. The leading logarithms that arise for emissions off incoming heavy quarks, logarithms of the type $(\alpha_s \log(Q^2/m_Q^2))^n$, with Q^2 the scale of the hard-scattering process and m_Q the quark mass, are summed to all orders in QCD when using heavy-quark parton distribution functions at the factorisation scale $\mu_F \sim Q$ and considering the incoming quarks as massless [64, 65]. A scheme to consistently incorporate explicit masses for incoming heavy quarks, relying on modified heavy-quark density functions [66], has recently been presented in [67].

3. Kinematics of the individual splittings

In the following sections, sections 3.1–3.4, the actual parton shower built on Catani-Seymour subtraction terms is constructed. To this end, all combinations of initial- and final-state emitter and spectator partons are considered in detail, following closely the original publications on the subtraction method [30, 31]. First, the kinematic variables characterising the individual splitting under consideration are discussed. Then the explicit form of the phase space element for the three-parton state under consideration is re-expressed through the kinematic variables above, and their respective bounds are given. In a next step, the polarisation-averaged splitting kernels for the respective emitter-spectator configuration are listed. This allows to give the factorised form of matrix elements with one additional parton in the soft and collinear limits of its production and the factorised form of the corresponding differential cross section, which includes both matrix element and phase space factorisation. From there, it is quite straightforward to deduce the actual Sudakov form factor for the emitter-spectator configuration.[6] Finally, the actual kinematics of the splitting is constructed, which may slightly differ from the evolution parameters due to mass effects. For each case then also the more familiar massless limit is briefly discussed. In section 3.5 the QCD splitting functions for supersymmetric particles are presented.

3.1 Final-state emitter and final-state spectator

The first case to be investigated is when both the emitter and the spectator parton are in the final state, cf. figure 1. Accordingly, the splitting $\{\widetilde{ij}, \tilde{k}\} \rightarrow \{i, j, k\}$ has to be studied. When considering processes without colour-charged initial-state particles, such as

---

[6]Note that some of the Catani-Seymour dipole functions may assume negative values in certain, non-singular regions of phase space. This would spoil their probabilistic interpretation as splitting operators in a parton cascade. Accordingly, for these phase-space regions the splitting probabilities are set to zero. It has been tested that this happens typically with in a tiny, negligible fraction of events only. In any case, once this parton shower is merged with the matrix elements it is anticipated that these events do not occur any longer.
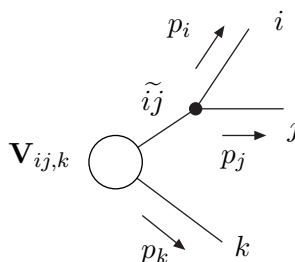
Figure 1: Effective diagram for the splitting of a final-state parton connected to a final-state spectator. The blob denotes the m-parton matrix element, and the outgoing lines label the final-state partons participating in the splitting.

jet production in lepton-lepton collisions, this is the only QCD radiation process and thus constitutes the basis of a corresponding final-state parton shower. However, the observed factorisation of the differential cross section for producing an additional parton also holds in the presence of initial-state partons, where only the additional branching channels discussed below then have to be taken into account as well.

3.1.1 Massive case

In the most general case all partons involved in the splitting can have arbitrary masses, i.e. $\tilde{p}_{ij}^2 = m_{ij}^2$, $\tilde{p}_k^2 = p_k^2 = m_k^2$, $p_i^2 = m_i^2$ and $p_j^2 = m_j^2$, respectively. In order to avoid on-shell decays, which should be described by their respective proper matrix element, only those situations are considered, where $m_{ij} \leq m_i + m_j$.

- Kinematics.
  Exact four-momentum conservation is ensured by the requirement

$$\tilde{p}_{ij} + \tilde{p}_k = p_i + p_j + p_k \equiv Q. \tag{3.1}$$

The splitting is characterised by the dimensionless variables $y_{ij,k}$, $\tilde{z}_i$ and $\tilde{z}_j$. They are given by

$$y_{ij,k} = \frac{p_i p_j}{p_i p_j + p_i p_k + p_j p_k}, \quad \tilde{z}_i = 1 - \tilde{z}_j = \frac{p_i p_k}{p_i p_k + p_j p_k}. \tag{3.2}$$

With these definitions the invariant transverse momentum of partons i and j, defined in eq. (1.19), can be written as

$$\mathbf{k}_\perp^2 = \left(Q^2 - m_i^2 - m_j^2 - m_k^2\right) y_{ij,k}\, \tilde{z}_i(1 - \tilde{z}_i) - (1 - \tilde{z}_i)^2 m_i^2 - \tilde{z}_i^2 m_j^2. \tag{3.3}$$

For convenience, the rescaled parton masses

$$\mu_n = \frac{m_n}{\sqrt{Q^2}} \quad (n = i, j, k, ij), \tag{3.4}$$

and the relative velocities between $p_i + p_j$ and p_i (p_k), $v_{ij,i}$ ($v_{ij,k}$),

$$v_{ij,i} = \frac{\sqrt{(1 - \mu_i^2 - \mu_j^2 - \mu_k^2)^2 y_{ij,k}^2 - 4\mu_i^2 \mu_j^2}}{(1 - \mu_i^2 - \mu_j^2 - \mu_k^2)y_{ij,k} + 2\mu_i^2} , \tag{3.5}$$

$$v_{ij,k} = \frac{\sqrt{\left[2\mu_k^2 + (1 - \mu_i^2 - \mu_j^2 - \mu_k^2)(1 - y_{ij,k})\right]^2 - 4\mu_k^2}}{(1 - \mu_i^2 - \mu_j^2 - \mu_k^2)(1 - y_{ij,k})} , \tag{3.6}$$

as well as the velocity between $\tilde{p}_{ij}$ and $\tilde{p}_k$,

$$\tilde{v}_{ij,k} = \frac{\sqrt{\lambda\left(1, \mu_{ij}^2, \mu_k^2\right)}}{1 - \mu_{ij}^2 - \mu_k^2} , \tag{3.7}$$

are introduced.

- Phase space.

  In the case of a final-state emitter with a final-state spectator, the corresponding three-parton phase space $d\Phi(p_i, p_j, p_k; Q)$ must be analyzed. It exactly factorises into a two-parton contribution $d\Phi(\tilde{p}_{ij}, \tilde{p}_k; Q)$ and a single-parton phase space factor $[dp_i(\tilde{p}_{ij}, \tilde{p}_k)]$,

  $$d\Phi(p_i, p_j, p_k; Q) = d\Phi(\tilde{p}_{ij}, \tilde{p}_k; Q) \, [dp_i(\tilde{p}_{ij}, \tilde{p}_k)] \, \Theta(1 - \mu_i - \mu_j - \mu_k) , \tag{3.8}$$

  where the latter is given by

  $$[dp_i(\tilde{p}_{ij}, \tilde{p}_k)] = \frac{(\tilde{p}_{ij} + \tilde{p}_k)^2}{16\pi^2} \frac{\left(1 - \mu_i^2 - \mu_j^2 - \mu_k^2\right)^2}{\sqrt{\lambda(1, \mu_{ij}^2, \mu_k^2)}} (1 - y_{ij,k}) \, dy_{ij,k} \, d\tilde{z}_i \frac{d\phi}{2\pi} . \tag{3.9}$$

  Here and in the following, λ denotes the Källen function,

  $$\lambda(x, y, z) = x^2 + y^2 + z^2 - 2(xy + xz + yz) . \tag{3.10}$$

  The boundaries of the full, unconstrained, phase space read $\phi \in [0, 2\pi]$, whereas the lower and upper limits for $\tilde{z}_i$ and $y_{ij,k}$ are

  $$z_{\mp} = \frac{2\mu_i^2 + (1 - \mu_i^2 - \mu_j^2 - \mu_k^2)y_{ij,k}}{2(\mu_i^2 + \mu_j^2 + (1 - \mu_i^2 - \mu_j^2 - \mu_k^2)y_{ij,k})}(1 \mp v_{ij,i}v_{ij,k}) , \tag{3.11}$$

  $$y_- = \frac{2\mu_i\mu_j}{1 - \mu_i^2 - \mu_j^2 - \mu_k^2} , \quad \text{and} \quad y_+ = 1 - \frac{2\mu_k(1 - \mu_k)}{1 - \mu_i^2 - \mu_j^2 - \mu_k^2} , \tag{3.12}$$

  respectively.

- Splitting kernels.

  The polarisation-averaged QCD splitting kernels $\langle \mathbf{V}_{ij,k} \rangle$ read

  $$\langle \mathbf{V}_{Q_i g_j, k}(\tilde{z}_i, y_{ij,k}) \rangle = C_F \left\{ \frac{2}{1 - \tilde{z}_i + \tilde{z}_i y_{ij,k}} - \frac{\tilde{v}_{ij,k}}{v_{ij,k}} \left(1 + \tilde{z}_i + \frac{m_i^2}{p_i p_j} \right) \right\}, \quad (3.13)$$

  $$\langle \mathbf{V}_{g_i g_j, k}(\tilde{z}_i, y_{ij,k}) \rangle = 2C_A \left\{ \frac{1}{1 - \tilde{z}_i + \tilde{z}_i y_{ij,k}} + \frac{1}{\tilde{z}_i + y_{ij,k} - \tilde{z}_i y_{ij,k}} \right.$$
  $$\left. + \frac{\tilde{z}_i (1 - \tilde{z}_i) - z_+ z_- - 2}{v_{ij,k}} \right\}, \quad (3.14)$$

  $$\langle \mathbf{V}_{Q_i Q_j, k}(\tilde{z}_i) \rangle = T_R \frac{1}{v_{ij,k}} \left\{ 1 - 2 \left[\tilde{z}_i (1 - \tilde{z}_i) - z_+ z_- \right] \right\}. \quad (3.15)$$

  Here, eq. (3.13) describes the QCD splitting $Q \to Qg$, of a massive quark Q, the case of a splitting anti-quark is formally identical. The corresponding expressions for the splitting $g \to gg$, or $g \to Q\bar{Q}$ are given in eqs. (3.14) and (3.15), respectively. Note that in the above splitting kernels the free parameter κ that occurs in the full NLO subtraction scheme [31] has been set to zero to obtain the simplest expressions for the different $\langle \mathbf{V}_{ij,k} \rangle$.

  It should be stressed here that the scalar product $p_i p_j$ present in eq. (3.13) can be written solely in terms of the splitting variables and the scale $\mathbf{k}_\perp^2$:

  $$p_i p_j = \frac{\mathbf{k}_\perp^2}{2\tilde{z}_i (1 - \tilde{z}_i)} + \frac{(1 - \tilde{z}_i) m_i^2}{2\tilde{z}_i} + \frac{\tilde{z}_i m_j^2}{2(1 - \tilde{z}_i)}. \quad (3.16)$$

  However, in eq. (3.13) the final-state gluon is massless and correspondingly $m_j^2 = 0$ such that the last term of eq. (3.16) vanishes in this specific case.

- Matrix element.

  Using the above splitting functions, the full $(m+1)$-parton matrix element factorises in the soft and collinear limit according to

  $$|\mathcal{M}_{m+1}|^2 = |\mathcal{M}_m|^2 \sum_{ij} \sum_{k \neq ij} \frac{1}{(p_i + p_j)^2 - m_{ij}^2} \frac{1}{\mathcal{N}_{ij}^{\mathrm{spec}}} 8\pi\alpha_s \langle \mathbf{V}_{ij,k}(\tilde{z}_i, y_{ij,k}) \rangle, \quad (3.17)$$

  cf. [30], where the sum covers all the possible emitter-spectator pairs. When combining this with the $(m+1)$-parton phase space a fully factorised expression for the differential cross section is obtained, namely

  $$d\hat{\sigma}_{m+1} = d\hat{\sigma}_m \sum_{ij} \sum_{k \neq ij} \frac{dy_{ij,k}}{y_{ij,k}} d\tilde{z}_i \frac{d\phi}{2\pi} \frac{\alpha_s}{2\pi} \frac{1}{\mathcal{N}_{ij}^{\mathrm{spec}}} J(y_{ij,k}) \langle \mathbf{V}_{ij,k}(\tilde{z}_i, y_{ij,k}) \rangle, \quad (3.18)$$

  where the Jacobian

  $$J(y_{ij,k}) = \frac{1 - \mu_i^2 - \mu_j^2 - \mu_k^2}{\sqrt{\lambda(1, \mu_{ij}^2, \mu_k^2)}} \frac{1 - y_{ij,k}}{1 + \frac{\mu_i^2 + \mu_j^2 - \mu_{ij}^2}{y_{ij,k}(1 - \mu_i^2 - \mu_j^2 - \mu_k^2)}} \quad (3.19)$$

  emerges from the phase-space factors of eq. (3.9) combined with the propagator term of eq. (3.17).

- Sudakov form factor.

A first step toward the construction of the corresponding Sudakov form factor is achieved by realising that the $y_{ij,k}$-integration in the equation above, eq. (3.18), can be replaced by an integration over the ordering parameter, the transverse momentum, according to

$$\frac{\mathrm{d}y_{ij,k}}{y_{ij,k}} = \frac{\mathrm{d}\mathbf{k}_\perp^2}{\mathbf{k}_\perp^2}\,. \tag{3.20}$$

Cutting the available phase space through the requirement of a minimal relative transverse momentum squared $\mathbf{k}_\perp^2 > \mathbf{k}_{\perp,0}^2 > 0$ and some upper limit $\mathbf{k}_{\perp,\max}^2$ for the splitting products i and j, the $\tilde{z}_i$ integration boundaries become

$$z_-\left(\mathbf{k}_{\perp,\max}^2, \mathbf{k}_{\perp,0}^2\right) = \mathrm{Max}\left(\frac{1}{2}\left(1 - \sqrt{1 - \frac{\mathbf{k}_{\perp,0}^2}{\mathbf{k}_{\perp,\max}^2}}\right),\, z_-\right),\, \tag{3.21}$$

$$z_+\left(\mathbf{k}_{\perp,\max}^2, \mathbf{k}_{\perp,0}^2\right) = \mathrm{Min}\left(\frac{1}{2}\left(1 + \sqrt{1 - \frac{\mathbf{k}_{\perp,0}^2}{\mathbf{k}_{\perp,\max}^2}}\right),\, z_+\right),\, \tag{3.22}$$

with $z_\mp$ taken from eq. (3.11). Having chosen a valid pair for $\mathbf{k}_\perp^2$ and $\tilde{z}_i$ this can then easily be solved for $y_{ij,k}$,

$$y_{ij,k} = \frac{1}{Q^2 - m_i^2 - m_j^2 - m_k^2}\left(\frac{\mathbf{k}_\perp^2}{\tilde{z}_i(1-\tilde{z}_i)} + \frac{(1-\tilde{z}_i)m_i^2}{\tilde{z}_i} + \frac{\tilde{z}_i m_j^2}{1-\tilde{z}_i}\right)\,. \tag{3.23}$$

If the calculated $y_{ij,k}$ fulfils the requirement $y_{ij,k} \in [y_-, y_+]$, with $y_\mp$ defined in eq. (3.12), a valid splitting has been constructed, i.e. a physical branching allowed by phase space.

The Sudakov form factor corresponding to having no emission from one of the process' final-final dipoles between the maximum transverse momentum squared $\mathbf{k}_{\perp,\max}^2$ and the infrared cut-off $\mathbf{k}_{\perp,0}^2$ reads

$$\Delta_{\mathrm{FF}}\left(\mathbf{k}_{\perp,\max}^2, \mathbf{k}_{\perp,0}^2\right) \tag{3.24}$$

$$= \exp\left(-\sum_{ij}\sum_{k\neq ij}\frac{1}{\mathcal{N}_{ij}^{\mathrm{spec}}}\int\limits_{\mathbf{k}_{\perp,0}^2}^{\mathbf{k}_{\perp,\max}^2}\frac{\mathrm{d}\mathbf{k}_\perp^2}{\mathbf{k}_\perp^2}\int\limits_{z_-}^{z_+}\mathrm{d}\tilde{z}_i\,\frac{\alpha_\mathrm{s}(\mathbf{k}_\perp^2)}{2\pi}\,J(y_{ij,k})\langle\mathbf{V}_{ij,k}(\tilde{z}_i, y_{ij,k})\rangle\right)\,.$$

As already advertised in section 2.3, the scale of the running coupling has thereby been chosen equal to the current transverse momentum squared.

- Physical kinematics.

Having a valid set of splitting variables, the actual physical branching kinematics must be constructed in order to fully specify the splitting $\{\widetilde{ij}, \tilde{k}\} \to \{i, j, k\}$. In the most general case, both the emitter and the spectator parton are massive, prohibiting

a simple Sudakov parametrisation of p_i and p_j in terms of light-like momenta $\tilde{p}_{ij}$ and $\tilde{p}_k$. Instead they are expressed in light-cone kinematics with massive base momenta. The new spectator momentum is determined in the emitter-spectator centre-of-mass frame,

$$p_k = \frac{\sqrt{\left[2\mu_k^2 + (1 - \mu_i^2 - \mu_j^2 - \mu_k^2)(1 - y_{ij,k})\right]^2 - 4\mu_k^2}}{\sqrt{\lambda(1, \mu_{ij}^2, \mu_k^2)}} \left(\tilde{p}_k - \frac{1}{2}\left[1 + \mu_k^2 - \mu_{ij}^2\right] Q\right)$$
$$+ \left[\frac{1}{2}(1 - \mu_i^2 - \mu_j^2 - \mu_k^2)(1 - y_{ij,k}) + \mu_k^2\right] Q \,. \tag{3.25}$$

Then the situation is most easily discussed in a frame where $Q - p_k$ is at rest and the momentum p_k points along the z-direction. In this frame, the light-cone momenta of $Q - p_k$ and p_k can be written as

$$Q - p_k = \left(M, M, \vec{0}\right) \quad \text{and} \quad p_k = \left(m_k\, e^x, m_k\, e^{-x}, \vec{0}\right) \,. \tag{3.26}$$

The ansatz for the light-cone momenta of the new emerging final-state partons reads

$$p_i = \left(m_{i,\perp}\, e^y, m_{i,\perp}\, e^{-y}, \vec{l}_\perp\right) \,, \quad p_j = \left(m_{j,\perp}\, e^z, m_{j,\perp}\, e^{-z}, -\vec{l}_\perp\right) \,, \tag{3.27}$$

with $m_\perp$ being the transverse mass of the respective parton, defined according to

$$m_\perp = \sqrt{m^2 + \vec{l}_\perp^2} \,. \tag{3.28}$$

The kinematics is fully determined through energy-momentum conservation and the constraint

$$\tilde{z}_i = 1 - \tilde{z}_j = \frac{p_i p_k}{p_i p_k + p_j p_k} \,. \tag{3.29}$$

Then,

$$\vec{l}_\perp^2 = \left(\frac{M^2 + m_i^2 + m_j^2}{2M}\right)^2 - m_i^2 - \left(\frac{M^2 + m_i^2 + m_j^2 - 2M^2 \tilde{z}_i}{2M} \left(\frac{\cosh x}{\sinh x}\right)\right)^2 \tag{3.30}$$

and

$$\cosh y = \frac{M^2 + m_i^2 - m_j^2}{2M m_{i,\perp}} \,, \quad \sinh y = \frac{\cosh x}{\sinh x}\left(\cosh y - \frac{M \tilde{z}_i}{m_{i,\perp}}\right) \,, \tag{3.31}$$

$$\cosh z = \frac{M^2 - m_i^2 + m_j^2}{2M m_{j,\perp}} \,, \quad \sinh z = \frac{\cosh x}{\sinh x}\left(\cosh z - \frac{M(1 - \tilde{z}_i)}{m_{j,\perp}}\right) \,. \tag{3.32}$$

Expressed through ordinary four-vectors the parton momenta in this frame read

$$p_i = (m_{i,\perp} \cosh y, l_\perp \cos\phi, l_\perp \sin\phi, m_{i,\perp} \sinh y) \,, \tag{3.33}$$
$$p_j = (m_{j,\perp} \cosh z, -l_\perp \cos\phi, -l_\perp \sin\phi, m_{j,\perp} \sinh z) \,, \tag{3.34}$$

with the angle ϕ not fixed by the splitting and therefore uniformly distributed in the transverse plane. The kinematics is completed by rotating and boosting back the momenta p_i, p_j and p_k into the laboratory frame.

If the spectator is massless, the new final-state momenta can alternatively be given in a simple Sudakov parametrisation:

$$p_i = \tilde{z}_i\,\tilde{p}_{ij} + \frac{\mathbf{k}_\perp^2 - \tilde{z}_i^2 m_{ij}^2 + m_i^2}{\tilde{z}_i\,2\tilde{p}_{ij}\tilde{p}_k}\,\tilde{p}_k + k_\perp\,, \tag{3.35}$$

$$p_j = (1 - \tilde{z}_i)\,\tilde{p}_{ij} + \frac{\mathbf{k}_\perp^2 - (1-\tilde{z}_i)^2 m_{ij}^2 + m_j^2}{(1-\tilde{z}_i)\,2\tilde{p}_{ij}\tilde{p}_k}\,\tilde{p}_k - k_\perp\,, \tag{3.36}$$

$$p_k = \left(\frac{(1 - \mu_i^2 - \mu_j^2)(1 - y_{ij,k})}{1 - \mu_{ij}^2}\right)\tilde{p}_k\,. \tag{3.37}$$

with the spacelike transverse-momentum vector $k_\perp$ pointing in a direction perpendicular to both the emitter and the spectator momentum.

3.1.2 Massless case

The case of a final-final splitting is considerably simpler in the massless limit, i.e. where all occurring partons can be treated as massless, $\tilde{p}_{ij}^2 = \tilde{p}_k^2 = p_k^2 = p_i^2 = p_j^2 = 0$. In this case, of course, the variables chosen to specify the splitting remain unchanged with respect to the fully massive case. However, neglecting masses the ordering parameter reduces to

$$\mathbf{k}_\perp^2 = Q^2 y_{ij,k}\,\tilde{z}_i(1 - \tilde{z}_i) = 2\tilde{p}_{ij}\tilde{p}_k\,y_{ij,k}\,\tilde{z}_i\,(1 - \tilde{z}_i)\,, \tag{3.38}$$

with the identification of $Q^2 = 2\tilde{p}_{ij}\tilde{p}_k$ this is identical with the transverse momentum defined in eq. (1.9). The full phase space for the emission of an extra parton extends to $\tilde{z}_i \in [0,1]$, $y_{ij,k} \in [0,1]$, whereas ϕ again uniformly covers the interval $[0, 2\pi]$.

In the massless limit also the spin averaged splitting kernels $\langle \mathbf{V}_{ij,k} \rangle$ simplify considerably, namely to

$$\langle \mathbf{V}_{\mathrm{q}_i \mathrm{g}_j,k}(\tilde{z}_i, y_{ij,k}) \rangle = C_{\mathrm{F}} \left\{ \frac{2}{1 - \tilde{z}_i + \tilde{z}_i y_{ij,k}} - (1 + \tilde{z}_i) \right\}\,, \tag{3.39}$$

$$\langle \mathbf{V}_{\mathrm{g}_i \mathrm{g}_j,k}(\tilde{z}_i, y_{ij,k}) \rangle = 2C_{\mathrm{A}} \left\{ \frac{1}{1 - \tilde{z}_i + \tilde{z}_i y_{ij,k}} + \frac{1}{\tilde{z}_i + y_{ij,k} - \tilde{z}_i y_{ij,k}} - 2 + \tilde{z}_i\,(1 - \tilde{z}_i) \right\}\,, \tag{3.40}$$

$$\langle \mathbf{V}_{\mathrm{q}_i \mathrm{q}_j,k}(\tilde{z}_i) \rangle = T_{\mathrm{R}} \left\{ 1 - 2\tilde{z}_i\,(1 - \tilde{z}_i) \right\}\,. \tag{3.41}$$

When combining the factorised form of the $(m + 1)$-parton phase space,

$$\mathrm{d}\Phi_{m+1} = \mathrm{d}\Phi_m \sum_{ij} \sum_{k \neq ij} \frac{2p_i p_j}{16\pi^2} \frac{\mathrm{d}y_{ij,k}}{y_{ij,k}}\,d\tilde{z}_i \frac{d\phi}{2\pi}\,(1 - y_{ij,k})\,\Theta(\tilde{z}_i\,(1 - \tilde{z}_i))\,\Theta(y_{ij,k}(1 - y_{ij,k}))\,, \tag{3.42}$$

with the corresponding expression for the $(m + 1)$-parton matrix element,

$$|\mathcal{M}_{m+1}|^2 = |\mathcal{M}_m|^2 \sum_{ij} \sum_{k \neq ij} \frac{1}{2p_i p_j} \frac{1}{\mathcal{N}_{ij}^{\mathrm{spec}}}\,8\pi\alpha_{\mathrm{s}}\,\langle \mathbf{V}_{ij,k}(\tilde{z}_i, y_{ij,k}) \rangle\,, \tag{3.43}$$

the fully factorised form of the $(m+1)$-parton differential cross section is recovered

$$d\hat{\sigma}_{m+1} = d\hat{\sigma}_m \sum_{ij} \sum_{k \neq ij} \frac{dy_{ij,k}}{y_{ij,k}} d\tilde{z}_i \frac{d\phi}{2\pi} \frac{\alpha_s}{2\pi} \frac{1}{\mathcal{N}_{ij}^{spec}} J(y_{ij,k}) \langle \mathbf{V}_{ij,k}(\tilde{z}_i, y_{ij,k}) \rangle . \qquad (3.44)$$

However, in this case, the Jacobian $J(y_{ij,k})$ simply is given by

$$J(y_{ij,k}) = 1 - y_{ij,k} . \qquad (3.45)$$

With the transverse momentum defined according to eq. (3.38) again the identity

$$\frac{dy_{ij,k}}{y_{ij,k}} = \frac{d\mathbf{k}_\perp^2}{\mathbf{k}_\perp^2} , \qquad (3.46)$$

is found. Choosing $\mathbf{k}_\perp^2$ as the evolution variable with its lower cut-off given by $\mathbf{k}_{\perp,0}^2$ and the upper limit by $\mathbf{k}_{\perp,max}^2$ the $\tilde{z}_i$ integration range reduces to

$$z_\mp(\mathbf{k}_{\perp,max}^2, \mathbf{k}_{\perp,0}^2) = \frac{1}{2} \left(1 \mp \sqrt{1 - \frac{\mathbf{k}_{\perp,0}^2}{\mathbf{k}_{\perp,max}^2}} \right) . \qquad (3.47)$$

Given a valid set of $\mathbf{k}_\perp^2$ and $\tilde{z}_i$ this can be solved for

$$y_{ij,k} = \frac{\mathbf{k}_\perp^2}{Q^2 \tilde{z}_i (1 - \tilde{z}_i)} , \qquad (3.48)$$

completing the determination of the splitting variables. Making the necessary replacements when going from massive partons to massless the Sudakov form factor given in eq. (3.24) yields the corresponding non-branching probability. The massless kinematics can be derived from eqs. (3.35)–(3.37) by setting $\mu_{ij} = \mu_i = \mu_j = 0$, accordingly

$$p_i = \tilde{z}_i \tilde{p}_{ij} + \frac{\mathbf{k}_\perp^2}{\tilde{z}_i 2\tilde{p}_{ij}\tilde{p}_k} \tilde{p}_k + k_\perp , \qquad (3.49)$$

$$p_j = (1 - \tilde{z}_i) \tilde{p}_{ij} + \frac{\mathbf{k}_\perp^2}{(1 - \tilde{z}_i) 2\tilde{p}_{ij}\tilde{p}_k} \tilde{p}_k - k_\perp , \qquad (3.50)$$

$$p_k = (1 - y_{ij,k}) \tilde{p}_k . \qquad (3.51)$$

3.2 Final-state emitter and initial-state spectator

In this section, the case of a final-state emission with the spectator being an initial-state parton a is worked out. The splitting schematically reads $\{\widetilde{ij}, \tilde{a}\} \to \{i, j, a\}$, for a pictorial representation of the configuration, cf. figure 2. This configuration emerges for the first time when considering deep-inelastic lepton scattering (DIS), where one incoming line carries colour charge, or in configurations like vector boson fusion, with no colour exchange between the two hadrons. However, besides the singularity related to a final-state splitting, there is also a singular region for the splitting of the initial-state QCD parton, which needs to be included in such processes. This situation will be investigated in detail in section 3.3.
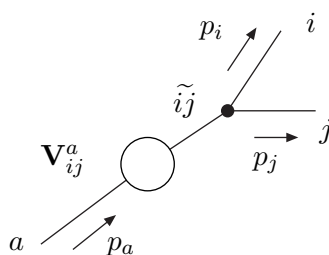
Figure 2: Sketch of the splitting of a final-state parton accompanied by an initial-state spectator. The blob denotes the m-parton matrix element. The incoming and outgoing lines label the initial- and final-state partons, respectively.

3.2.1 Massive case

The initial line is always assumed to be massless, however, all final-state particles can be massive. Accordingly,

$$\tilde{p}_{ij}^2 = m_{ij}^2 \quad \tilde{p}_a^2 = p_a^2 = 0 \quad p_i^2 = m_i^2, \quad p_j^2 = m_j^2. \tag{3.52}$$

To avoid on-shell decays being described incorrectly, again $m_{ij} \leq m_i + m_j$ should hold true.

- Kinematics.
  Four-momentum conservation is incorporated through the condition

$$\tilde{p}_{ij} - \tilde{p}_a = p_i + p_j - p_a \equiv Q. \tag{3.53}$$

  Defining the Lorentz-invariants

$$x_{ij,a} = \frac{p_i p_a + p_j p_a - p_i p_j + \frac{1}{2}\left(m_{ij}^2 - m_i^2 - m_j^2\right)}{p_i p_a + p_j p_a}, \tag{3.54}$$

$$\tilde{z}_i = \frac{p_i p_a}{p_i p_a + p_j p_a}, \quad \tilde{z}_j = \frac{p_j p_a}{p_i p_a + p_j p_a} = 1 - \tilde{z}_i, \tag{3.55}$$

  the relative transverse momentum of the new emerging final-state partons is given by

$$\mathbf{k}_\perp^2 = 2\tilde{p}_a \tilde{p}_{ij} \frac{1 - x_{ij,a}}{x_{ij,a}} \tilde{z}_i (1 - \tilde{z}_i) - (1 - \tilde{z}_i)^2 m_i^2 - \tilde{z}_i^2 m_j^2. \tag{3.56}$$

- Phase space.
  The factorised form of the three-parton phase space reads [31]

$$\mathrm{d}\Phi(p_i, p_j; Q + p_a) = \int_0^1 \mathrm{d}x \mathrm{d}\Phi(\tilde{p}_{ij}; Q + xp_a) \left[\mathrm{d}p_i(\tilde{p}_{ij}; p_a, x)\right] \Theta(x_+ - x), \tag{3.57}$$

  with the single-parton phase space factor

$$\left[\mathrm{d}p_i(\tilde{p}_{ij}; p_a, x)\right] = \frac{2\tilde{p}_{ij} p_a}{16\pi^2} \frac{\mathrm{d}\phi}{2\pi} \mathrm{d}\tilde{z}_i \, \mathrm{d}x_{ij,a} \, \delta(x - x_{ij,a}), \tag{3.58}$$

and the integration boundaries

$$x_- = 0, \quad x_+ = 1 + \mu_{ij}^2 - (\mu_i + \mu_j)^2, \tag{3.59}$$

$$z_\mp = \frac{1 - x + \mu_{ij}^2 + \mu_i^2 - \mu_j^2 \mp \sqrt{(1 - x + \mu_{ij}^2 - \mu_i^2 - \mu_j^2)^2 - 4\mu_i^2 \mu_j^2}}{2(1 - x + \mu_{ij}^2)}. \tag{3.60}$$

Here, again rescaled parton masses have been introduced,

$$\mu_n = \frac{m_n}{\sqrt{2\tilde{p}_{ij}\tilde{p}_a/x_{ij,a}}} \quad (n = i, j, ij). \tag{3.61}$$

- Splitting kernels.
  The polarisation-averaged QCD dipole splitting kernels $\langle \mathbf{V}_{ij}^a(\tilde{z}_i, x_{ij,a}) \rangle$ read

$$\langle \mathbf{V}_{Q_i g_j}^a(\tilde{z}_i, x_{ij,a}) \rangle = C_F \left\{ \frac{2}{1 - \tilde{z}_i + (1 - x_{ij,a})} - (1 + \tilde{z}_i) - \frac{m_i^2}{p_i p_j} \right\}, \tag{3.62}$$

$$\langle \mathbf{V}_{g_i g_j}^a(\tilde{z}_i, x_{ij,a}) \rangle = 2C_A \left\{ \frac{1}{1 - \tilde{z}_i + (1 - x_{ij,a})} + \frac{1}{\tilde{z}_i + (1 - x_{ij,a})} - 2 + \tilde{z}_i (1 - \tilde{z}_i) \right\}, \tag{3.63}$$

$$\langle \mathbf{V}_{Q_i Q_j}^a(\tilde{z}_i) \rangle = T_R \left\{ 1 - 2(z_+ - \tilde{z}_i)(z_- - \tilde{z}_i) \right\}. \tag{3.64}$$

The scalar product of the a priori unknown momenta p_i and p_j in eq. (3.62) can again be expressed according to eq. (3.16). The two functions $\langle \mathbf{V}_{Q_i g_j}^a \rangle$ and $\langle \mathbf{V}_{g_i g_j}^a \rangle$ can take negative values in non-singular regions of the emission phase space. Here they are explicitly set equal to zero instead.

- Matrix element.
  Combining the $(m + 1)$-parton phase space with the factorised form of the matrix element,

$$|\mathcal{M}_{m+1}|^2 = |\mathcal{M}_m|^2 \sum_{ij} \sum_a \frac{1}{(p_i+p_j)^2 - m_{ij}^2} \frac{1}{\mathcal{N}_{ij}^{\mathrm{spec}}} \frac{1}{x_{ij,a}} 8\pi\alpha_s \langle \mathbf{V}_{ij}^a(\tilde{z}_i, x_{ij,a}) \rangle, \tag{3.65}$$

one obtains the fully differential cross section for the emission of one additional parton in that configuration

$$d\hat{\sigma}_{m+1} = d\hat{\sigma}_m \sum_{ij} \sum_a \frac{dx_{ij,a}}{x_{ij,a}} d\tilde{z}_i \frac{d\phi}{2\pi} \frac{\alpha_s}{2\pi} \frac{1}{\mathcal{N}_{ij}^{\mathrm{spec}}} \frac{1}{1 - x_{ij,a}} \langle \mathbf{V}_{ij}^a(\tilde{z}_i, x_{ij,a}) \rangle, \tag{3.66}$$

where the sum covers all the possible colour-connected emitter-spectator pairings. The Jacobian of the variable transformation in this case reads

$$J(x_{ij,a}) = \frac{1}{1 - x_{ij,a}}. \tag{3.67}$$

Taking into account that the initial parton actually stems from a hadronic initial state, a corresponding parton distribution function (PDF) emerges. Absorbing it into the Jacobian yields

$$\tilde{J}(x_{ij,a}; \mu_F^2) = \frac{1}{1 - x_{ij,a}} \frac{f_a(\eta_a/x_{ij,a}, \mu_F^2)}{f_a(\eta_a, \mu_F^2)}. \tag{3.68}$$

Here, η_a is the momentum fraction of the spectator parton a and $f_a(\eta_a, \mu_F^2)$ the corresponding hadronic PDF evaluated at some scale μ_F^2. In section 2.3 this scale has been set to $\mu_F = \mathbf{k}_\perp$. The parton distribution function $f_a(\eta_a/x_{ij,a}, \mu_F^2)$ corresponds to the new incoming momentum and is also evaluated at scale μ_F^2.

- Sudakov form factor.
  Note that eq. (3.56) implies that

$$\frac{\mathrm{d}x_{ij,a}}{x_{ij,a}} = (1 - x_{ij,a})\frac{\mathrm{d}\mathbf{k}_\perp^2}{\mathbf{k}_\perp^2}. \tag{3.69}$$

With $\mathbf{k}_\perp^2$ taken as the evolution scale with an upper limit $\mathbf{k}_{\perp,\mathrm{max}}^2$ and the cut-off $\mathbf{k}_{\perp,0}^2$ the $\tilde{z}_i$ integration boundaries therefore are given by

$$z_- \left(\mathbf{k}_{\perp,\mathrm{max}}^2, \mathbf{k}_{\perp,0}^2\right) = \mathrm{Max}\left(\frac{1}{2}\left(1 - \sqrt{1 - \frac{\mathbf{k}_{\perp,0}^2}{\mathbf{k}_{\perp,\mathrm{max}}^2}}\right), z_-\right), \tag{3.70}$$

$$z_+ \left(\mathbf{k}_{\perp,\mathrm{max}}^2, \mathbf{k}_{\perp,0}^2\right) = \mathrm{Min}\left(\frac{1}{2}\left(1 + \sqrt{1 - \frac{\mathbf{k}_{\perp,0}^2}{\mathbf{k}_{\perp,\mathrm{max}}^2}}\right), z_+\right) \tag{3.71}$$

with $z_\pm$ given in eq. (3.59). Having determined $\mathbf{k}_\perp^2$ and $\tilde{z}_i$ the variable $x_{ij,a}$ is calculated through

$$x_{ij,a} = 1 - \frac{\mathbf{k}_\perp^2 + (1 - \tilde{z}_i)^2 m_i^2 + \tilde{z}_i^2 m_j^2 - \tilde{z}_i(1 - \tilde{z}_i)(m_{ij}^2 - m_i^2 - m_j^2)}{\mathbf{k}_\perp^2 + (1 - \tilde{z}_i)^2 m_i^2 + \tilde{z}_i^2 m_j^2 + \tilde{z}_i(1 - \tilde{z}_i)(Q^2 + 2m_i^2 + 2m_j^2)}, \tag{3.72}$$

and has to fulfil the condition

$$x_{ij,a} \in [\eta_a/\eta_{\mathrm{max}}, x_+] \tag{3.73}$$

to yield a valid branching. Here, η_{max} corresponds to the maximal allowed Bjørken-x for the PDF (typically, $\eta_{\mathrm{max}} = 1$). Having at hand all ingredients, the Sudakov form factor associated to the splitting of a final-state parton with an initial-state spectator reads

$$\Delta_{\mathrm{FI}}(\mathbf{k}_{\perp,\mathrm{max}}^2, \mathbf{k}_{\perp,0}^2) \tag{3.74}$$

$$= \exp\left(-\sum_{ij}\sum_a \frac{1}{\mathcal{N}_{ij}^{\mathrm{spec}}} \int_{\mathbf{k}_{\perp,0}^2}^{\mathbf{k}_{\perp,\mathrm{max}}^2} \frac{\mathrm{d}\mathbf{k}_\perp^2}{\mathbf{k}_\perp^2} \int_{z_-}^{z_+} \mathrm{d}\tilde{z}_i \frac{\alpha_\mathrm{s}(\mathbf{k}_\perp^2)}{2\pi} \frac{f_a(\eta_a/x_{ij,a}, \mathbf{k}_\perp^2)}{f_a(\eta_a, \mathbf{k}_\perp^2)} \langle \mathbf{V}_{ij}^a(\tilde{z}_i, x_{ij,a})\rangle\right).$$

- Physical kinematics.
  The actual branching kinematics can be given in a Sudakov parametrisation

$$p_i = \tilde{z}_i\,\tilde{p}_{ij} + \frac{\mathbf{k}_\perp^2 + m_i^2 - \tilde{z}_i^2\,m_{ij}^2}{\tilde{z}_i\,2\tilde{p}_{ij}\tilde{p}_a}\,\tilde{p}_a + k_\perp, \tag{3.75}$$

$$p_j = (1 - \tilde{z}_i)\,\tilde{p}_{ij} + \frac{\mathbf{k}_\perp^2 + m_j^2 - (1 - \tilde{z}_i)^2\,m_{ij}^2}{(1 - \tilde{z}_i)\,2\tilde{p}_{ij}\tilde{p}_a}\,\tilde{p}_a - k_\perp, \tag{3.76}$$

They are evaluated in the Breit-frame of the emitter and spectator with the spacelike-$k_\perp$ being perpendicular to both the momenta. After the splitting the spectator remains parallel to $\tilde{p}_a$ but is rescaled according to

$$p_a = \frac{1}{x_{ij,a}} \tilde{p}_a \,. \tag{3.77}$$

3.2.2 Massless case

The modifications emerging in the massless limit are briefly discussed. The splitting variable $x_{ij,a}$ simplifies to

$$x_{ij,a} = \frac{p_i p_a + p_j p_a - p_i p_j}{p_i p_a + p_j p_a} \,, \tag{3.78}$$

whereas the momentum fractions $\tilde{z}_i$ and $\tilde{z}_j$ are still defined according to eq. (3.55). The invariant spacelike transverse momentum is simplified and reads

$$\mathbf{k}_\perp^2 = 2\tilde{p}_a \tilde{p}_{ij} \frac{1 - x_{ij,a}}{x_{ij,a}} \, \tilde{z}_i \left(1 - \tilde{z}_i\right) \,. \tag{3.79}$$

While the g $\to$ gg splitting function remains the same, the mass dependent terms drop out in the q $\to$ qg and g $\to$ q$\overline{\text{q}}$ kernels,

$$\langle \mathbf{V}_{\mathrm{q}_i \mathrm{g}_j}^a (\tilde{z}_i, x_{ij,a}) \rangle = C_{\mathrm{F}} \left\{ \frac{2}{1 - \tilde{z}_i + (1 - x_{ij,a})} - (1 + \tilde{z}_i) \right\} \,, \tag{3.80}$$

$$\langle \mathbf{V}_{\mathrm{q}_i \mathrm{q}_j}^a (\tilde{z}_i) \rangle = T_{\mathrm{R}} \left\{ 1 - 2\tilde{z}_i \left(1 - \tilde{z}_i\right) \right\} \,. \tag{3.81}$$

Incorporating the factorisation of the $(m + 1)$-parton matrix element and the corresponding phase space the fully differential $(m + 1)$-parton cross section is still given by eq. (3.66), with the appropriate Jacobian for hadronic initial states. In the massless limit the phase-space boundaries are no longer constrained through finite mass terms, and therefore extend to

$$x_{ij,a}, \, \tilde{z}_i \in [0, 1] \,. \tag{3.82}$$

Eq. (3.79) still implies that

$$\frac{\mathrm{d}x_{ij,a}}{x_{ij,a}} = (1 - x_{ij,a}) \frac{\mathrm{d}\mathbf{k}_\perp^2}{\mathbf{k}_\perp^2} \,. \tag{3.83}$$

When evolving in $\mathbf{k}_\perp^2$ from $\mathbf{k}_{\perp,\mathrm{max}}^2$ and asking for a minimum separation $\mathbf{k}_{\perp,0}^2$ the allowed $\tilde{z}_i$ range is reduced to

$$\tilde{z}_i \in \left[\frac{1}{2} \left(1 - \sqrt{1 - \frac{\mathbf{k}_{\perp,0}^2}{\mathbf{k}_{\perp,\mathrm{max}}^2}} \right) , \, \frac{1}{2} \left(1 + \sqrt{1 - \frac{\mathbf{k}_{\perp,0}^2}{\mathbf{k}_{\perp,\mathrm{max}}^2}} \right) \right] \tag{3.84}$$

in the massless case. The expression of the Sudakov from factor, eq. (3.74), of course remains unaltered.
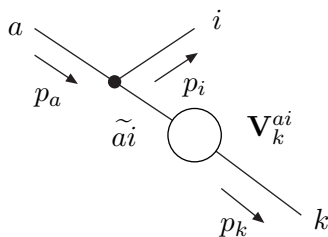
Figure 3: Splitting of an initial-state parton accompanied by a final-state spectator. The blob denotes the m-parton matrix element. The incoming and outgoing lines label the initial- and final-state partons, respectively.

The kinematics of the new final-state partons simplify to

$$p_i = \tilde{z}_i \, \tilde{p}_{ij} + \frac{\mathbf{k}_\perp^2}{\tilde{z}_i \, 2\tilde{p}_{ij}\tilde{p}_a} \, \tilde{p}_a + k_\perp \,, \tag{3.85}$$

$$p_j = (1 - \tilde{z}_i) \, \tilde{p}_{ij} + \frac{\mathbf{k}_\perp^2}{(1 - \tilde{z}_i) \, 2\tilde{p}_{ij}\tilde{p}_a} \, \tilde{p}_a - k_\perp \,, \tag{3.86}$$

with $k_\perp$ still being perpendicular to both the emitter and the spectator momentum. The new spectator momentum is still given by

$$p_a = \frac{1}{x_{ij,a}} \tilde{p}_a \,, \tag{3.87}$$

with $x_{ij,a}$ taken from eq. (3.78).

3.3 Initial-state emitter and final-state spectator

The case of an initial-state parton branching $(\widetilde{ai})$, accompanied by a final-state spectator $(\tilde{k})$ is sketched in figure 3. This accounts for the situation where the emitter and the spectator parton studied in section 3.2 exchange their rôles.

3.3.1 Massive case

As stated above, treating initial-state particles as massless, final-state particles emitted from the initial state are assumed massless as well, the spectator mass, however, is arbitrary. Accordingly, the momenta involved in the splitting $\{\widetilde{ai}, \tilde{k}\} \rightarrow \{a, i, k\}$ have to fulfil the mass-shell relations

$$\tilde{p}_{ai}^2 = p_i^2 = p_a^2 = 0 \,, \quad \tilde{p}_k^2 = p_k^2 = m_k^2 \,. \tag{3.88}$$

and the momentum conservation condition

$$\tilde{p}_k - \tilde{p}_{ai} = p_i + p_k - p_a \equiv Q \,. \tag{3.89}$$

- Kinematics.

  The splitting can be specified by the variables

$$x_{ik,a} = \frac{p_i p_a + p_k p_a - p_i p_k}{p_i p_a + p_k p_a}, \quad u_i = \frac{p_i p_a}{p_i p_a + p_k p_a}. \tag{3.90}$$

  The transverse momentum squared parametrising the singular region where the emitted parton i becomes collinear with the initial-state parton a then reads

$$\mathbf{k}_\perp^2 = 2\tilde{p}_{ai}\tilde{p}_k \frac{1 - x_{ik,a}}{x_{ik,a}} u_i(1 - u_i). \tag{3.91}$$

  To allow for a more compact notation, the rescaled spectator mass

$$\mu_k = \frac{m_k}{\sqrt{2\tilde{p}_{ai}\tilde{p}_k/x_{ik,a}}} \tag{3.92}$$

  is introduced.

- Splitting kernels.

  The QCD splitting kernels, taking into account possible non-zero spectator masses, read

$$\langle \mathbf{V}_k^{\mathrm{q}_a \mathrm{g}_i}(x_{ik,a}, u_i) \rangle = C_\mathrm{F} \left\{ \frac{2}{1 - x_{ik,a} + u_i} - (1 + x_{ik,a}) \right\}, \tag{3.93}$$

$$\langle \mathbf{V}_k^{\mathrm{q}_a \mathrm{q}_i}(x_{ik,a}) \rangle = C_\mathrm{F} \left\{ x_{ik,a} + 2\frac{1 - x_{ik,a}}{x_{ik,a}} - \frac{2\mu_k^2}{x_{ik,a}} \frac{u_i}{1 - u_i} \right\}, \tag{3.94}$$

$$\langle \mathbf{V}_k^{\mathrm{g}_a \mathrm{g}_i}(x_{ik,a}, u_i) \rangle = 2C_\mathrm{A} \left\{ \frac{1}{1 - x_{ik,a} + u_i} + \frac{1 - x_{ik,a}}{x_{ik,a}} - 1 \right.$$
$$\left. + x_{ik,a}(1 - x_{ik,a}) - \frac{\mu_k^2}{x_{ik,a}} \frac{u_i}{1 - u_i} \right\}, \tag{3.95}$$

$$\langle \mathbf{V}_k^{\mathrm{g}_a \mathrm{q}_i}(x_{ik,a}) \rangle = T_\mathrm{R} \left\{ 1 - 2x_{ik,a}(1 - x_{ik,a}) \right\}. \tag{3.96}$$

  Note that $\langle \mathbf{V}_k^{\mathrm{q}_a \mathrm{g}_i} \rangle$ can turn negative outside the singular region and is set to zero for those rare cases.

- Phase space.

  The three-parton phase space is again obtained by a convolution of a two-parton piece and a single-parton part,

$$\mathrm{d}\Phi(p_i, p_k; Q + p_a) = \int_0^1 \mathrm{d}x \, \mathrm{d}\Phi(\tilde{p}_k; Q + xp_a) \left[\mathrm{d}p_i(\tilde{p}_k; p_a, x)\right], \tag{3.97}$$

  where

$$[\mathrm{d}p_i(\tilde{p}_k; p_a, x)] = \frac{\mathrm{d}^4 p_i}{2\pi} \delta(p_i^2) \, \Theta(x) \, \Theta(1 - x) \, \delta(x - x_{ik,a}) \frac{1}{1 - u_i}, \tag{3.98}$$

  or, more conveniently,

$$[\mathrm{d}p_i(\tilde{p}_k; p_a, x)] = \frac{2\tilde{p}_k p_a}{16\pi^2} \frac{\mathrm{d}\phi}{2\pi} \mathrm{d}x_{ik,a} \mathrm{d}u_i \Theta(u_i(1 - u_i)) \Theta(x(1 - x)) \delta(x - x_{ik,a}). \tag{3.99}$$

The upper limit for the u_i-integration contains a dependence on the spectator mass,

$$u_+ = \frac{1 - x_{ik,a}}{1 - x_{ik,a} + \mu_k^2} \, . \tag{3.100}$$

- Matrix element.
  Using the factorisation property of the $(m+1)$-parton matrix element

$$|\mathcal{M}_{m+1}|^2 = |\mathcal{M}_m|^2 \sum_{ai} \sum_k \frac{1}{2p_a p_i} \frac{1}{\mathcal{N}_{ai}^{\mathrm{spec}}} \frac{1}{x_{ik,a}} \, 8\pi\alpha_{\mathrm{s}} \, \langle \mathbf{V}_k^{ai}(x_{ik,a}, u_i) \rangle \tag{3.101}$$

in the soft and collinear limits and the relation

$$\frac{2\tilde{p}_k p_a}{2p_a p_i} = \frac{1}{u_i} \tag{3.102}$$

the $(m+1)$-parton fully differential cross section reads

$$\mathrm{d}\hat{\sigma}_{m+1} = \mathrm{d}\hat{\sigma}_m \sum_{ai} \sum_k \frac{\mathrm{d}u_i}{u_i} \, \mathrm{d}x_{ik,a} \, \frac{\mathrm{d}\phi}{2\pi} \frac{\alpha_{\mathrm{s}}}{2\pi} \frac{1}{\mathcal{N}_{ai}^{\mathrm{spec}}} \frac{1}{x_{ik,a}} \, \langle \mathbf{V}_k^{ai}(x_{ik,a}, u_i) \rangle \, . \tag{3.103}$$

The integration range of the variables u_i and $x_{ik,a}$ is $[0, u_+]$ and $[0, 1]$, respectively, and $[0, 2\pi]$ for ϕ. The Jacobian

$$J(x_{ik,a}) = \frac{1}{x_{ik,a}} \tag{3.104}$$

for the parton matrix element again is changed in hadronic interactions to include the effect of the PDFs, such that

$$\tilde{J}(x_{ik,a}; \mu_F^2) = \frac{1}{x_{ik,a}} \frac{f_a(\eta_{ai}/x_{ik,a}, \mu_F^2)}{f_{ai}(\eta_{ai}, \mu_F^2)} \, , \tag{3.105}$$

where again, in the implementation here the choice for the factorisation scale is $\mu_F = \mathbf{k}_\perp$, cf. section 2.3. Note that the Jacobian takes into account not only a change in Bjørken-x but also a possible flavour change in the process' initial state.

- Sudakov form factor.
  The integration over u_i in eq. (3.103) can be replaced by an integration over $\mathbf{k}_\perp^2$ according to

$$\frac{\mathrm{d}u_i}{u_i} = \frac{1 - u_i}{1 - 2u_i} \frac{\mathrm{d}\mathbf{k}_\perp^2}{\mathbf{k}_\perp^2} \, . \tag{3.106}$$

The arising Jacobian is combined with the function $\tilde{J}(x_{ik,a}; \mu_F^2)$ to

$$\tilde{J}(x_{ik,a}, u_i; \mu_F^2) = \frac{1 - u_i}{1 - 2u_i} \frac{1}{x_{ik,a}} \frac{f_a(\eta_{ai}/x_{ik,a}, \mu_F^2)}{f_{ai}(\eta_{ai}, \mu_F^2)} \, . \tag{3.107}$$

With $\mathbf{k}_\perp^2 > 0$ as the evolution variable and its cut-off being $\mathbf{k}_{\perp,0}^2$ the $x_{ik,a}$ phase-space boundaries are

$$x_{ik,a} \in \left[\frac{\eta_{ai}}{\eta_{\mathrm{max}}} , \frac{Q^2}{Q^2 + 4\mathbf{k}_{\perp,0}^2} \right] , \tag{3.108}$$

with $\eta_{\max}$ the maximal allowed Bjørken-x of the PDF. With $\mathbf{k}_\perp^2$ and $x_{ik,a}$ given, u_i can be calculated and yields

$$u_i = \frac{1}{2}\left(1 - \sqrt{1 - \frac{4\mathbf{k}_\perp^2\, x_{ik,a}}{Q^2(1 - x_{ik,a})}}\right).$$
(3.109)

When $u_i \leq u_+$ an allowed branching is found. Thus the Sudakov form factor for having no emission from an initial-state parton accompanied by a final-state spectator between scales $\mathbf{k}_{\perp,\max}^2$ and $\mathbf{k}_{\perp,0}^2$ can be written down,

$$\Delta_{\mathrm{IF}}(\mathbf{k}_{\perp,\max}^2, \mathbf{k}_{\perp,0}^2)$$
$$= \exp\left(-\sum_{ai}\sum_k \frac{1}{\mathcal{N}_{ai}^{\mathrm{spec}}} \int_{\mathbf{k}_{\perp,0}^2}^{\mathbf{k}_{\perp,\max}^2} \frac{\mathrm{d}\mathbf{k}_\perp^2}{\mathbf{k}_\perp^2} \int_{x_-}^{x_+} \mathrm{d}x_{ik,a}\, \frac{\alpha_{\mathrm{s}}(\mathbf{k}_\perp^2/4)}{2\pi}\, \tilde{J}(x_{ik,a}, u_i; \mathbf{k}_\perp^2) \langle \mathbf{V}_k^{ai}(x_{ik,a}, u_i)\rangle\right).$$
(3.110)

- Physical kinematics.
  The new initial-state particle a remains parallel to the original initial-state parton, and is just rescaled by the splitting variable $x_{ik,a}$ such that

$$p_a = \frac{1}{x_{ik,a}} \tilde{p}_{ai}.$$
(3.111)

The two final-state momenta are most conveniently evaluated in the rest-frame of $Q + p_a$ with p_a pointing along the positive z-axis. The corresponding light-cone momenta read

$$Q + p_a = \left(M, M, \vec{0}\right) \quad \text{and} \quad p_a = \left(2E_a, 0, \vec{0}\right).$$
(3.112)

Note that the massless vector p_a only has a light-cone $+$-component, given by twice the energy of the parton. For p_i and p_k the ansatz

$$p_i = \left(l_\perp e^y, l_\perp e^{-y}, \vec{l}_\perp\right), \quad p_k = \left(m_{k,\perp} e^z, m_{k,\perp} e^{-z}, -\vec{l}_\perp\right),$$
(3.113)

is used, with $m_\perp$ being the transverse mass. Besides the energy- and momentum-conservation requirement the momenta are constrained by the splitting variables,

$$u_i = \frac{p_i p_a}{(p_i + p_k)p_a} = \frac{l_\perp e^{-y}}{M}.$$
(3.114)

yielding

$$\vec{l}_\perp^2 = \left(M^2 - m_k^2\right) u_i - M^2 u_i^2,$$
(3.115)

for the transverse momentum squared. This equals the physical transverse momentum squared of parton i, $\mathbf{k}_\perp^2$. Employing the relations

$$\cosh y = \frac{M^2 - m_k^2}{2Ml_\perp}, \quad \sinh y = \frac{1}{2}\left(\frac{l_\perp}{Mu_i} - \frac{Mu_i}{l_\perp}\right),$$
(3.116)

$$\cosh z = \frac{M^2 + m_k^2}{2Mm_{k,\perp}}, \quad \sinh z = \frac{1}{2}\left(\frac{m_{k,\perp}}{M(1-u_i)} - \frac{M(1-u_i)}{m_{k,\perp}}\right),$$
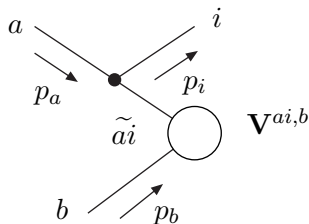(3.117)

Figure 4: Schematical view of the splitting of an initial-state parton with an initial-state parton as spectator. The blob denotes the m-parton matrix element. Incoming and outgoing lines label the initial- and final-state partons, respectively.

the four-momenta of the final-state partons, in the frame specified above, read

$$p_i = (l_\perp \cosh y, l_\perp \cos \phi, l_\perp \sin \phi, l_\perp \sinh y), \tag{3.118}$$

$$p_k = (m_{k,\perp} \cosh z, -l_\perp \cos \phi, -l_\perp \sin \phi, m_{k,\perp} \sinh z). \tag{3.119}$$

Again, ϕ has been uniformly distributed in the transverse plane. The kinematics is completed by rotating and boosting the momenta p_a, p_i and p_k back in the laboratory frame.

3.3.2 Massless case

The massless limit of the scenario above, initial-state splittings accompanied by final-state spectators, $\{\widetilde{ai}, \tilde{k}\} \to \{a, i, k\}$, corresponds to neglecting the spectator mass, $\tilde{p}_k^2 = p_k^2 = 0$. Apart from that, the splitting variables remain unchanged and the dependence on m_k, of course, disappears in the corresponding phase space boundaries.

Dropping the explicit mass terms present in $\langle \mathbf{V}_k^{q_a q_i}(x_{ik,a}) \rangle$ and $\langle \mathbf{V}_k^{g_a g_i}(x_{ik,a}, u_i) \rangle$ given in eqs. (3.94) and (3.95), respectively, the factorised form of the fully differential cross section can completely be taken over.

Neglecting the finite spectator masses the splitting kinematics is significantly simplified. They are given by

$$p_a = \frac{1}{x_{ik,a}} \tilde{p}_{ai}, \tag{3.120}$$

$$p_i = (1 - u_i) \frac{1 - x_{ik,a}}{x_{ik,a}} \tilde{p}_{ai} + u_i \tilde{p}_k + k_\perp, \tag{3.121}$$

$$p_k = u_i \frac{1 - x_{ik,a}}{x_{ik,a}} \tilde{p}_{ai} + (1 - u_i) \tilde{p}_k - k_\perp, \tag{3.122}$$

and they are conveniently evaluated in the emitter-spectator Breit-frame with $k_\perp$ perpendicular to both the emitter and the spectator.

3.4 Initial-state emitter and initial-state spectator

The last scenario to be studied is the splitting of an initial-state particle $\widetilde{ai}$, with the spectator b being an initial-state parton as well, cf. figure 4. This type of branching occurs

when considering hadron-hadron collisions, where both the initial-state particles are colour charged and therefore can be colour connected. The simplest example for this configuration is the lowest order Drell-Yan process, where both the incoming quark and anti-quark can serve as emitter and spectator.

In contrast to all other cases discussed before, it turns out to be convenient to preserve the spectator momentum p_b in this branching. Since also the emitter momentum remains parallel to p_a,

$$\tilde{p}_{ai} = x_{i,ab}\, p_a\,, \quad \text{with} \quad x_{i,ab} = \frac{p_a p_b - p_i p_a - p_i p_b}{p_a p_b}\,, \tag{3.123}$$

the transverse momentum of the emitted parton, p_i, has to be balanced by *all* other final-state momenta k_j. This does not only include the QCD partons, but all non-QCD particles, e.g. leptons, as well.

- Kinematics.
  Defining the variable

$$\tilde{v}_i = \frac{p_i p_a}{p_a p_b} \tag{3.124}$$

  the transverse momentum squared of parton i is given by

$$\mathbf{k}_\perp^2 = 2\tilde{p}_{ai} p_b\, \tilde{v}_i\, \frac{1 - x_{i,ab} - \tilde{v}_i}{x_{i,ab}}\,. \tag{3.125}$$

  The four-momenta of the m-parton ensemble fulfil

$$\tilde{p}_{ai} + p_b - \sum_{j=1}^{m} \tilde{k}_j = 0\,, \tag{3.126}$$

  correspondingly the full set of $m + 1$ particles has to satisfy

$$p_a + p_b - \sum_{j=1}^{m} k_j - p_i = 0\,. \tag{3.127}$$

- Splitting kernels.
  The polarisation-averaged splitting kernels $\langle \mathbf{V}^{ai,b}\rangle$ depend on $x_{i,ab}$ only and read

$$\langle \mathbf{V}^{\mathrm{q}_a \mathrm{g}_i, b}(x_{i,ab})\rangle = C_{\mathrm{F}} \left\{ \frac{2}{1 - x_{i,ab}} - (1 + x_{i,ab}) \right\}\,, \tag{3.128}$$

$$\langle \mathbf{V}^{\mathrm{q}_a \mathrm{q}_i, b}(x_{i,ab})\rangle = C_{\mathrm{F}} \left\{ x_{i,ab} + 2\frac{1 - x_{i,ab}}{x_{i,ab}} \right\}\,, \tag{3.129}$$

$$\langle \mathbf{V}^{\mathrm{g}_a \mathrm{g}_i, b}(x_{i,ab})\rangle = 2C_{\mathrm{A}} \left\{ \frac{1}{1 - x_{i,ab}} + \frac{1 - x_{i,ab}}{x_{i,ab}} - 1 + x_{i,ab}(1 - x_{i,ab}) \right\}\,, \tag{3.130}$$

$$\langle \mathbf{V}^{\mathrm{g}_a \mathrm{q}_i, b}(x_{i,ab})\rangle = T_{\mathrm{R}} \left\{ 1 - 2x_{i,ab}(1 - x_{i,ab}) \right\}\,. \tag{3.131}$$

- **Phase space.**

  The final-state phase space can be written as follows [31]

  $$\mathrm{d}\Phi(p_i, k_1, \ldots; p_a + p_b) = \int\limits_0^1 \mathrm{d}x \, \mathrm{d}\Phi(\tilde{k}_1, \ldots; x p_a + p_b) \, [\mathrm{d}p_i(p_a, p_b, x)], \quad (3.132)$$

  with

  $$[\mathrm{d}p_i(p_a, p_b, x)] = \frac{2p_a p_b}{16\pi^2} \frac{\mathrm{d}\phi}{2\pi} \mathrm{d}x_{i,ab} \mathrm{d}\tilde{v}_i \Theta(x(1-x)) \Theta(\tilde{v}_i) \Theta\left(1 - \frac{\tilde{v}_i}{1-x}\right) \delta(x - x_{i,ab}), \quad (3.133)$$

  where ϕ is the polar angle in the plane perpendicular to p_a and p_b.

- **Matrix element.**

  Combining this with the expression for the $(m+1)$-parton matrix element

  $$|\mathcal{M}_{m+1}|^2 = |\mathcal{M}_m|^2 \sum_{ai} \sum_{b \neq ai} \frac{1}{2p_a p_i} \frac{1}{\mathcal{N}_{ai}^{\mathrm{spec}}} \frac{1}{x_{i,ab}} 8\pi\alpha_s \langle \mathbf{V}^{ai,b}(x_{i,ab}) \rangle \quad (3.134)$$

  the differential cross section becomes

  $$\mathrm{d}\hat{\sigma}_{m+1} = \mathrm{d}\hat{\sigma}_m \sum_{ai} \sum_{b \neq ai} \frac{\mathrm{d}\tilde{v}_i}{\tilde{v}_i} \mathrm{d}x_{i,ab} \frac{\mathrm{d}\phi}{2\pi} \frac{\alpha_s}{2\pi} \frac{1}{\mathcal{N}_{ai}^{\mathrm{spec}}} \frac{1}{x_{i,ab}} \langle \mathbf{V}^{ai,b}(x_{i,ab}) \rangle, \quad (3.135)$$

  where $1 - x_{i,ab} - \tilde{v}_i > 0$ has to hold. The Jacobian can be read off as

  $$J(x_{i,ab}) = \frac{1}{x_{i,ab}}, \quad (3.136)$$

  or, including again the PDFs,

  $$\tilde{J}(x_{i,ab}; \mu_F^2) = \frac{1}{x_{i,ab}} \frac{f_a(\eta_{ai}/x_{i,ab}, \mu_F^2)}{f_{ai}(\eta_{ai}, \mu_F^2)}. \quad (3.137)$$

- **Sudakov form factor.**

  Regarding the transverse momentum given by eq. (3.125) the identity

  $$\frac{\mathrm{d}\tilde{v}_i}{\tilde{v}_i} = \frac{1 - x_{i,ab} - \tilde{v}_i}{1 - x_{i,ab} - 2\tilde{v}_i} \frac{\mathrm{d}\mathbf{k}_\perp^2}{\mathbf{k}_\perp^2}, \quad (3.138)$$

  can be employed to replace the $\tilde{v}_i$ integration with a $\mathbf{k}_\perp^2$-integral. The resulting Jacobian, combined with $\tilde{J}(x_{i,ab}; \mu_F^2)$, amounts to

  $$\tilde{J}(x_{i,ab}, \tilde{v}_i; \mu_F^2) = \frac{1 - x_{i,ab} - \tilde{v}_i}{1 - x_{i,ab} - 2\tilde{v}_i} \frac{1}{x_{i,ab}} \frac{f_a(\eta_{ai}/x_{i,ab}, \mu_F^2)}{f_{ai}(\eta_{ai}, \mu_F^2)}. \quad (3.139)$$

  When evolving in $\mathbf{k}_\perp^2$ the dependence of the $x_{i,ab}$-integration boundaries on the cut-off $\mathbf{k}_{\perp,0}^2$ read

  $$x_{i,ab} \in \left[\frac{\eta_{ai}}{\eta_{\max}}, \frac{2\tilde{p}_a p_b}{2\tilde{p}_a p_b + 4\mathbf{k}_{\perp,0}^2} \right]. \quad (3.140)$$

$\tilde{v}_i$ can be calculated from $\mathbf{k}_\perp^2$ and $x_{i,ab}$,

$$\tilde{v}_i = \frac{1 - x_{i,ab}}{2} \left(1 - \sqrt{1 - \frac{2\mathbf{k}_\perp^2 \, x_{i,ab}}{\tilde{p}_a p_b (1 - x_{i,ab})^2}} \right) . \tag{3.141}$$

The Sudakov form factor then reads

$$\Delta_{\mathrm{II}}(\mathbf{k}_{\perp,\mathrm{max}}^2, \mathbf{k}_{\perp,0}^2) \tag{3.142}$$

$$= \exp\left(-\sum_{ai} \sum_{b \neq ai} \frac{1}{\mathcal{N}_{ai}^{\mathrm{spec}}} \int_{\mathbf{k}_{\perp,0}^2}^{\mathbf{k}_{\perp,\mathrm{max}}^2} \frac{\mathrm{d}\mathbf{k}_\perp^2}{\mathbf{k}_\perp^2} \int_{x_-}^{x_+} \mathrm{d}x_{i,ab} \, \frac{\alpha_\mathrm{s}(\mathbf{k}_\perp^2/4)}{2\pi} \tilde{J}(x_{i,ab}, \tilde{v}_i; \mathbf{k}_\perp^2) \langle \mathbf{V}^{ai,b}(x_{i,ab}) \rangle \right) .$$

- Physical kinematics.

  The momenta of the $(m+1)$-parton ensemble, expressed through the emitter and spectator momentum and the momenta of all other final-state particles of the m-parton process, read

$$p_a = \frac{1}{x_{i,ab}} \tilde{p}_{ai} , \tag{3.143}$$

$$p_i = \frac{1 - x_{i,ab} - \tilde{v}_i}{x_{i,ab}} \tilde{p}_{ai} + \tilde{v}_i \, p_b + k_\perp , \tag{3.144}$$

$$k_j = \Lambda(\tilde{p}_{ai} + p_b, p_a + p_b - p_i) \, \tilde{k}_j , \tag{3.145}$$

with $k_\perp / \sqrt{\mathbf{k}_\perp^2}$ uniformly distributed in the transverse plane and $\Lambda(\tilde{p}_{ai} + p_b, p_a + p_b - p_i) = \Lambda(\tilde{K}, K)$ being a proper Lorentz transformation given by

$$\Lambda^\mu{}_\nu(\tilde{K}, K) = g^\mu{}_\nu - \frac{2\,(\tilde{K} + K)^\mu (\tilde{K} + K)_\nu}{(\tilde{K} + K)^2} + \frac{2\, K^\mu \tilde{K}_\nu}{\tilde{K}^2} . \tag{3.146}$$

Accordingly, the full set of final-state momenta compensates for the transverse momentum of p_i, although they do not participate in the splitting.

3.5 SUSY QCD splitting functions

In the minimal supersymmetric extension of the Standard Model the sector of strongly interacting particles is extended by the superpartners of the ordinary quark- and gluon-fields [61]. The new particles participating in the strong interaction are the scalar-quarks, called squarks and the gluino. While the former are colour-triplets the gluino is a Majorana fermion in the adjoint representation, a colour-octet.

In order to be consistent with todays experimental (non-)observations the assumed SUSY particles have to be rather heavy. This renders the massless limit for these fields not applicable when describing their QCD interactions at the energies of the forthcoming colliders. Based on that argument it is beyond the present scope to describe possible branchings like $g \to \tilde{q}\tilde{q}^*$, $g \to \tilde{g}\tilde{g}$ in a quasi-collinear limit. Rather, they are appropriately described using exact matrix element methods, as discussed e.g. in [68, 69].
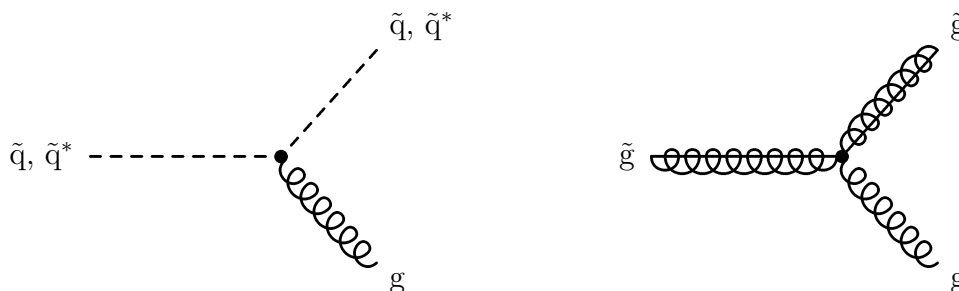
Figure 5: The SUSY QCD vertices corresponding to gluon emission off (anti-)squarks and gluinos.

Since the spin and the flavour of the spectator parton do not enter the splitting functions, the branchings of the Standard Model particles are not altered in supersymmetric extensions. The only SUSY QCD splittings that appear to be relevant in the context of a parton shower formulation are related to the emission of a gluon off a squark or antisquark and off a gluino, cf. figure 5. Further, assuming that supersymmetric particles do not appear as partonic initial states those are solely final-state splittings. The associated spectator, however, can be either in the final state or in the initial state.

Due to its fermionic nature the splitting functions involving gluinos are equal to the corresponding splittings of massive quarks, cf. eq. (3.13) and eq. (3.62), only the colour factors have to be adapted from C_F to C_A.

The kernel of the branching $\tilde{q} \to \tilde{q}g$ with the spectator also in the final state reads

$$\langle \mathbf{V}_{\tilde{q}_i g_j, k}(\tilde{z}_i, y_{ij,k}) \rangle = C_F \left\{ \frac{2}{1 - \tilde{z}_i + \tilde{z}_i y_{ij,k}} - \frac{\tilde{v}_{ij,k}}{v_{ij,k}} \left(2 + \frac{m_i^2}{p_i p_j} \right) \right\} , \qquad (3.147)$$

where all the variables have been defined in section 3.1.1. If the spectator is in the initial state this becomes

$$\langle \mathbf{V}_{\tilde{q}_i g_j}^a(\tilde{z}_i, x_{ij,a}) \rangle = C_F \left\{ \frac{2}{1 - \tilde{z}_i + (1 - x_{ij,a})} - 2 - \frac{m_i^2}{p_i p_j} \right\} , \qquad (3.148)$$

for the definitions of the variables used see section 3.2.1.

Apart from the splitting kernels all the results derived in the corresponding sections describing the branchings of massive final-state partons with spectators in the final- or initial state can be taken over without any alteration. This includes the exact phase-space factorisation as well as the parton kinematics defined there.

4. Comparing the hardest emission with matrix elements

In the following, the predictions for the hardest (first) emission of the parton shower algorithm will be worked out for different processes and compared with corresponding exact tree-level matrix element calculations. The set of processes to be considered covers three-jet production in e^+e^- collisions, cf. section 4.1, the first order real correction process to DIS, cf. section 4.2, and the production of a weak gauge boson accompanied by a light jet
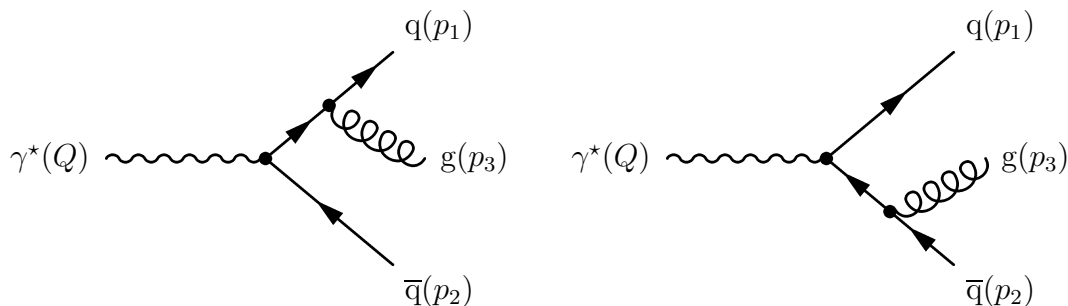
Figure 6: The two first order α_{s} Feynman diagrams contributing to $\gamma^{\star} \to \mathrm{q}\overline{\mathrm{q}}\mathrm{g}$.

at hadron colliders, cf. section 4.3. These three examples constitute a full set of generic processes to reliably test the first emission of the proposed parton shower approach.

4.1 Three-jet production at lepton-colliders

In this example the production of three jets at a lepton-collider is investigated. Jet production proceeds via the s-channel exchange of a colour-singlet particle, namely a $\gamma^{\star}$ or Z^0-boson. The latter will be ignored in the discussion here. At first perturbative order in α_{s}, two Feynman diagrams contribute to the matrix element $\gamma^{\star} \to \mathrm{q}\overline{\mathrm{q}}\mathrm{g}$, corresponding to the emission of a gluon from either the final-state quark or the anti-quark, cf. figure 6.

For convenience, the centre-of mass energy

$$E_{\mathrm{c.m.}} \equiv \sqrt{Q^2} \,, \tag{4.1}$$

and the momentum fractions

$$x_i \equiv \frac{2 p_i Q}{Q^2} \,. \tag{4.2}$$

are introduced. Neglecting the masses of the final-state particles the Lorentz-invariant Mandelstam variables for the $1 \to 3$ process become

$$\hat{s} \equiv (p_1 + p_3)^2 = 2 p_1 p_3 = Q^2 (1 - x_2) \,, \tag{4.3}$$

$$\hat{t} \equiv (p_2 + p_3)^2 = 2 p_2 p_3 = Q^2 (1 - x_1) \,, \tag{4.4}$$

$$\hat{u} \equiv (p_1 + p_2)^2 = 2 p_1 p_2 = Q^2 (1 - x_3) \,. \tag{4.5}$$

Energy-momentum conservation implies that

$$x_1 + x_2 + x_3 = 2 \quad \text{and} \quad \hat{s} + \hat{t} + \hat{u} = Q^2 \,. \tag{4.6}$$

The partonic differential decay rate with respect to the quark and anti-quark momentum fractions $x_{1,2}$ reads

$$\frac{\mathrm{d}\hat{\Gamma}}{\mathrm{d}x_1 \mathrm{d}x_2}\bigg|_{\mathrm{ME}} = \hat{\Gamma}_0 \, \frac{\alpha_{\mathrm{s}}}{2\pi} \, C_{\mathrm{F}} \left[\frac{x_1^2 + x_2^2}{(1 - x_1)(1 - x_2)} \right] \,, \tag{4.7}$$

where $\hat{\Gamma}_0$ denotes the total decay rate for $\gamma^\star \to q\bar{q}$,

$$\hat{\Gamma}_0 = 2\alpha_{\text{qed}} e_q^2 E_{\text{c.m.}} \,, \tag{4.8}$$

see for instance [70].

In the parton shower approach, two contributions occur as well. They correspond to the timelike splitting of either the quark or the anti-quark, and the total result is just the incoherent sum of the two pieces. To work this out, consider the case of the quark splitting with the anti-quark being the spectator parton. Then, the shower variables are, cf. section 3.1.2,

$$y_{13,2} = \frac{p_1 p_3}{p_1 p_3 + p_1 p_2 + p_2 p_3} = \frac{\hat{s}}{\hat{s} + \hat{u} + \hat{t}} = \frac{\hat{s}}{Q^2} \,, \tag{4.9}$$

$$\tilde{z}_1 = \frac{p_1 p_2}{p_1 p_2 + p_3 p_2} = \frac{\hat{u}}{\hat{u} + \hat{t}} \,, \tag{4.10}$$

which, expressed in terms of the x_i, translate into

$$y_{13,2} = 1 - x_2 \quad \text{and} \quad \tilde{z}_1 = \frac{1 - x_3}{x_2} = 1 - \frac{1 - x_1}{x_2} \,. \tag{4.11}$$

Accordingly, the decay rate for the emission off the quark can be cast into the form

$$\frac{d\hat{\Gamma}}{dx_1 dx_2}\bigg|_{\text{PSq}} = \hat{\Gamma}_0 \frac{\alpha_s}{2\pi} C_F \left[\frac{1}{1 - x_2} \left(\frac{2}{2 - x_1 - x_2} - (1 + x_1) \right) + \frac{1 - x_1}{x_2} \right] \,. \tag{4.12}$$

The result for the emission of a gluon off the anti-quark can be obtained from eq. (4.12) by $1 \leftrightarrow 2$. Taken together, the parton shower decay rate yields

$$\frac{d\hat{\Gamma}}{dx_1 dx_2}\bigg|_{\text{PS}} = \frac{d\hat{\Gamma}}{dx_1 dx_2}\bigg|_{\text{PSq}} + \frac{d\hat{\Gamma}}{dx_1 dx_2}\bigg|_{\text{PS}\bar{q}}$$

$$= \hat{\Gamma}_0 \frac{\alpha_s}{2\pi} C_F \left[\frac{x_1^2 + x_2^2}{(1 - x_1)(1 - x_2)} + \frac{1 - x_1}{x_2} + \frac{1 - x_2}{x_1} \right] \,. \tag{4.13}$$

Obviously, the parton shower reproduces the matrix element calculation in both the soft and the collinear limit. The only difference between the two results are two non-singular terms in the parton shower result that vanish as $x_{1,2} \to 1$.

4.2 Real corrections to leading order DIS

The simplest physical process involving initial-state hadrons is deep-inelastic lepton-nucleon scattering (DIS), i.e. $e^\pm p \to e^\pm + X$. At leading order, two partonic processes contribute, namely $e^\pm q \to e^\pm q$ and $e^\pm \bar{q} \to e^\pm \bar{q}$, both of which must be convoluted with the initial hadron's PDF to obtain the hadronic cross section. The interaction is mediated by virtual-photon and Z^0-boson exchange. In the following, however, only the $\gamma^\star$ channel is taken into account, for which the two partonic cross sections are equal.

At next-to-leading order the quark can radiate a gluon before or after its interaction with the virtual photon, cf. figure 7. Beyond this, at NLO the incoming quark may originate from a gluon in the initial hadron that produces a quark-anti-quark pair which the $\gamma^\star$ then
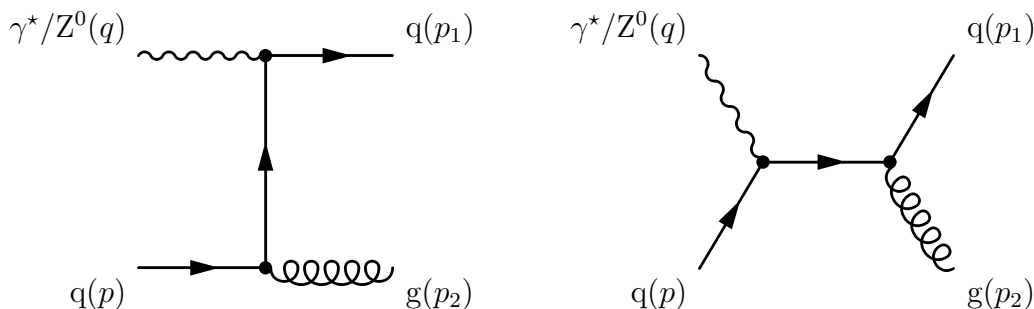
Figure 7: The two leading order Feynman diagrams contributing to $\gamma^\star q \to qg$.
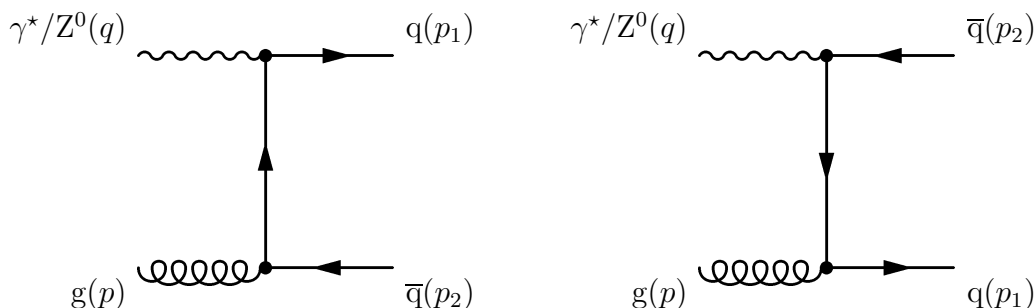

Figure 8: The two possible Feynman diagrams for $\gamma^\star g \to q\overline{q}$.

couples to, cf. figure 8. The real emission matrix elements can be expressed through the kinematic variables

$$Q^2 = -q^2\,, \quad x = \frac{Q^2}{2pq}, \quad z_i = \frac{p_i p}{pq}\,, \tag{4.14}$$

where q denotes the four-momentum of the off-shell photon, p the incoming parton momentum and the p_i label the momenta of the final-state partons. The Mandelstam variables for the $2 \to 2$ processes $\gamma^\star(q)q(p) \to q(p_1)g(p_2)$ and $\gamma^\star(q)g(p) \to q(p_1)\overline{q}(p_2)$ are

$$\hat{s} \equiv (q+p)^2 = 2pq - Q^2 = Q^2\frac{1-x}{x}\,, \tag{4.15}$$

$$\hat{t} \equiv (p_1-q)^2 = -2p_1q - Q^2 = -Q^2\frac{1-z_1}{x}\,, \tag{4.16}$$

$$\hat{u} \equiv (p_2-q)^2 = -2p_2q - Q^2 = -Q^2\frac{1-z_2}{x}\,. \tag{4.17}$$

Momentum conservation implies that $q + p = p_1 + p_2$ and

$$\hat{s} + \hat{t} + \hat{u} + Q^2 = 0\,. \tag{4.18}$$

In the following, the two real emission processes will be discussed in detail.

4.2.1 The gluon emission process

The matrix element of the gluon emission channel $\gamma^\star(q)q(p) \to q(p_1)g(p_2)$ reads [30, 70]

$$|\mathcal{M}_{2,\mathrm{q}}(p_1, p_2; p)|^2_{\mathrm{ME}} = \frac{8\pi\alpha_\mathrm{s}}{Q^2} C_\mathrm{F} \left[\frac{x^2 + z_1^2}{(1-x)(1-z_1)} + 2(1 - 3xz_1) \right] \cdot |\mathcal{M}_{1,\mathrm{q}}(q + xp; xp)|^2 \,, \tag{4.19}$$

with $\mathcal{M}_{1,\mathrm{q}}(q + p; p)$ the matrix element of the lowest order process.

In the parton shower approach two contributions to this final state emerge. First, the emission of the gluon from the initial-state quark with the final-state parton serving as spectator (IF) has to be considered. Second, the initial-state parton acts as the spectator of the final-state splitting $\mathrm{q} \to \mathrm{qg}$ (FI).

- IF.

  The "parton shower"-matrix element of the initial-state splitting with final-state spectator is obtained from eq. (3.101) and is given by

$$|\mathcal{M}_{2,\mathrm{q}}(p_1, p_2; p)|^2_{\mathrm{PSif}} \tag{4.20}$$
$$= \frac{1}{2pp_2} \frac{1}{x_{21,p}} 8\pi\alpha_\mathrm{s}\, C_\mathrm{F} \left[\frac{2}{1 - x_{21,p} + u_2} - (1 + x_{21,p}) \right] \cdot |\mathcal{M}_{1,\mathrm{q}}(q + xp; xp)|^2 \,,$$

  where the appropriate splitting function, eq. (3.93) with $\mu_k^2 = 0$, has been inserted. Employing the identities

$$x_{21,p} = \frac{p_1 p + p_2 p - p_2 p_1}{p_1 p + p_2 p} = \frac{\hat{u} + \hat{t} + \hat{s}}{\hat{u} + \hat{t}} = \frac{Q^2}{\hat{s} + Q^2} = x \,, \tag{4.21}$$

$$u_2 = \frac{p_2 p}{p_2 p + p_1 p} = \frac{\hat{t}}{\hat{u} + \hat{t}} = z_2 = 1 - z_1 \,, \tag{4.22}$$

$$\frac{1}{2pp_2 x} = \frac{1}{Q^2 pp_2/pq} = \frac{1}{Q^2(1 - z_1)} \,, \tag{4.23}$$

  the expression above becomes

$$|\mathcal{M}_{2,\mathrm{q}}(p_1, p_2; p)|^2_{\mathrm{PSif}} = \frac{8\pi\alpha_\mathrm{s}}{Q^2(1 - z_1)} C_\mathrm{F} \left[\frac{2}{2 - x - z_1} - (1 + x) \right] \cdot |\mathcal{M}_{1,\mathrm{q}}(q + xp; xp)|^2 \,. \tag{4.24}$$

- FI.

  In full analogy the shower expression for the final-state emission process yields

$$|\mathcal{M}_{2,\mathrm{q}}(p_1, p_2; p)|^2_{\mathrm{PSfi}}$$
$$= \frac{1}{2p_1 p_2} \frac{1}{x_{12,p}} 8\pi\alpha_\mathrm{s}\, C_\mathrm{F} \left[\frac{2}{1 - \tilde{z}_1 + (1 - x_{12,p})} - (1 + \tilde{z}_1) \right] \cdot |\mathcal{M}_{1,\mathrm{q}}(q + xp; xp)|^2 \,.$$

  With

$$x_{12,p} = \frac{p_1 p + p_2 p - p_1 p_2}{p_1 p + p_2 p} = x \quad \text{and} \quad \tilde{z}_1 = \frac{p_1 p}{p_1 p + p_2 p} = z_1 \,, \tag{4.25}$$

this can be cast into the form

$$|\mathcal{M}_{2,\mathrm{q}}(p_1, p_2; p)|^2_{\mathrm{PSfi}} = \frac{8\pi\alpha_\mathrm{s}}{Q^2(1-x)} C_\mathrm{F} \left[\frac{2}{2-x-z_1} - (1+z_1) \right] \cdot |\mathcal{M}_{1,\mathrm{q}}(q+xp; xp)|^2 ,$$
(4.26)

where in addition

$$2p_1 p_2 = Q^2 \frac{1-x}{x}$$
(4.27)

has been employed.

Combining the two parton shower contributions yields the final result, namely

$$|\mathcal{M}_{2,\mathrm{q}}(p_1, p_2; p)|^2_{\mathrm{PS}} = |\mathcal{M}_{2,\mathrm{q}}(p_1, p_2; p)|^2_{\mathrm{PSif}} + |\mathcal{M}_{2,\mathrm{q}}(p_1, p_2; p)|^2_{\mathrm{PSfi}}$$
$$= \frac{8\pi\alpha_\mathrm{s}}{Q^2} C_\mathrm{F} \left[\frac{x^2 + z_1^2}{(1-x)(1-z_1)} \right] \cdot |\mathcal{M}_{1,\mathrm{q}}(q+xp; xp)|^2 .$$
(4.28)

When comparing this with the exact perturbative result of eq. (4.19), it can be inferred that the parton shower exactly reproduces the soft and collinear singular structure of the matrix element as $z_1 \to 1$ or $x \to 1$. The only difference is an additional finite non-singular term present in the exact result.

4.2.2 The initial-state gluon channel

Expressed in terms of the leading order matrix element the exact real emission next-to-leading order result for the process $\gamma^\star(q)\mathrm{g}(p) \to \mathrm{q}(p_1)\overline{\mathrm{q}}(p_2)$ reads [30, 70]

$$|\mathcal{M}_{2,\mathrm{g}}(p_1, p_2; p)|^2_{\mathrm{ME}}$$
(4.29)
$$= \frac{8\pi\alpha_\mathrm{s}}{Q^2} T_\mathrm{R} \left[\frac{(z_1^2 + (1-z_1)^2)(x^2 + (1-x)^2)}{z_1(1-z_1)} + 8x(1-x) \right] \cdot |\mathcal{M}_{1,\mathrm{q}}(q+xp; xp)|^2 .$$

Starting from the leading order matrix element $\gamma^\star(q)\mathrm{q}(p) \to \mathrm{q}(p_1)$ there is only one possibility in the parton shower to reach the $2 \to 2$ process, the splitting of an initial-state gluon into $\mathrm{q}\overline{\mathrm{q}}$ and the q interacting with the off-shell photon. The second matrix element diagram, corresponding to the interaction of the anti-quark with the $\gamma^\star$, here has no parton shower counterpart. However, when starting the shower from the charge conjugated leading order process, namely $\gamma^\star(q)\overline{\mathrm{q}}(p) \to \overline{\mathrm{q}}(p_1)$, this contribution will occur while the $\gamma^\star \mathrm{q}$ interaction will be missing instead. The two terms are evaluated separately and then added incoherently.

- Emission off the quark.
  The case of an internal quark propagator is discussed first. According to eqs. (3.101) and (3.96) the parton shower approximation to the matrix element reads

  $$|\mathcal{M}_{2,\mathrm{g}}(p_1, p_2; p)|^2_{\mathrm{PSq}}$$
  $$= \frac{1}{2pp_2} \frac{1}{x_{21,p}} 8\pi\alpha_\mathrm{s} T_\mathrm{R} [1 - 2x_{21,p}(1-x_{21,p})] \cdot |\mathcal{M}_{1,\mathrm{q}}(q+xp; xp)|^2$$
  $$= \frac{8\pi\alpha_\mathrm{s}}{Q^2(1-z_1)} T_\mathrm{R} [1 - 2x(1-x)] \cdot |\mathcal{M}_{1,\mathrm{q}}(q+xp; xp)|^2 .$$
  (4.30)

- Emission off the anti-quark.

  Starting instead the shower from the $\overline{q}$ initiated process, and emitting the quark into the final state yields, correspondingly,

  $$|\mathcal{M}_{2,\mathrm{g}}(p_1, p_2; p)|^2_{\mathrm{PS}\overline{q}}$$

  $$= \frac{1}{2pp_1} \frac{1}{x_{12,p}} 8\pi\alpha_{\mathrm{s}} T_{\mathrm{R}} \left[1 - 2x_{12,p}(1 - x_{12,p})\right] \cdot |\mathcal{M}_{1,\overline{q}}(q + xp; xp)|^2$$

  $$= \frac{8\pi\alpha_{\mathrm{s}}}{Q^2 z_1} T_{\mathrm{R}} \left[1 - 2x(1 - x)\right] \cdot |\mathcal{M}_{1,\overline{q}}(q + xp; xp)|^2 . \qquad (4.31)$$

Due to the charge conjugation invariance of the leading order matrix element,

$$|\mathcal{M}_{1,\overline{q}}(q + xp; xp)|^2 = |\mathcal{M}_{1,\mathrm{q}}(q + xp; xp)|^2 , \qquad (4.32)$$

the two parton shower contributions can directly be combined and yield

$$|\mathcal{M}_{2,\mathrm{g}}(p_1, p_2; p)|^2_{\mathrm{PS}} = |\mathcal{M}_{2,\mathrm{g}}(p_1, p_2; p)|^2_{\mathrm{PSq}} + |\mathcal{M}_{2,\mathrm{g}}(p_1, p_2; p)|^2_{\mathrm{PS}\overline{q}}$$

$$= \frac{8\pi\alpha_{\mathrm{s}}}{Q^2} T_{\mathrm{R}} \left[\frac{x^2 + (1 - x)^2}{z_1(1 - z_1)}\right] \cdot |\mathcal{M}_{1,\mathrm{q}}(q + xp; xp)|^2 . \qquad (4.33)$$

Again the parton shower matches the soft and collinear behaviour of the matrix element given in eq. (4.29) and reproduces the exact result up to non-singular terms.

4.3 Associated production of a weak gauge boson and a light parton

The lowest order production process of weak gauge bosons ($W^{\pm}$, Z^0, $\gamma^{\star}$) at a hadron collider proceeds via the s-channel fusion of two initial-state quarks. Without losing generality $W^{\pm}$ boson production will be investigated in the following. The leading order process then simply reads $q\overline{q}' \to W^{\pm}$. At order α_{s} there are three processes emerging: $q\overline{q}' \to W^{\pm}g$, $g\overline{q}' \to W^{\pm}\overline{q}$ and $qg \to W^{\pm}q'$. Considering on-shell $W^{\pm}$ bosons for simplicity,[7] only $2 \to 2$ processes have to be discussed, which can be described using the Mandelstam variables

$$\hat{s} \equiv (p_1 + p_2)^2 = 2p_1 p_2 , \qquad (4.34)$$

$$\hat{t} \equiv (p_1 - p_3)^2 = -2p_1 p_3 , \qquad (4.35)$$

$$\hat{u} \equiv (p_2 - p_3)^2 = -2p_2 p_3 . \qquad (4.36)$$

Momentum conservation then implies that

$$\hat{s} + \hat{t} + \hat{u} = m_{\mathrm{W}}^2 , \qquad (4.37)$$

where m_{W} denotes the $W^{\pm}$-boson mass.

4.3.1 The gluon emission channel

The first channel to be discussed is the gluon emission process $q\overline{q}' \to W^{\pm}g$. At tree-level, there are two Feynman diagrams contributing to the matrix element, cf. figure 9. The

---

[7]This corresponds to neglecting the off-shell gauge boson decays which, however, do not affect the QCD dynamics of the processes under consideration. The decay products of the gauge boson can be introduced into the process using the narrow-width-approximation, or by incorporating the full off-shell $W^{\pm}$ propagator.
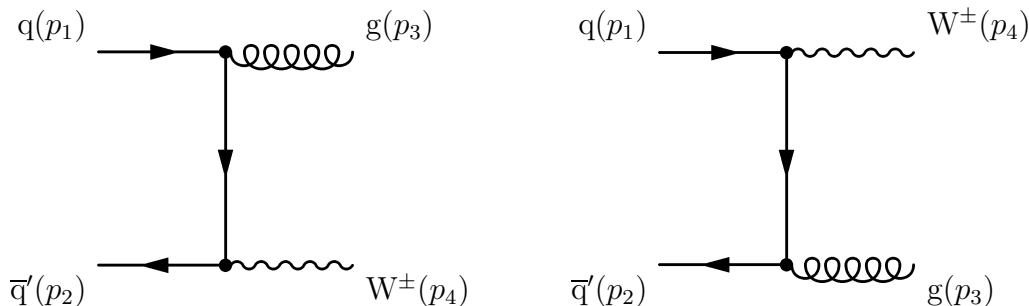
Figure 9: The leading order Feynman diagrams contributing to the process $q\overline{q}' \to W^\pm g$.

partonic differential cross section can be written as [70]

$$\frac{d\hat{\sigma}}{d\hat{t}}\bigg|_{ME} = \frac{\hat{\sigma}_0}{\hat{s}} \frac{\alpha_s}{2\pi} C_F \left[\frac{\hat{t}^2 + \hat{u}^2 + 2m_W^2 \hat{s}}{\hat{t}\hat{u}} \right], \qquad (4.38)$$

with $\hat{\sigma}_0$ the cross section of the leading order process $q\overline{q}' \to W^\pm$

$$\hat{\sigma}_0 = \frac{\pi}{3\hat{s}} \frac{g_W^2}{4}, \qquad (4.39)$$

where CKM-effects have been ignored. In the parton shower approach there are two ways to produce the final-state gluon, which have to be added incoherently: either the gluon can be emitted from the initial-state quark or from the anti-quark.

- Emission off the quark.

  As a first step, the kinematical variables used in the parton shower approximation should be related to the Mandelstam variables. In the first case, the initial quark as emitter and the initial anti-quark as spectator, the parton shower variables become, cf. section 3.4,

$$\tilde{v}_3 = \frac{p_3 p_1}{p_1 p_2} = -\frac{\hat{t}}{\hat{s}} \quad \text{and} \quad x_{3,12} = \frac{p_1 p_2 - p_3 p_1 - p_3 p_2}{p_1 p_2} = \frac{\hat{s} + \hat{t} + \hat{u}}{\hat{s}} = \frac{m_W^2}{\hat{s}}. \quad (4.40)$$

Using the appropriate splitting function of eq. (3.128), the parton shower differential cross section

$$\frac{d\hat{\sigma}}{d\tilde{v}_3}\bigg|_{PSq} = \hat{\sigma}_0 \frac{\alpha_s}{2\pi} \frac{1}{\tilde{v}_3} C_F \left[\frac{2}{1 - x_{3,12}} - (1 - x_{3,12}) \right] \qquad (4.41)$$

can be cast into

$$\frac{d\hat{\sigma}}{d\hat{t}}\bigg|_{PSq} = \hat{\sigma}_0 \frac{\alpha_s}{2\pi} C_F \frac{1}{-\hat{t}} \left[\frac{2}{1 - x_{3,12}} - (1 - x_{3,12}) \right]. \qquad (4.42)$$

Using the relation

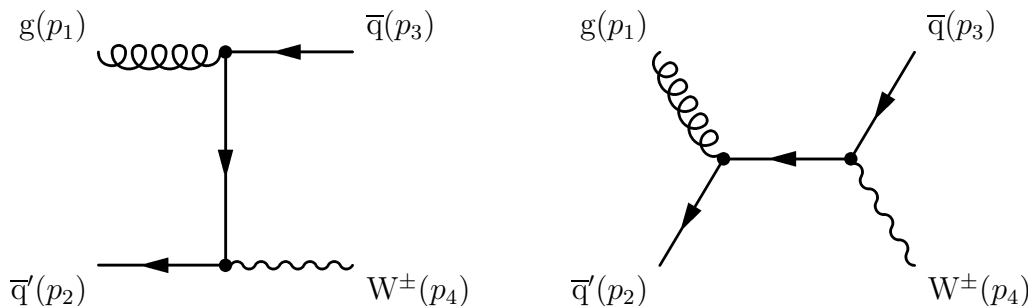$$(1 - x_{3,12}) = -\frac{\hat{t} + \hat{u}}{\hat{s}} \qquad (4.43)$$

Figure 10: The leading order Feynman diagrams contributing to the process $g\overline{q}' \to W^{\pm}\overline{q}$.

and multiplying with $\hat{s}/\hat{s}$ yields

$$\left.\frac{d\hat{\sigma}}{d\hat{t}}\right|_{\mathrm{PSq}} = \frac{\hat{\sigma}_0}{\hat{s}}\,\frac{\alpha_{\mathrm{s}}}{2\pi}\,C_{\mathrm{F}}\left[\frac{\hat{s}^2+m_{\mathrm{W}}^4}{\hat{t}(\hat{t}+\hat{u})}\right]\;. \tag{4.44}$$

- Emission off the anti-quark.

  Swapping the rôle of the emitter and the spectator parton amounts to only interchanging $\hat{t}$ and $\hat{u}$ in the results above. Accordingly, the differential cross section in this case is given by

$$\left.\frac{d\hat{\sigma}}{d\hat{t}}\right|_{\mathrm{PS}\overline{q}} = \frac{\hat{\sigma}_0}{\hat{s}}\,\frac{\alpha_{\mathrm{s}}}{2\pi}\,C_{\mathrm{F}}\left[\frac{\hat{s}^2+m_{\mathrm{W}}^4}{\hat{u}(\hat{t}+\hat{u})}\right]\;. \tag{4.45}$$

The full parton shower result is the sum of the two contributions and reads

$$\left.\frac{d\hat{\sigma}}{d\hat{t}}\right|_{\mathrm{PS}} = \left.\frac{d\hat{\sigma}}{d\hat{t}}\right|_{\mathrm{PSq}} + \left.\frac{d\hat{\sigma}}{d\hat{t}}\right|_{\mathrm{PS}\overline{q}} = \frac{\hat{\sigma}_0}{\hat{s}}\,\frac{\alpha_{\mathrm{s}}}{2\pi}\,C_{\mathrm{F}}\left[\frac{\hat{s}^2+m_{\mathrm{W}}^4}{\hat{t}\hat{u}}\right]\;. \tag{4.46}$$

Again, the parton shower approach provides the correct description for soft and collinear phase-space configurations but misses non-singular terms. The difference of the parton shower and the exact result can be quantified by the ratio

$$\frac{d\hat{\sigma}/d\hat{t}|_{\mathrm{ME}}}{d\hat{\sigma}/d\hat{t}|_{\mathrm{PS}}} = \frac{\hat{t}^2+\hat{u}^2+2m_{\mathrm{W}}^2\hat{s}}{\hat{s}^2+m_{\mathrm{W}}^4} = 1 - \frac{2\hat{t}\hat{u}}{\hat{s}^2+m_{\mathrm{W}}^4}\,, \tag{4.47}$$

which can take values between 0.5 and 1 in full agreement with the result of the parton shower algorithm implemented in PYTHIA [71]. This indicates that the parton shower approximation tends to overestimate the matrix element - a feature also present in $e^+e^- \to q\bar{q}g$, but not in the deep inelastic scattering processes.

4.3.2 The initial-state gluon case

There are two Feynman diagrams, cf. figure 10, contributing to the channel with an initial-state gluon, i.e. to the process $g\overline{q}' \to W^{\pm}\overline{q}$. The result of the full matrix element calculation reads [70]

$$\left.\frac{d\hat{\sigma}}{d\hat{t}}\right|_{\mathrm{ME}} = \frac{\hat{\sigma}_0}{\hat{s}}\,\frac{\alpha_{\mathrm{s}}}{2\pi}\,T_{\mathrm{R}}\left[\frac{\hat{s}^2+\hat{u}^2+2m_{\mathrm{W}}^2\hat{t}}{-\hat{s}\hat{t}}\right]\;. \tag{4.48}$$

In the parton shower approach only one emission process contributes to this channel, corresponding to the t-channel diagram. The s-channel contribution is not realised in the shower ansatz. Using the definitions of the shower variables as given above and the corresponding splitting function, cf. eq. (3.131), the parton shower cross section reads

$$
\left.\frac{\mathrm{d}\hat{\sigma}}{\mathrm{d}\hat{t}}\right|_{\mathrm{PS}} = \frac{\hat{\sigma}_0}{\hat{s}} \frac{\alpha_{\mathrm{s}}}{2\pi} T_{\mathrm{R}} \frac{\hat{s}}{-\hat{t}} \left[1 - 2x_{3,12}(1 - x_{3,12})\right]
$$
$$
= \frac{\hat{\sigma}_0}{\hat{s}} \frac{\alpha_{\mathrm{s}}}{2\pi} T_{\mathrm{R}} \left[\frac{\hat{s}^2 + 2m_{\mathrm{W}}^2(\hat{t} + \hat{u})}{-\hat{s}\hat{t}}\right] , \tag{4.49}
$$

where

$$
(1 - x_{3,12}) = -\frac{\hat{t} + \hat{u}}{\hat{s}} \quad \text{and} \quad x_{3,12} = m_{\mathrm{W}}^2/\hat{s} \tag{4.50}
$$

has been used. The ratio of the parton shower and the matrix element result is

$$
\frac{\mathrm{d}\hat{\sigma}/\mathrm{d}\hat{t}|_{\mathrm{ME}}}{\mathrm{d}\hat{\sigma}/\mathrm{d}\hat{t}|_{\mathrm{PS}}} = \frac{\hat{s}^2 + \hat{u}^2 + 2m_{\mathrm{W}}^2\hat{t}}{\hat{s}^2 + m_{\mathrm{W}}^4(\hat{t} + \hat{u})} = 1 + \frac{\hat{u}(\hat{u} - 2m_{\mathrm{W}}^2)}{(\hat{s} - m_{\mathrm{W}}^2)^2 + m_{\mathrm{W}}^4} , \tag{4.51}
$$

varying between 1 and 3 [71]. Accordingly, the parton shower ansatz tends to undershoot the exact matrix element. However, the shower is constructed to give the correct answer in the logarithmically enhanced phase-space regions and thus has the correct limiting behaviour in the soft and collinear limits. The differences identified here are a result of differences in the non-singular terms, contributing only in hard regions of phase space. The process qg → W$^{\pm}$q$'$ closely follows the above example solely $\hat{t}$ and $\hat{u}$ have to be exchanged. This leads to the same qualitative results and the same conclusions.

5. Applications

In this section, the abilities of the newly developed parton shower formulation in describing QCD dynamics will be highlighted by comparing its results for various physics processes with experimental data and other calculations: In section 5.1, the predictions for hadron production in e^+e^- collisions as measured at LEP will be studied and some results related to a future machine operated at $\sqrt{s} = 500\,\mathrm{GeV}$ will be discussed. In section 5.2, emphasis is put on the capabilities of the shower to describe particle production at hadron colliders such as the Tevatron or the upcoming LHC.

5.1 Jet production at e^+e^- colliders

Measurements of hadronic final states produced in e^+e^- collisions provide a very precise probe of QCD dynamics in the final state and an excellent means to deduce its fundamental parameters such as the value of $\alpha_S(m_Z)$, see for instance [72], and the colour charges C_F and C_A in three- and four-jet events as discussed e.g. in [72]–[75]. Therefore it is not surprising that in the past years calculations for relevant three-jet observables, such as thrust, have become available at NNLO [76] and that full parton-level Monte Carlo codes for four-jet final states at NLO have been constructed [77, 78]. Obviously such

observables also provide a critical test of the corresponding final-state radiation piece of a parton shower model. However, due to the fragmentation of partons into hadrons, which at the moment can be simulated with phenomenological models only, the parton shower predictions can not directly be compared with experimental data but rather have to be supplemented with a hadronisation model. The new parton shower presented here therefore has been interfaced to the Lund string fragmentation routines of Pythia version 6.2 [79] in the framework of the Sherpa event generator. The large number of very precisely measured observables at various energies allows tuning the intrinsic parameters of the parton shower in conjunction with the phenomenological parameters of the fragmentation model. Such a procedure has been performed, for instance, for the new parton shower and fragmentation code in Herwig++ [80]. In principle, such a tuning is a very time-consuming and delicate procedure, see for instance [81], deserving a publication in its own right. Recent developments to automatise the task of generator tuning and validation to a large extend are reported in [82]. Here, only a very limited tuning based on few parameters and observables only has been performed. The results of this tuning are presented in section 5.1.1. In section 5.1.2 the focus is on heavy-quark production at LEP1 and ILC energies to validate the treatment of finite parton masses in the shower model.

5.1.1 Comparison with LEP1 data

The most extensive data set available to validate QCD Monte Carlo predictions are LEP measurements at the Z^0 pole. A selection of event shape variables, multiplicity distributions, differential jet rates, four-jet angle measurements and various particle momentum distributions have been used to select values for the unconstrained, phenomenological parameters of the simulation, namely the value of the strong coupling constant at m_Z, the infrared shower cut-off $\mathbf{k}_{\perp,0}$ and the three Lund string hadronisation parameters a (PARP(41)), b (PARP(42)) and σ_q (PARP(21)). For the results presented in the following, they have been fixed to $\alpha_s(m_Z) = 0.125$, $\mathbf{k}_{\perp,0} = 0.63\,\text{GeV}$, $a = 0.33$, $b = 0.75\,\text{GeV}^{-2}$, and $\sigma_q = 0.358\,\text{GeV}$, respectively. This yields a mean charged multiplicity per event of $\langle N_{\text{ch}} \rangle = 20.87$ at $\sqrt{s} = m_Z$, in good agreement with the experimentally found value of $\langle N_{\text{ch}} \rangle = 20.92 \pm 0.24$ [83].

Figures 11 to 14 show some exemplary results obtained with the new shower implementation compared to Delphi LEP1 data at $\sqrt{s} = 91.2\,\text{GeV}$ [83].

In figure 11 the new algorithm, denoted as "CS shower" in the following, is compared with some event-shape measurements by Delphi [83]. The distributions of thrust, thrust-major, thrust-minor and aplanarity are displayed. The lower panel of each plot contains the bin-wise ratio (MC-data)/data, and the yellow bands show the statistical plus systematic error of the respective measurements. All the observables are sensitive to the pattern of QCD radiation probing both soft and hard emissions off the shower initiating $q\bar{q}$ pair. The Monte Carlo predictions agree very well with the event-shape data. There is some slight excess at very low $1 - T$ corresponding to two-jet like events. This region of phase space however is very sensitive to hadronisation corrections and therefore dominated by non-perturbative physics. The same reasoning holds for the major and minor distributions at low M or m.
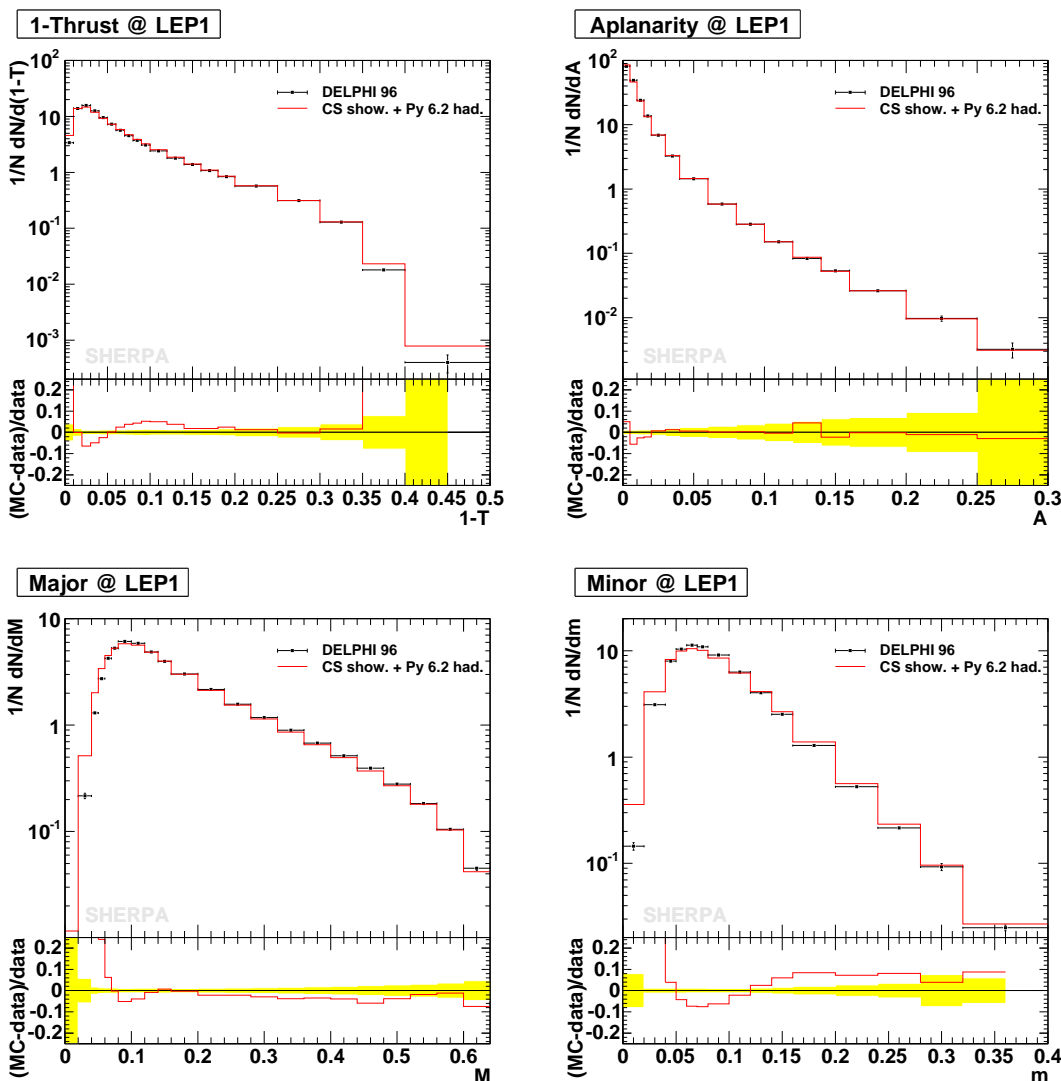
Figure 11: The event-shape variables 1−Thrust $(1 − T)$, Aplanarity (A), Major (M) and Minor (m) in comparison with DELPHI data [83].

The transverse-momentum distribution within and out of the event plane defined by the thrust and thrust-major axes, (p_T^{in}) and (p_T^{out}), respectively, are presented in figure 12. While p_T^{in} is quite well modeled by the Catani-Seymour shower, p_T^{out} is significantly underestimated for values above 1 GeV. This tendency, however, is observed in other QCD Monte Carlo simulations as well [83].

In figure 13 the predictions for the exclusive two-, three-, four- and five-jet rates in the Durham algorithm [84] as a function of the jet resolution y_{cut}^{Durham} are compared with data taken by the DELPHI experiment [85]. They all exhibit a sufficient agreement with data within the experimental uncertainty bands. For the four- and five-jet rate the shower seems to underestimate the region of $y_{cut}^{Durham} \approx 0.001$, however, this region is also affected by
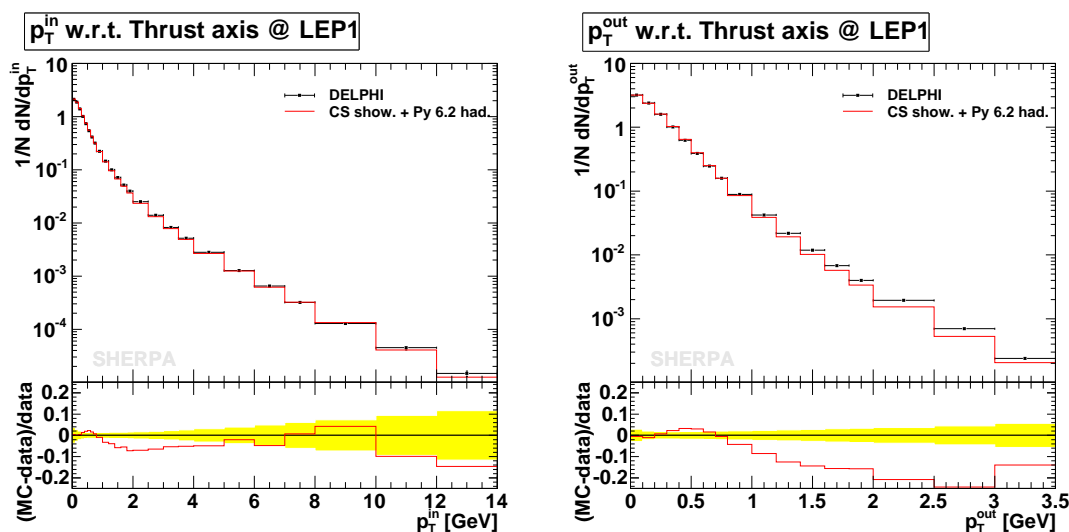
Figure 12: The p_T^{in} and p_T^{out} observables measured with respect to the thrust axis compared to a DELPHI measurement [83].

hadronisation effects and a more sophisticated tuning may provide an even better agreement with data here. The dependence on the choice of hadronisation parameters is even more pronounced for jet resolutions smaller than 0.001 where the results for the new shower preferably lie on the upper side of the experimental uncertainty band.

The last observables to be considered are jet angular distributions in events with four jets. These observables can not be expected to be too well described by this parton shower model as they should probe spin correlations of the produced partons. Such correlations, however, are not taken into account here. Anyway, a complete description of these effects requires full matrix element calculations (eventually combined with a parton shower) [11, 86]. In figure 14, the predictions for the Bengtsson-Zerwas [87] and the Nachtmann-Reiter [88] angle are compared with DELPHI data [85] for events with four jets, defined in the Durham algorithm with at a jet resolution $y_{\mathrm{cut}}^{\mathrm{Durham}} = 0.008$. Both results agree surprisingly well with data. A similar level of agreement is observed for the other two prominent four-jet angles, α_{34} and the Körner-Schierholz-Willrodt angle, that are not shown here.

5.1.2 Jet rates in heavy-quark production

The leading order of heavy-quark production at lepton colliders also proceeds through an intermediate γ^* or Z^0 in the s-channel. Since pair production of top-quarks was outside the kinematical reach of LEP, only the production of bottom-quarks is available at these energies to discuss the treatment of heavy quarks in the new parton shower algorithm. At a future international linear collider (ILC), operating at or around $\sqrt{s} = 500\,\mathrm{GeV}$, pair production of top-quarks will play a key rôle in the physics programme. This is also true for the LHC where top-quarks will copiously be produced and constitute a major background in nearly all searches for new physics. Therefore, a correct description of the radiation pattern of heavy quarks will be of enormous importance. As already hinted at in
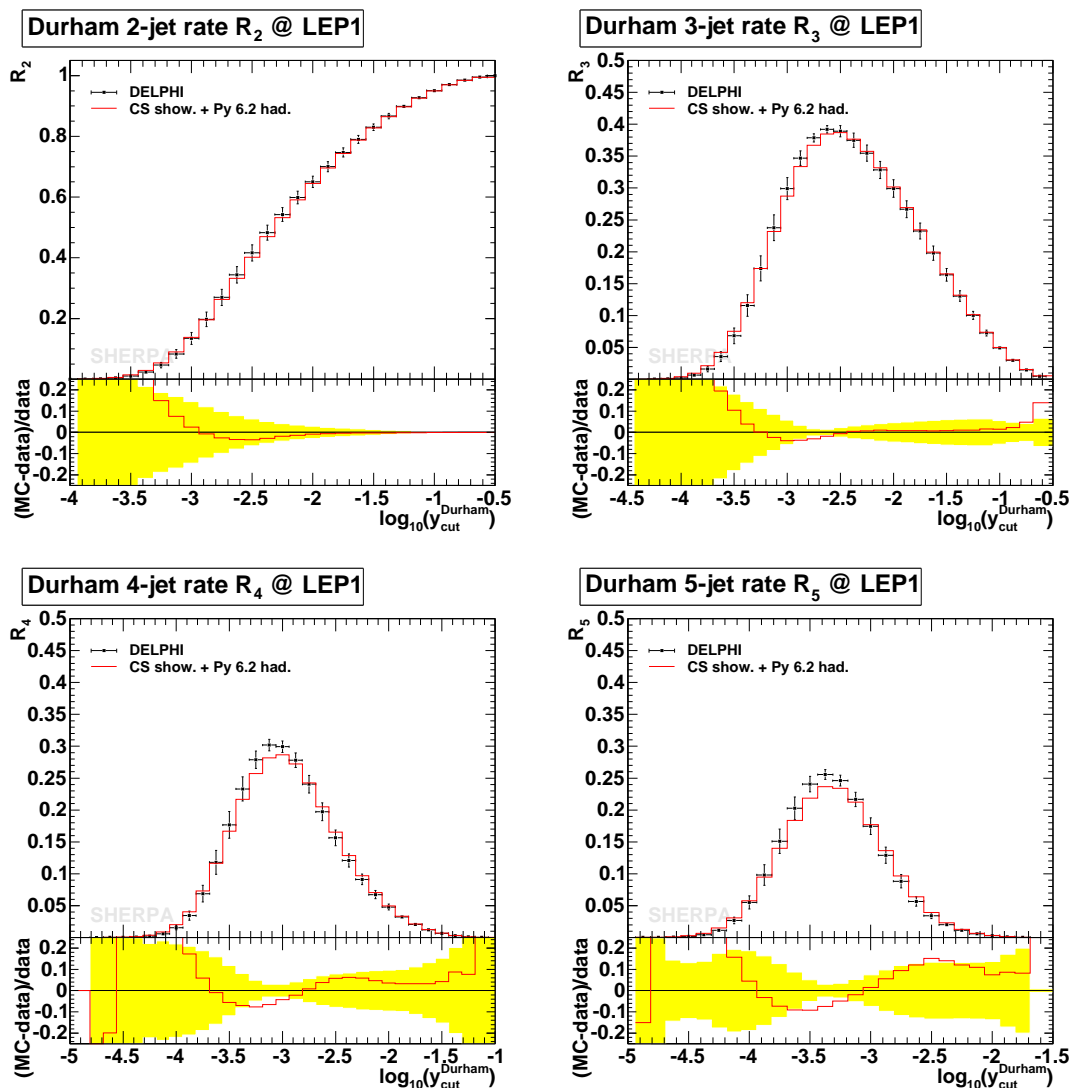
Figure 13: The n-jet rates R_n for the Durham jet algorithm as a function of the jet-resolution parameter y_{cut}^{Durham}. Data taken from [85].

section 3.1.1, radiation off massive quarks is suppressed with respect to the case $m_Q = 0$, also known as "dead-cone"-effect [46]. The impact is however rather small when considering b-quark masses of $4.8\,\mathrm{GeV}$ at collider energies that are much larger. To illustrate the impact of the finite b-quark mass in the shower approach the Durham two- and three-jet rates for $b\bar{b}$-production at LEP1 are presented in the left panel of figure 15. There, results are shown for the fully massive case (i.e. the mass has fully been taken into account in the splitting kernels, the phase-space boundaries and the splitting kinematics) and for the massless case are depicted. As expected, in the massive case both R_2 and R_3 are slightly enhanced at low values of y_{cut}^{Durham}, corresponding to the suppressions of additional radiation that turns a two-jet event into three-jet and a three-jet into a four-jet event at the scale of the emission.
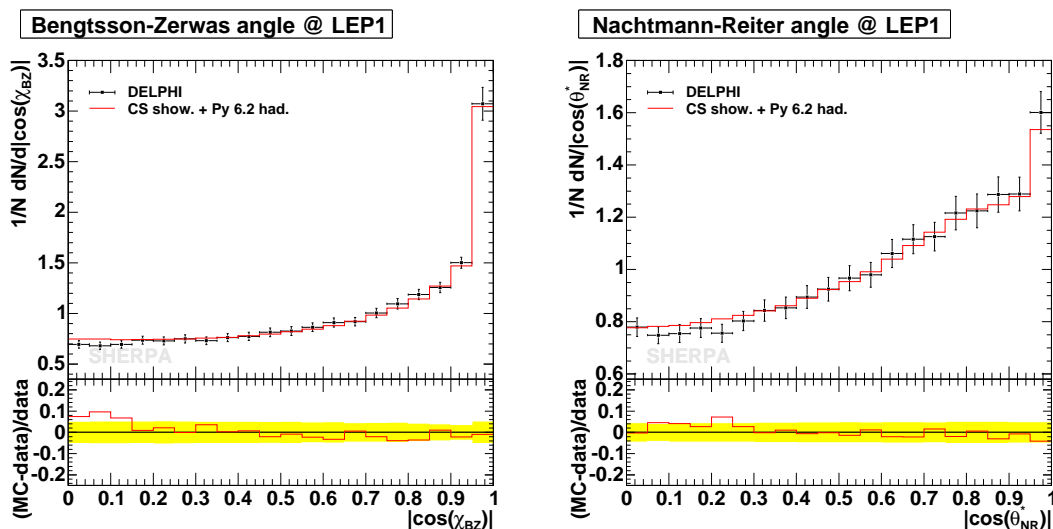
Figure 14: The Bengtsson-Zerwas and Nachtmann-Reiter four-jet angles compared with DELPHI data [85].
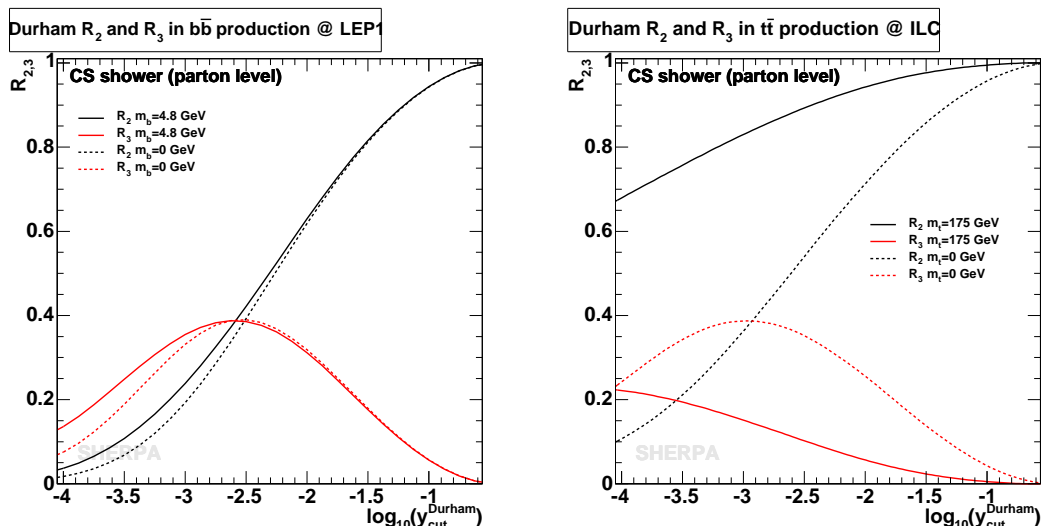
Figure 15: The exclusive Durham two- and three-jet rates in inclusive $b\bar{b}$ production at LEP1 (left panel) and $t\bar{t}$ production at a $500\,\mathrm{GeV}$ linear collider (right panel). The solid curves correspond to fully taking into account the quark masses in the parton shower simulation while for the dashed predictions the finite masses have been neglected.

In the right panel of figure 15 the same observables are presented, but this time for the pair-production of $175\,\mathrm{GeV}$ top-quarks at a $500\,\mathrm{GeV}$ ILC. Obviously, the finite mass has to be taken into account in the description of QCD radiation off top-quarks, since the differences with respect to the massless case can exceed an order of magnitude for the two-jet rate.

5.2 Particle production in hadron collisions

With the advent of the LHC era, the description and simulation of particle production processes at hadron colliders gained even more relevance. Due to the colour-charged partonic initial states, *every* hard process at hadron colliders is accompanied by initial- and subsequent final-state radiation. In the following, only two examples shall be considered to highlight the performance of the new parton shower model in such situations. First, the inclusive production of Drell-Yan lepton pairs, the simplest process that features initial-state emitter — initial-state spectator dipoles, and, second, QCD jet production are discussed. For the latter, besides looking at some inclusive two-jet distributions, three-jet observables sensitive to the inclusion of QCD colour coherence are considered and qualitatively compared with data.

For all the predictions presented below, the CTEQ6L set of PDFs [89] has been used, the strong coupling constant has been fixed to $\alpha_s(m_Z) = 0.118$ with its running taken at two-loop level, in accordance with the choice in the PDF, and the infrared cut-off of the shower is chosen to be $\mathbf{k}_{\perp,0} = 2\,\text{GeV}$. Hadronisation of the partonic shower final states is again accomplished by an interface to the Lund string routines of PYTHIA 6.2 [79].

5.2.1 Inclusive gauge boson production

The production of electroweak gauge bosons, e.g. $W^\pm$ and Z^0 bosons, and their subsequent decay into leptonic final states, is one of the most prominent processes at hadron colliders due to their clean signature. Although very interesting in their own right, their inclusive production, i.e. their production together with additional QCD jets, represents a serious background to many other interesting processes, like, e.g. the production and decay of top-quarks or SUSY particles. Therefore, many theoretical efforts have been undertaken to predict gauge boson production as precisely as possible, both at fixed order in the strong coupling, see for instance [90]–[94], or focusing on the analytical resummation of large logarithms from soft gluon emissions, see for example [95]–[99]. An important ingredient in all cases have been parametrisations of the PDFs and a good perturbative control over their scaling behaviour, which by now is known at the three-loop level [100]. In addition, in the past few years, Drell-Yan production formed the testbed for approaches aiming at the combination of tree-level matrix elements with parton shower Monte Carlos [17, 20, 27, 101, 102]. Parton shower Monte Carlos thereby have to deliver the correct description for the bulk of the events where the bosons are accompanied by rather soft emissions only.

In the following, Drell-Yan production of γ^*/Z^0 at Tevatron Run I energies is considered with the bosons decaying into e^+e^--pairs. They are constrained to fall into a mass-window of $66\text{ GeV} < M_{e^+e^-} < 116\text{ GeV}$. The predictions of the new shower algorithm will directly be compared to results obtained with the matrix element-parton shower merging approach as implemented in SHERPA. To this end, an inclusive sample combining matrix elements for no extra emission and one extra final-state QCD parton has been generated with SHERPA version 1.0.10. In the figures this sample will be denoted by "SHERPA 1.0.10 CKKW (0+1 jet ME)".
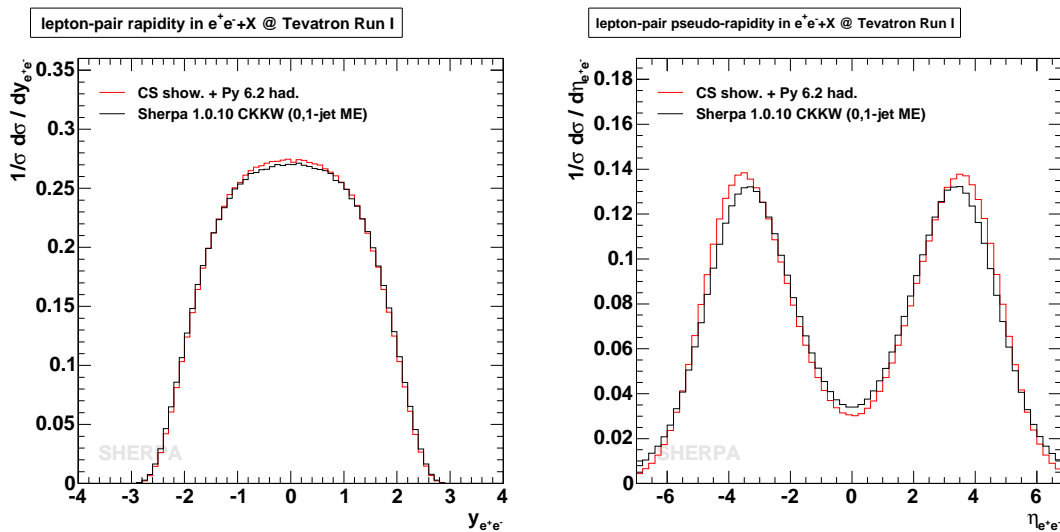
Figure 16: The rapidity- (left panel) and pseudo-rapidity (right panel) distribution of e^+e^- Drell-Yan pairs produced in $p\bar{p}$ collisions at $\sqrt{s} = 1800\,\text{GeV}$.

The discussion of the results starts with the rapidity- and pseudo-rapidity distributions of the produced lepton-pair, see figure 16. As the shape of the former is already described well at the leading order, i.e. without any radiation, there is hardly any difference visible for the two results. The gauge boson pseudo-rapidity distribution however, only emerges when there is some additional QCD radiation. The radiation pattern, and especially the hardest emission, determines this leptonic observable. The pure shower result is in excellent agreement with the merged result, which contains the exact tree-level matrix element for the first hard emission. However, the shower distribution is somewhat lower at central pseudo-rapidity and slightly exceeds the merged SHERPA result for the two maxima around $\eta_{e^+e^-} \approx \pm 4$. These differences can be traced back to the lack of sufficiently hard radiation in the shower, which is constrained from above through the default shower start scale for this process, namely the invariant mass squared of the initial dipoles, $M_{e^+e^-}^2$. Below that scale, however, the parton shower can be expected to deliver reliable results, and in order to fill the phase space above that scale, matrix element-parton shower merging techniques should be added.

The smaller amount of hard radiation can be further quantified by looking at the differential jet rates d_1 and d_2 for the $k_\perp$-jet algorithm [103], displayed in figure 17. These observables determine the scales where the first (d_1) and second (d_2) additional parton gets resolved as a jet from the core process. The results for the Catani-Seymour based shower and the merged SHERPA sample agree well for small cluster scales but, as can be expected, the shower is significantly lower for values of $d_i > m_Z$.

The last observable to be considered is the transverse momentum distribution of the lepton-pair. This distribution has been measured with high precision by the Tevatron experiments. Like the Drell-Yan pseudo-rapidity it is very sensitive to both soft and hard radiation accompanying the produced boson. Figure 18 contains a comparison of the
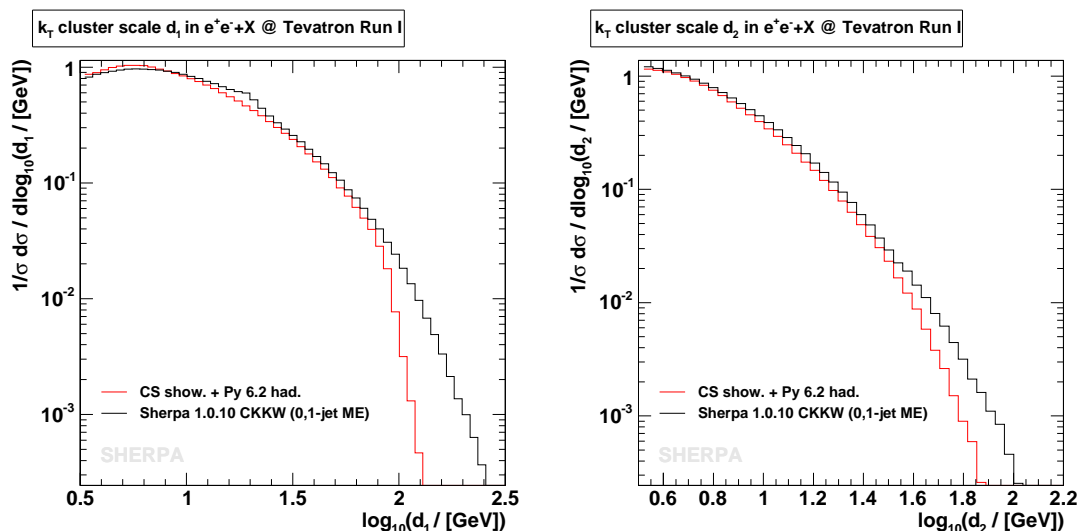
Figure 17: The $k_\perp$ differential jet rates d_1 and d_2 in $e^+e^- + X$ production at Tevatron Run I.
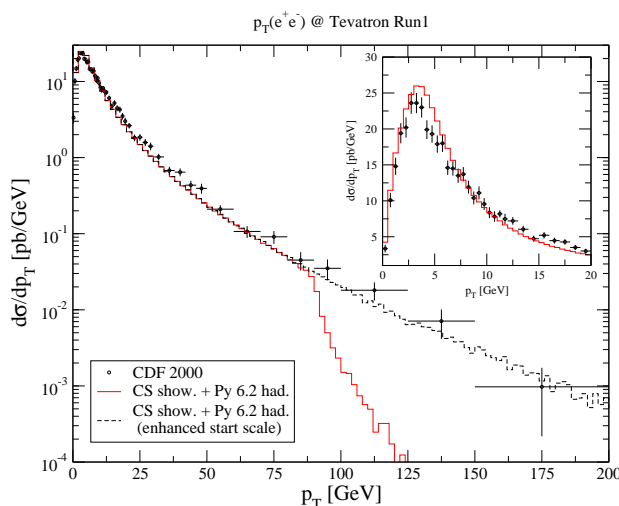

Figure 18: The $p_\perp$ distribution of e^+e^- Drell-Yan pairs in comparison with data from CDF at the Tevatron, Run I [104].

prediction from the new shower model with a CDF measurement [104].[8] The agreement between data and simulation is quite good up to p_T's of approximately 80 GeV. The upper-right part of figure 18 contains a blow-up of the low transverse-momentum region of $p_T <$ 20 GeV, this time, however, on a linear scale. There, the parton shower describes the turn-on of the distribution quite nicely, the actual peak, however, is slightly higher and a bit broader than seen in data. To describe the very low transverse-momentum region a

---

[8]A comparison of the merged SHERPA prediction with this data has already been presented in [17].

Gaussian-smeared intrinsic $k_\perp$ was introduced, with a mean of $0.52\,\mathrm{GeV}$ and a width of $0.8\,\mathrm{GeV}$. This smearing is applied, after the shower terminated, to the primary, low-scale "initiator" partons, and it can be thought of as a residual effect due to their binding in the proton. In this model, similar to the one in Pythia, the intrinsic primordial transverse momentum is spread over all final state particles in due proportion, since the $k_\perp$-kick rotates the full shower. A more detailed tuning of these values combined with the shower cut-off $\mathbf{k}_{\perp,0}$ may yield an even better description of the distribution's peak.[9] Above $80\,\mathrm{GeV}$ the parton shower dies off very rapidly due to its phase space being constrained by the choice of the starting scale, $\mathbf{k}_{\perp,\mathrm{max}}^2 = M_{e^+e^-}^2$. For illustrative purposes a prediction has been added where the start scale has been enhanced to $4M_{e^+e^-}^2$. While the results at low p_T do not change significantly, the distribution continues in the tail, thereby following the experimental data. But, of course, with this choice of parton shower starting scale, there is a similar drop-off of the distribution at scales of around $4M_{e^+e^-}^2$. However, since there is no guarantee that the parton shower kernels perform well enough at large scales, i.e. outside the soft- and collinear phase-space regions, it seems to be overly optimistic to stretch its predictions to such high scales. Instead, the parton shower description should consistently be improved by incorporating exact higher-order corrections.

5.2.2 Inclusive jet production

The most obvious QCD production process to look for at hadron colliders is inclusive jet production. However, from a theoretical point of view this is quite a complicated process. Besides tree-level calculations for up-to six final-state jets, so far, there merely exist full next-to-leading order results up-to three-jet production [38, 106]–[109]. Despite of strong efforts, culminating in evaluating the complete set of necessary matrix elements [110]–[114] and in developing methods to isolate the infrared divergences in the real correction part [115] a full NNLO calculation for inclusive jet production has not been finished yet. Also, from the point of view of the parton shower presented here, jet production at hadron colliders is rather involved. This is because the $2 \rightarrow 2$ hard process will contain all possible colour connections between initial-state and final-state partons. Hence, QCD jet production constitutes a severe test of the entire shower algorithm. The input parameters for the simulations have been chosen as specified above. The starting scale of the shower, however, is related to the transverse momentum of the $2 \rightarrow 2$ core process' outgoing partons, namely $\mathbf{k}_{\perp,\mathrm{max}}^2 = p_{\perp,j}^2$.

The first thing to be looked at is a very inclusive quantity, the dijet invariant mass. This has been measured by DØ during Run I [116]. The jets considered there have been reconstructed using a jet-cone algorithm with a cone opening angle of $R = 0.7$ in the $\eta - \phi$ space

---

[9]It should be noted here that in this parton shower model, apart from some intrinsic $k_\perp$, the lepton pair receives transverse momentum from splitting initial-initial dipoles only. Therefore, the first gluon emission into the final-state dominates the boson's p_T distribution. However, from [105] it is known that at sufficiently high energies the low-p_T region is also populated by events where two or more relatively high-p_T partons compensate each other. In this approach, such effects are mostly absent apart from configurations where an initial gluon splits into an initial and a final-state quark. The impact of those compensating configurations still remains to be studied.
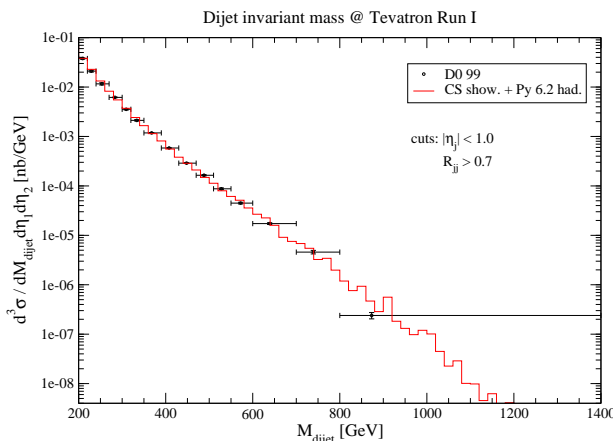
Figure 19: Dijet mass M_{dijet} measured by DØ at Tevatron Run I [116].

and with jet transverse energies above 30 GeV. Dijet candidates have then been subjected to the requirement that both jets satisfy $|\eta_j| < 1.0$. Figure 19 exhibits the resulting dijet-mass distribution starting at $M_{\mathrm{dijet}} > 200\,\mathrm{GeV}$. It is a very steeply falling spectrum spanning six orders of magnitude in the mass range under consideration. To compare with data the result of the (leading order) simulation has been normalised to the cross section observed in experiment. In fact, the prediction of the proposed shower algorithm then is in very good agreement with the data and almost everywhere exactly hits the weighted bin centers.

Another interesting observable when studying dijet events is the azimuthal angle between the two highest-p_T jets. If there is no additional QCD radiation the two jets have equal transverse momenta and they are oriented back-to-back. Thus, in this case, their azimuthal separation $\Delta\phi_{\mathrm{dijet}} = |\phi_1 - \phi_2|$ equals π. In the presence of merely soft radiation the azimuthal angles remain strongly correlated, the strength of the decorrelation rises with the presence of additional hard radiation. Therefore, the dijet decorrelation provides a testbed for soft- and hard QCD emissions without the necessity to reconstruct further jets. Figure 20 contains the results of a recent DØ measurement for cone jets found for $R = 0.7$ [117]. The data fall into different ranges of the leading-jet transverse momentum and are then multiplied with different constant prefactors in order to display them in one plot. In all cases, the second-leading jet was required to have a transverse momentum $p_T > 40\,\mathrm{GeV}$ and both jets are constrained to the central-rapidity region, $|y_j| < 0.5$. The data are overlayed with the respective predictions of the Catani-Seymour dipole shower approach. The simulation agrees very well with the data over the whole interval of $\Delta\phi_{\mathrm{dijet}}$ spanned by the experimental measurements. This is a very satisfying result as it proves that the proposed shower formulation not only correctly accounts for phase space regions related to soft and collinear radiation but also yields qualitatively and quantitatively correct estimates for rather hard emissions as well. Furthermore, since this observable is quite sensitive to model-intrinsic scale choices such as the shower start scale and scales entering the running coupling constant and parton density functions, this agreement proves that the defaults have been chosen correctly.
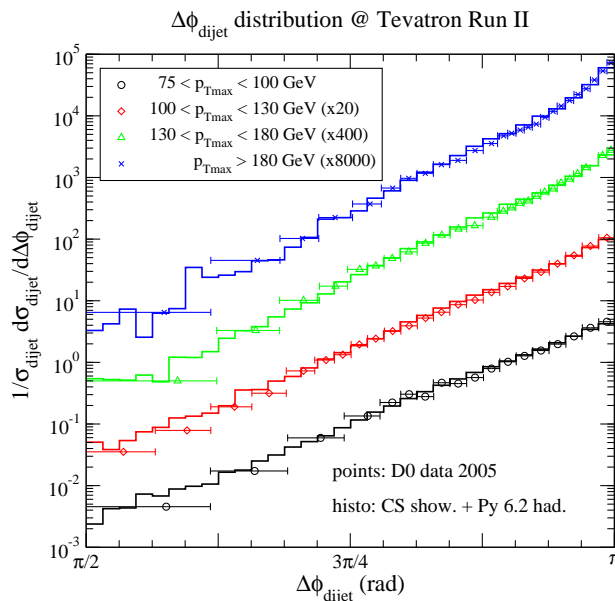
Figure 20: Azimuthal decorrelation in dijet events measured by DØ at Tevatron Run II [117].

The last item to be discussed are observables in QCD jet production at hadron colliders that are known to be sensitive to the correct treatment of QCD soft colour coherence in the parton shower simulation. Colour-coherence effects have been widely studied for e^+e^- collisions, for an early review see e.g. [118]. They manifest themselves in the fact that soft emissions are forbidden outside a certain angular cone around the emitting particle's direction, known as angular ordering [46, 50]. To account for this in shower Monte Carlos the phase space for allowed emissions has to be properly constrained. Within the HERWIG Monte Carlo for instance this is realised by evolving the shower in terms of cone-opening angles. While the situation for pure final-state showers is quite clear, in hadronic collisions the situation is slightly more complicated due to the presence of more colour flows, among them those that connect initial- and final-state partons. As colour-coherence here already influences the first emission from the initial- and final-state partons QCD three-jet events are the best place to look for the pattern of these phenomena at hadron colliders.

In one of the pioneering studies [119] three-jet events that feature a hard leading jet and a rather soft third jet have been considered. Observables potentially sensitive to colour coherence are spatial correlations between the third jet and the leading ones. In [119] such discriminating variables have been found and by comparison with Monte Carlo simulations evidence for the observation of colour coherence in hadron collisions has been provided. This ultimately has led to a refinement of the PYTHIA shower algorithm in order to appropriately model colour coherence in the spirit of [120]. In the CDF study [119] jets have been defined through a cone algorithm with a cone radius of $R = 0.7$ and the following event selection criteria have been applied:

- For the two leading jets the pseudo-rapidity is constrained to $|\eta_1| < 0.7$ and $|\eta_2| < 0.7$;
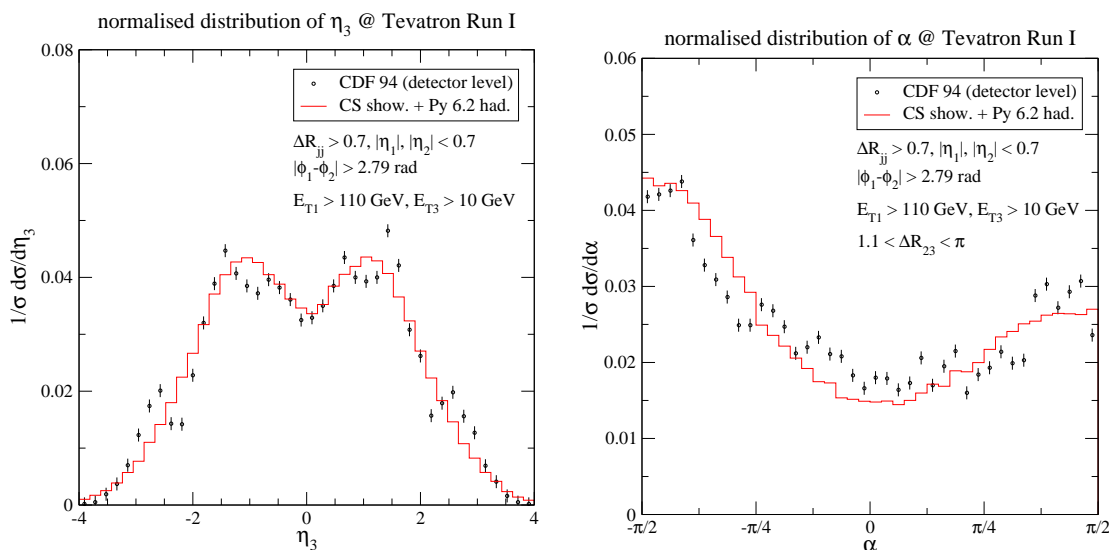
Figure 21: The pseudo-rapidity distribution of the third-hardest jet (left panel) and the distribution of the angle α (right panel) in inclusive QCD three-jet production in comparison with CDF data taking during Tevatron Run I. Experimental errors are statistical only. Histograms are normalised to one.

- they have to be back-to-back within 20 degrees in the transverse plane, corresponding to $|\phi_1 - \phi_2| > 2.79$ radian;

- and the transverse energy of the leading jet, E_{T1}, has to exceed $110\,\text{GeV}$, the third jet is required to have $E_{T3} > 10\,\text{GeV}$.

- Only for the study of the α variable defined below the additional cut $1.1 < \Delta R_{23} < \pi$, where $\Delta R_{23} = \sqrt{(\eta_2 - \eta_3)^2 + (\phi_2 - \phi_3)^2}$, is imposed.

A number of observables has been considered, the two most convenient and discriminating ones have been the pseudo-rapidity distribution of the third jet, η_3, and the polar angle in the space parametrised by $\Delta\phi = \phi_3 - \phi_2$ and $\Delta H = \text{sign}(\eta_2)(\eta_3 - \eta_2)$, namely $\alpha = \arctan(\Delta H/|\Delta\phi|)$.[10] It should be stressed that the published results, used for the comparison, are not corrected for detector effects, such as finite resolution and uninstrumented regions, and therefore can only qualitatively be compared with theoretical calculations. The results of the Monte Carlo simulations exhibited in [119] have passed the full chain of the CDF detector simulation. In figure 21 the measurements are compared with simulated events at the hadron level.[11] In the left panel the η_3 distribution is shown and the right

---

[10] A further observable considered in the CDF study is the spatial separation of the second- and third jet in the $\eta - \phi$ space, ΔR_{23}. This observable, however, seems to be less discriminatory between theoretical models. In addition, and more importantly, detector effects seem to have a larger impact on its discriminating power. Therefore it is not taken into account here.

[11] In [119] it is found that detector corrections are rather small for the η_3 distribution but somewhat larger for α. The basic shape of the distributions, however, is not altered by these effects.

panel contains the comparison of the α distribution. Both predictions agree well with the data. The η_3 distribution tends to be broader in models that take into account colour-coherence effects and only then theoretical calculations show the significant dip around $\eta_3 \approx 0$ seen in data.[12] The α variable is also very sensitive to the inclusion of colour coherence. It decreases from $\alpha = -\pi/2$ to $\alpha = 0$ but then the slope changes and the distribution rises as $\alpha \to \pi/2$. This trend is clearly seen for the simulation with the new shower algorithm. Models not taking into account coherence fail to describe the distribution's rise towards $\alpha \to \pi/2$ and have a clear excess of events at small $|\alpha|$. Concerning the interpretation of these results the missing detector smearing for the shower simulation has to be kept in mind. However, in ref. [119] estimates for the size of the detector effects are given, showing that the impact of the finite detector resolution is much smaller than the size of the physical effects. The generic features of the two observables presented here are not dependent on detector effects, and they are well described by the new shower formulation.

The conclusion of this is that the proposed parton shower algorithm with its notion of emitter-spectator dipoles associated with the color flow of the event and using transverse momenta as evolution variable accounts for soft colour coherence and yields a very satisfying description, both on the qualitative and the quantitative level. It can be anticipated that such non-trivial quantum phenomena are of large importance at the LHC, since the phase space for jet production is much larger and hard jets are produced copiously. For a solid description of QCD therefore the systematic and correct inclusion of these effects is paramount.

6. Conclusions and outlook

In this publication a parton shower model based on Catani-Seymour dipole subtraction kernels has been presented, which was proposed for the first time in [1, 2]. In the present implementation, the original proposal is extended to cover also initial-state splittings, finite parton masses, and QCD radiation off SUSY particles.

Choices concerning the evolution parameter of the parton shower and the various scales entering running coupling constants, PDFs, etc. have been detailed, fixing the full algorithm. The kinematics of massive splittings has been presented in some detail, and the corresponding massless limits have been discussed. By direct comparison with some benchmark processes, at first order in α_s, the differences of the parton shower approximation with respect to exact results have been worked out. It has been shown that indeed the parton shower algorithm presented here reproduces the soft and collinear limits of the exact matrix elements and that differences between both results are non-singular terms only. Some first results with this new parton shower formulation have been presented and show very encouraging agreement with other models and with experimental data.

In the near future, this new algorithm will be fully incorporated into the SHERPA framework and it will be made publicly available in the next releases of the code. This

---

[12]The HERWIG Monte Carlo, incorporating colour coherence through explicit angular ordering, describes the data very well. Switching on the approximate version of angular ordering in PYTHIA, realised by a veto on rising opening angles during shower evolution, significantly improves PYTHIA's agreement with data.

will also involve a more careful tuning of the shower parameters and the inputs of the hadronisation models provided by or linked to SHERPA, which surely will further improve the agreement with data. Planned is a detailed comparison against another new shower ansatz that is based on splitting colour dipoles [121], and that is also being developed in the SHERPA framework at present. In addition, a full merging with multi-leg matrix elements in the spirit of [11] will be implemented. It can furthermore be anticipated that this new shower implementation will lend itself to incorporation of MC@NLO-techniques [7, 9].

Acknowledgments

References

[1] Z. Nagy and D.E. Soper, *Matching parton showers to NLO computations*, *JHEP* **10** (2005) 024 [hep-ph/0503053].

[2] Z. Nagy and D.E. Soper, *A new parton shower algorithm: shower evolution, matching at leading and next-to-leading order level*, hep-ph/0601021.

[3] T. Sjöstrand, *High-energy physics event generation with* PYTHIA 5.7 *and JETSET 7.4*, *Comput. Phys. Commun.* **82** (1994) 74.

[4] T. Sjöstrand, S. Mrenna and P. Skands, PYTHIA 6.4 *physics and manual*, *JHEP* **05** (2006) 026 [hep-ph/0603175].

[5] G. Corcella et al., HERWIG 6: *an event generator for hadron emission reactions with interfering gluons (including supersymmetric processes)*, *JHEP* **01** (2001) 010 [hep-ph/0011363].

[6] G. Corcella et al., HERWIG 6.5 *release note*, hep-ph/0210213.

[7] S. Frixione and B.R. Webber, *Matching NLO QCD computations and parton shower simulations*, *JHEP* **06** (2002) 029 [hep-ph/0204244].

[8] S. Frixione, P. Nason and B.R. Webber, *Matching NLO QCD and parton showers in heavy flavour production*, *JHEP* **08** (2003) 007 [hep-ph/0305252].

[9] P. Nason and G. Ridolfi, *A positive-weight next-to-leading-order Monte Carlo for Z pair hadroproduction*, *JHEP* **08** (2006) 077 [hep-ph/0606275].

[10] S. Frixione and B.R. Webber, *The MC@NLO 3.3 event generator*, hep-ph/0612272.

[11] S. Catani, F. Krauss, R. Kuhn and B.R. Webber, *QCD matrix elements + parton showers*, *JHEP* **11** (2001) 063 [hep-ph/0109231].

[12] F. Krauss, *Matrix elements and parton showers in hadronic interactions*, *JHEP* **08** (2002) 015 [hep-ph/0205283].

[13] L. Lönnblad, *Correcting the colour-dipole cascade model with fixed order matrix elements*, *JHEP* **05** (2002) 046 [hep-ph/0112284].

[14] M.L. Mangano, M. Moretti and R. Pittau, *Multijet matrix elements and shower evolution in hadronic collisions: $Wb\bar{b} + (n)jets$ as a case study*, *Nucl. Phys.* **B 632** (2002) 343 [hep-ph/0108069].

[15] M.L. Mangano, M. Moretti, F. Piccinini and M. Treccani, *Matching matrix elements and shower evolution for top-quark production in hadronic collisions*, *JHEP* **01** (2007) 013 [hep-ph/0611129].

[16] T. Gleisberg, S. Höche, F. Krauss, A. Schälicke, S. Schumann and J.C. Winter, SHERPA 1.*alpha, a proof-of-concept version*, *JHEP* **02** (2004) 056 [hep-ph/0311263].

[17] F. Krauss, A. Schälicke, S. Schumann and G. Soff, *Simulating $W / Z + jets$ production at the Tevatron*, *Phys. Rev.* **D 70** (2004) 114009 [hep-ph/0409106].

[18] A. Schälicke and F. Krauss, *Implementing the ME+PS merging algorithm*, *JHEP* **07** (2005) 018 [hep-ph/0503281].

[19] L. Lönnblad, ARIADNE *version 4: a program for simulation of QCD cascades implementing the color dipole model*, *Comput. Phys. Commun.* **71** (1992) 15.

[20] N. Lavesson and L. Lönnblad, *$W + jets$ matrix elements and the dipole cascade*, *JHEP* **07** (2005) 054 [hep-ph/0503293].

[21] M.L. Mangano, M. Moretti, F. Piccinini, R. Pittau and A.D. Polosa, ALPGEN, *a generator for hard multiparton processes in hadronic collisions*, *JHEP* **07** (2003) 001 [hep-ph/0206293].

[22] T. Stelzer and W.F. Long, *Automatic generation of tree level helicity amplitudes*, *Comput. Phys. Commun.* **81** (1994) 357 [hep-ph/9401258].

[23] F. Maltoni and T. Stelzer, MADEVENT: *automatic event generation with* MADGRAPH, *JHEP* **02** (2003) 027 [hep-ph/0208156].

[24] J. Alwall et al., MADGRAPH/ MADEVENT *v4: the new web generation*, arXiv:0706.2334.

[25] A. Kanaki and C.G. Papadopoulos, HELAC: *a package to compute electroweak helicity amplitudes*, *Comput. Phys. Commun.* **132** (2000) 306 [hep-ph/0002082].

[26] C.G. Papadopoulos and M. Worek, *Multi-parton cross sections at hadron colliders*, *Eur. Phys. J.* **C 50** (2007) 843 [hep-ph/0512150].

[27] J. Alwall et al., *Comparative study of various algorithms for the merging of parton showers and matrix elements in hadronic collisions*, *Eur. Phys. J.* **C 53** (2008) 473 [arXiv:0706.2569].

[28] S. Gieseke, P. Stephens and B. Webber, *New formalism for QCD parton showers*, *JHEP* **12** (2003) 045 [hep-ph/0310083].

[29] T. Sjöstrand and P.Z. Skands, *Transverse-momentum-ordered showers and interleaved multiple interactions*, *Eur. Phys. J.* **C 39** (2005) 129 [hep-ph/0408302].

[30] S. Catani and M.H. Seymour, *A general algorithm for calculating jet cross sections in NLO QCD*, *Nucl. Phys.* **B 485** (1997) 291 [*Erratum ibid.* **B 510** (1998) 503] [hep-ph/9605323].

[31] S. Catani, S. Dittmaier, M.H. Seymour and Z. Trócsányi, *The dipole formalism for next-to-leading order QCD calculations with massive partons*, *Nucl. Phys.* **B 627** (2002) 189 [hep-ph/0201036].

[32] M. Dinsdale, M. Ternick and S. Weinzierl, *Parton showers from the dipole formalism*, *Phys. Rev.* **D 76** (2007) 094003 [arXiv:0709.1026].

[33] D.A. Kosower, *Antenna factorization of gauge-theory amplitudes*, *Phys. Rev.* **D 57** (1998) 5410 [hep-ph/9710213].

[34] J.M. Campbell, M.A. Cullen and E.W.N. Glover, *Four jet event shapes in electron positron annihilation*, *Eur. Phys. J.* **C 9** (1999) 245 [hep-ph/9809429].

[35] W.T. Giele, D.A. Kosower and P.Z. Skands, *A simple shower and matching algorithm*, arXiv:0707.3652.

[36] J.M. Campbell and R.K. Ellis, *An update on vector boson pair production at hadron colliders*, *Phys. Rev.* **D 60** (1999) 113006 [hep-ph/9905386].

[37] W. Beenakker et al., *Higgs radiation off top quarks at the Tevatron and the LHC*, *Phys. Rev. Lett.* **87** (2001) 201805 [hep-ph/0107081].

[38] Z. Nagy, *Three-jet cross sections in hadron hadron collisions at next-to-leading order*, *Phys. Rev. Lett.* **88** (2002) 122003 [hep-ph/0110315].

[39] J. Campbell and R.K. Ellis, *Next-to-leading order corrections to $W + 2jet$ and $Z + 2jet$ production at hadron colliders*, *Phys. Rev.* **D 65** (2002) 113007 [hep-ph/0202176].

[40] V. Del Duca, F. Maltoni, Z. Nagy and Z. Trocsanyi, *QCD radiative corrections to prompt diphoton production in association with a jet at hadron colliders*, *JHEP* **04** (2003) 059 [hep-ph/0303012].

[41] J. Campbell, R.K. Ellis, F. Maltoni and S. Willenbrock, *Associated production of a Z boson and a single heavy-quark jet*, *Phys. Rev.* **D 69** (2004) 074021 [hep-ph/0312024].

[42] J. Campbell, R.K. Ellis and F. Tramontano, *Single top production and decay at next-to-leading order*, *Phys. Rev.* **D 70** (2004) 094012 [hep-ph/0408158].

[43] S. Dittmaier, P. Uwer and S. Weinzierl, *NLO QCD corrections to $t\bar{t}$ + jet production at hadron colliders*, *Phys. Rev. Lett.* **98** (2007) 262002 [hep-ph/0703120].

[44] T. Kinoshita, *Mass singularities of Feynman amplitudes*, *J. Math. Phys.* **3** (1962) 650.

[45] T.D. Lee and M. Nauenberg, *Degenerate systems and mass singularities*, *Phys. Rev.* **133** (1964) B1549.

[46] R.K. Ellis, W.J. Stirling and B.R. Webber, *QCD and collider physics*, *Camb. Monogr. Part. Phys. Nucl. Phys. Cosmol.* **8** (1996) 1.

[47] T. Sjöstrand, *A model for initial state parton showers*, *Phys. Lett.* **B 157** (1985) 321.

[48] M. Bengtsson, T. Sjöstrand and M. van Zijl, *Initial state radiation effects on W and jet production*, *Z. Physik* **C 32** (1986) 67.

[49] H.-U. Bengtsson and T. Sjöstrand, *The Lund Monte Carlo for hadronic processes:* PYTHIA *version 4.8*, *Comput. Phys. Commun.* **46** (1987) 43.

[50] G. Marchesini and B.R. Webber, *Monte Carlo simulation of general hard processes with coherent QCD radiation*, *Nucl. Phys.* **B 310** (1988) 461.

[51] B.I. Ermolaev and V.S. Fadin, *Log-log asymptotic form of exclusive cross-sections in quantum chromodynamics*, *JETP Lett.* **33** (1981) 269 [*Pisma Zh. Eksp. Teor. Fiz.* **33** (1981) 285].

[52] A.H. Mueller, *On the multiplicity of hadrons in QCD jets*, *Phys. Lett.* **B 104** (1981) 161.

[53] Y.L. Dokshitzer, V.S. Fadin and V.A. Khoze, *On the sensitivity of the inclusive distributions in parton jets to the coherence effects in QCD gluon cascades*, *Z. Physik* **C 18** (1983) 37.

[54] Y.L. Dokshitzer, V.A. Khoze, S.I. Troian and A.H. Mueller, *QCD coherence in high-energy reactions*, *Rev. Mod. Phys.* **60** (1988) 373.

[55] G. Gustafson, *Dual description of a confined color field*, *Phys. Lett.* **B 175** (1986) 453.

[56] B. Andersson, G. Gustafson, G. Ingelman and T. Sjöstrand, *Parton fragmentation and string dynamics*, *Phys. Rept.* **97** (1983) 31.

[57] B. Andersson, *The Lund model*, *Camb. Monogr. Part. Phys. Nucl. Phys. Cosmol.* **7** (1997) 1.

[58] B.R. Webber, *A QCD model for jet fragmentation including soft gluon interference*, *Nucl. Phys.* **B 238** (1984) 492.

[59] J.-C. Winter, F. Krauss and G. Soff, *A modified cluster-hadronization model*, *Eur. Phys. J.* **C 36** (2004) 381 [`hep-ph/0311085`].

[60] P. Stephens, *Computer simulations of high energy physics*, `hep-ph/0408363`.

[61] H.E. Haber and G.L. Kane, *The search for supersymmetry: probing physics beyond the standard model*, *Phys. Rept.* **117** (1985) 75.

[62] T. Appelquist, H.-C. Cheng and B.A. Dobrescu, *Bounds on universal extra dimensions*, *Phys. Rev.* **D 64** (2001) 035002 [`hep-ph/0012100`].

[63] A. Djouadi, *The anatomy of electro-weak symmetry breaking. II: the Higgs bosons in the minimal supersymmetric model*, `hep-ph/0503173`.

[64] D.A. Dicus and S. Willenbrock, *Higgs boson production from heavy quark fusion*, *Phys. Rev.* **D 39** (1989) 751.

[65] E. Boos and T. Plehn, *Higgs-boson production induced by bottom quarks*, *Phys. Rev.* **D 69** (2004) 094005 [`hep-ph/0304034`].

[66] J.C. Collins and X.-m. Zu, *Parton distribution functions suitable for Monte-Carlo event generators*, *JHEP* **06** (2002) 018 [`hep-ph/0204127`].

[67] B.P. Kersevan and I. Hinchliffe, *A consistent prescription for the production involving massive quarks in hadron collisions*, *JHEP* **09** (2006) 033 [`hep-ph/0603068`].

[68] K. Hagiwara et al., *Supersymmetry simulations with off-shell effects for LHC and ILC*, *Phys. Rev.* **D 73** (2006) 055005 [`hep-ph/0512260`].

[69] D. Berdine, N. Kauer and D. Rainwater, *Breakdown of the narrow width approximation for new physics*, *Phys. Rev. Lett.* **99** (2007) 111601 [`hep-ph/0703058`].

[70] R.D. Field, *Applications of perturbative QCD*, Addison-Wesley, Redwood City U.S.A. (1989).

[71] G. Miu and T. Sjöstrand, *W production in an improved parton shower approach*, *Phys. Lett.* **B 449** (1999) 313 [`hep-ph/9812455`].

[72] OPAL collaboration, G. Abbiendi et al., *A simultaneous measurement of the QCD colour factors and the strong coupling*, *Eur. Phys. J.* **C 20** (2001) 601 [`hep-ex/0101044`].

[73] DELPHI collaboration, P. Abreu et al., *Measurement of the triple gluon vertex from four - jet events at LEP*, *Z. Physik* **C 59** (1993) 357.

[74] OPAL collaboration, R. Akers et al., *A measurement of the QCD color factor ratios C_A/C_F and T_F / C_F from angular correlations in four jet events*, *Z. Physik* **C 65** (1995) 367.

[75] ALEPH collaboration, R. Barate et al., *A measurement of the QCD colour factors and a limit on the light gluino*, *Z. Physik* **C 76** (1997) 1.

[76] A. Gehrmann-De Ridder, T. Gehrmann, E.W.N. Glover and G. Heinrich, *Second-order QCD corrections to the thrust distribution*, arXiv:0707.1285.

[77] A. Signer, *MENLO_PARC: a program for $e^+e^- \to 4jets$ at next-to-leading order*, *Comput. Phys. Commun.* **106** (1997) 125.

[78] Z. Nagy and Z. Trócsányi, *Next-to-leading order calculation of four-jet observables in electron positron annihilation*, *Phys. Rev.* **D 59** (1999) 014020 [*Erratum ibid.* **D 62** (2000) 099902] [hep-ph/9806317].

[79] T. Sjöstrand, L. Lönnblad and S. Mrenna, Pythia 6.2*: physics and manual*, hep-ph/0108264.

[80] S. Gieseke, A. Ribon, M.H. Seymour, P. Stephens and B. Webber, Herwig++ 1.0*: an event generator for e^+e^- annihilation*, *JHEP* **02** (2004) 005 [hep-ph/0311208].

[81] K. Hamacher and M. Weierstall, *The next round of hadronic generator tuning heavily based on identified particle data*, hep-ex/9511011.

[82] A. Buckley, *CEDAR: tools for event generator tuning*, arXiv:0708.2655.

[83] DELPHI collaboration, P. Abreu et al., *Tuning and test of fragmentation models based on identified particles and precision event shape data*, *Z. Physik* **C 73** (1996) 11.

[84] S. Catani, Y.L. Dokshitzer, M. Olsson, G. Turnock and B.R. Webber, *New clustering algorithm for multi-jet cross-sections in e^+e^- annihilation*, *Phys. Lett.* **B 269** (1991) 432.

[85] H. Hoeth, *Messung der vierjet-winkelverteilungen und bestimmung der QCD-farbfaktoren mit hilfe des APACIC++-generators*, Diploma Thesis, Fachbereich Physik, Bergishce Universität Wuppertal, Germany (2003).

[86] Z. Nagy and Z. Trócsányi, *Four-jet angular distributions and color charge measurements: leading order versus next-to-leading order*, *Phys. Rev.* **D 57** (1998) 5793 [hep-ph/9712385].

[87] M. Bengtsson and P.M. Zerwas, *Four jet events in e^+e^- annihilation: testing the three gluon vertex*, *Phys. Lett.* **B 208** (1988) 306.

[88] O. Nachtmann and A. Reiter, *A test for the gluon selfcoupling in the reactions $e^+e^- \to$ four jets and $Z^0 \to$ four jets*, *Z. Physik* **C 16** (1982) 45.

[89] J. Pumplin et al., *New generation of parton distributions with uncertainties from global QCD analysis*, *JHEP* **07** (2002) 012 [hep-ph/0201195].

[90] G. Altarelli, R.K. Ellis and G. Martinelli, *Large perturbative corrections to the Drell-Yan process in QCD*, *Nucl. Phys.* **B 157** (1979) 461.

[91] J. Kubar-Andre and F.E. Paige, *Gluon corrections to the Drell-Yan model*, *Phys. Rev.* **D 19** (1979) 221.

[92] R. Hamberg, W.L. van Neerven and T. Matsuura, *A complete calculation of the order α_S^2 correction to the Drell-Yan K factor*, *Nucl. Phys.* **B 359** (1991) 343 [*Erratum ibid.* **B 644** (2002) 403].

[93] R.V. Harlander and W.B. Kilgore, *Next-to-next-to-leading order Higgs production at hadron colliders*, *Phys. Rev. Lett.* **88** (2002) 201801 [hep-ph/0201206].

[94] C. Anastasiou, L.J. Dixon, K. Melnikov and F. Petriello, *High-precision QCD at hadron colliders: electroweak gauge boson rapidity distributions at NNLO*, *Phys. Rev.* **D 69** (2004) 094008 [hep-ph/0312266].

[95] R.J. Gonsalves, J. Pawlowski and C.-F. Wai, *QCD radiative corrections to electroweak boson production at large transverse momentum in hadron collisions*, *Phys. Rev.* **D 40** (1989) 2245.

[96] R.K. Ellis and S. Veseli, *W and Z transverse momentum distributions: resummation in q_T-space*, *Nucl. Phys.* **B 511** (1998) 649 [hep-ph/9706526].

[97] C. Balázs and C.P. Yuan, *Soft gluon effects on lepton pairs at hadron colliders*, *Phys. Rev.* **D 56** (1997) 5558 [hep-ph/9704258].

[98] A. Kulesza, G. Sterman and W. Vogelsang, *Joint resummation in electroweak boson production*, *Phys. Rev.* **D 66** (2002) 014011 [hep-ph/0202251].

[99] R.J. Gonsalves, N. Kidonakis and A. Sabio Vera, *W production at large transverse momentum at the Large Hadron Collider*, *Phys. Rev. Lett.* **95** (2005) 222001 [hep-ph/0507317].

[100] A. Vogt, S. Moch and J.A.M. Vermaseren, *The three-loop splitting functions in QCD: the singlet case*, *Nucl. Phys.* **B 691** (2004) 129 [hep-ph/0404111].

[101] S. Mrenna and P. Richardson, *Matching matrix elements and parton showers with* HERWIG *and* PYTHIA, *JHEP* **05** (2004) 040 [hep-ph/0312274].

[102] F. Krauss, A. Schalicke, S. Schumann and G. Soff, *Simulating W/Z + jets production at the CERN LHC*, *Phys. Rev.* **D 72** (2005) 054017 [hep-ph/0503280].

[103] S. Catani, Y.L. Dokshitzer, M.H. Seymour and B.R. Webber, *Longitudinally invariant $k_\perp$ clustering algorithms for hadron hadron collisions*, *Nucl. Phys.* **B 406** (1993) 187.

[104] CDF collaboration, A.A. Affolder et al., *The transverse momentum and total cross section of e^+e^- pairs in the Z boson region from $p\bar{p}$ collisions at $\sqrt{s} = 1.8$ TeV*, *Phys. Rev. Lett.* **84** (2000) 845 [hep-ex/0001021].

[105] G. Parisi and R. Petronzio, *Small transverse momentum distributions in hard processes*, *Nucl. Phys.* **B 154** (1979) 427.

[106] Z. Kunszt and D.E. Soper, *Calculation of jet cross-sections in hadron collisions at order α_S^3*, *Phys. Rev.* **D 46** (1992) 192.

[107] W.T. Giele, E.W.N. Glover and D.A. Kosower, *Higher order corrections to jet cross-sections in hadron colliders*, *Nucl. Phys.* **B 403** (1993) 633 [hep-ph/9302225].

[108] W.B. Kilgore and W.T. Giele, *Hadronic three jet production at next-to-leading order*, hep-ph/9903361.

[109] Z. Trócsányi, *Three-jet cross section in hadron collisions at next-to-leading order: pure gluon processes*, *Phys. Rev. Lett.* **77** (1996) 2182 [hep-ph/9610499].

[110] Z. Bern, L.J. Dixon and D.A. Kosower, *A two-loop four-gluon helicity amplitude in QCD*, *JHEP* **01** (2000) 027 [hep-ph/0001001].

[111] C. Anastasiou, E.W.N. Glover, C. Oleari and M.E. Tejeda-Yeomans, *Two-loop QCD corrections to $q\bar{q} \to q\bar{q}$*, *Nucl. Phys.* **B 601** (2001) 341 [`hep-ph/0011094`].

[112] C. Anastasiou, E.W.N. Glover, C. Oleari and M.E. Tejeda-Yeomans, *Two-loop QCD corrections to massless quark gluon scattering*, *Nucl. Phys.* **B 605** (2001) 486 [`hep-ph/0101304`].

[113] E.W.N. Glover, C. Oleari and M.E. Tejeda-Yeomans, *Two-loop QCD corrections to gluon gluon scattering*, *Nucl. Phys.* **B 605** (2001) 467 [`hep-ph/0102201`].

[114] Z. Bern, A. De Freitas and L.J. Dixon, *Two-loop helicity amplitudes for gluon gluon scattering in QCD and supersymmetric Yang-Mills theory*, *JHEP* **03** (2002) 018 [`hep-ph/0201161`].

[115] A. Daleo, T. Gehrmann and D. Maître, *Antenna subtraction with hadronic initial states*, *JHEP* **04** (2007) 016 [`hep-ph/0612257`].

[116] D0 collaboration, B. Abbott et al., *The dijet mass spectrum and a search for quark compositeness in $\bar{p}p$ collisions at $\sqrt{s} = 1.8$ TeV*, *Phys. Rev. Lett.* **82** (1999) 2457 [`hep-ex/9807014`].

[117] D0 collaboration, V.M. Abazov et al., *Measurement of dijet azimuthal decorrelations at central rapidities in $p\bar{p}$ collisions at $\sqrt{s} = 1.96$ TeV*, *Phys. Rev. Lett.* **94** (2005) 221801 [`hep-ex/0409040`].

[118] V.A. Khoze and W. Ochs, *Perturbative QCD approach to multiparticle production*, *Int. J. Mod. Phys.* **A 12** (1997) 2949 [`hep-ph/9701421`].

[119] CDF collaboration, F. Abe et al., *Evidence for color coherence in $p\bar{p}$ collisions at $\sqrt{s} = 1.8$ TeV*, *Phys. Rev.* **D 50** (1994) 5562.

[120] M. Bengtsson and T. Sjöstrand, *A comparative study of coherent and noncoherent parton shower evolution*, *Nucl. Phys.* **B 289** (1987) 810.

[121] F. Krauss and J.C. Winter, *Initial-state showering based on colour dipoles connected to incoming parton lines*, `arXiv:0712.3913`.

[122] S. Höche and A. Schälicke, *The* COMPARE *tool*, http://www.freacafe.de/compare.

[123] R. Brun and F. Rademakers, ROOT*: an object oriented data analysis framework*, *Nucl. Instrum. Meth.* **A389** (1997) 81.

[124] T. Ohl, *Drawing Feynman diagrams with LATEX and metafont*, *Comput. Phys. Commun.* **90** (1995) 340 [`hep-ph/9505351`].

[125] J.A.M. Vermaseren, AXODRAW, *Comput. Phys. Commun.* **83** (1994) 45.